We are committed to providing accessible customer service.
If you need accessible formats or communications supports, please contact us.

Nous tenons à améliorer l’accessibilité des services à la clientèle.
Si vous avez besoin de formats accessibles ou d’aide à la communication, veuillez nous contacter.

# Assessment Report

**On the**

# Sturgeon Lake Property

**Located in: NTS 52G15**

**Six Mile Lake Area and Bell Lake Area**

**Patricia Mining Division**

**Northern Ontario, Canada**

## Prepared For:

**Odin Metals Ltd.**
**35 Richardson Street**

**West Perth, WA 6005**

**Prepared By:**
**B. Clark, G.I.T**
**Clark Expl. Consulting Inc.**
**Thunder Bay, Ontario**

**August, 2019**

## Table of Contents



## List of Figures

**List of Appendices**

## 1.0 Summary

The Sturgeon Lake Property (the “Property”) report was prepared for Odin Metals Ltd. (“Odin”). In March 2019 Geotech conducted an airborne survey in conjunction with Glencore over the Sturgeon Lake Belt. This report summarizes the findings of the airborne VTEM survey over the Property.

The mining claims that comprise the Property are located roughly 195 kilometres northwest of Thunder Bay (Figure 1). The Property is situated in the Bell Lake and Six Mile Lake Area Townships within NTS Area 52 G/15 in the Patricia Mining Division. The approximate UTM center point of the Property is 657390E, 5524806N (NAD 83, Zone 15N).

The Sturgeon Lake Property is comprised of 90 claims totalling 1547 hectares. The claims are shown in Figure 2 and are listed in Appendix I. The total work requirement for the claims is $26,800 annually.

.

## 2.0 Introduction

The Sturgeon Lake Property (the “Property”) report was prepared for Odin Metals Ltd. (“Odin”).

This report is based on assessment file data pertaining to NTS area 52-G/15 from the Ministry of Northern Development and Mines online database as well as the recent airborne survey conducted in March 2019.

The author has also relied on previous exploration reports as referenced in Section “References”. The historical exploration information was mostly gathered from the Ontario government databases. These reports may or may not have been completed by qualified persons as defined by N.I. 43-101. After reviewing the reports and associated data, the author is satisfied the data presented is accurate.

## 3.0 Reliance on Other Experts

Information presented in this report is based on the author’s personal knowledge of the property and the area in question. Although this report cites the work of other experts who may or may not be considered qualified persons, the interpretation of this information and the conclusions and recommendations made in this report are based on the author’s personal knowledge of the Property and are the sole responsibility of the author.

While title documents and option agreements were reviewed for this report, this report does not constitute nor is it intended to represent a legal, or any other opinion as to the validity of the title. The titles were reviewed utilizing the Ontario government website for claims using the claims list provided by the company within the option agreements. The title and option information were relied upon to describe the ownership of the property, claim summary and summary of the option agreement in Section 4.

## 4.0 Property Description and Location

The mining claims that comprise the Property are located roughly 195 kilometres northwest of Thunder Bay (Figure 1). The Property is situated in the Bell Lake and Six Mile Lake Area Townships within NTS Area 52 G/15 in the Patricia Mining Division. The approximate UTM center point of the Property is 657390E, 552806N (NAD 83, Zone 15U).

The Sturgeon Lake Property is comprised of 90 claims totalling 1547 hectares. The claims are shown in Figure 2 and are listed in Appendix I. The total work requirement for the claims is $26,800 annually.

The Ontario government registered claims provide a right to the owner to access exploration on the areas described. These claims are mineral rights only with a right to the surface rights on completion of specific expenditures on exploration and other administrative requirements.

## 5.0 Accessibility, Climate, Local Resources, Infrastructure and Physiography

The mining claims that comprise the Sturgeon Lake Property are adjacent to the Glencore Patents & Leases that comprise the past producing Mattabi Mine.

The property is located approximately 65 kilometers north-northeast of the town of Ignace, Ontario, approximately 85 kilometers east-southeast of Sioux-Lookout, Ontario, and is within four kilometers of the past-producing Lyon Lake, Creek, and Sturgeon Lake deposits(s) of the Sturgeon Lake VMS camp. The city of Thunder Bay in 195 kilometres southeast, has a population of 110,000 and provides support services, equipment and skilled labour for both mineral exploration and mining industry. Rail, national highway, port, and the airport at Thunder Bay has daily scheduled flights to Toronto, Ottawa, Calgary and Winnipeg.

Access to the Sturgeon Lake Property from Thunder Bay, the property can be reached by travelling west on Highway 11/17 and then 17 until the turnoff north of Highway 599 located as one enters Ignace, Ontario approximately 242 kilometers away. Highway 599 is followed for 60 kilometers north to Silver Dollar. The Mattabi Mine Road is located roughly 500 meters past Silver Dollar on Highway 599, and this road is taken for approximately 15 kilometers to the gate on the west side of the Sturgeon Lake VMS Camp. The Sturgeon Lake camp is currently held by Glencore and access is restricted to the past-producing mine workings and the active water treatment facility located on the property. Once through the gates, a series of well-maintained road networks is followed westward leading to a portion of the property that can no longer be travelled by pickup truck. A four kilometre winter drill road is then travelled into the western shore of Claw Lake. Alternatively, the property ay be accessed from Sioux Lookout or Sturgeon Lake areas via float or ski-equipped aircraft landing on Claw Lake.

The Property consists of topography characterized by small hills surrounded by narrow incised valleys that appear to align with both with structural features of the underlying bedrock and glacial direction (mean elevation 325 metres above sea level). Small wetland areas occupy topographic depressions. Tree cover consists of white and jack

pine, birch, spruce and balsam on elevated topography, and cedar, spruce, birch and tamarack in swampy lowlands. Overburden is comprised of boulder laden glacial till and outwash deposits, with muskeg and organic deposits in low-lying areas.

The area exhibits a northern boreal climate, with short, warm summers and cold winters with moderate snowfall. Freezing temperatures can be expected from late October through mid-May. Ground access to the property might be hampered in spring by wet and slippery conditions along roads and trails.

The current land holdings are sufficient to allow for exploration. There are currently no encumbrances on surface rights and the potential surface rights holdings can be triggered when the claims go to lease. However, it is beyond the author's scope to determine whether or not the current land holdings are sufficient for development of infrastructure to sustain a mining operation.

**Figure 1: Sturgeon Lake Property Location**

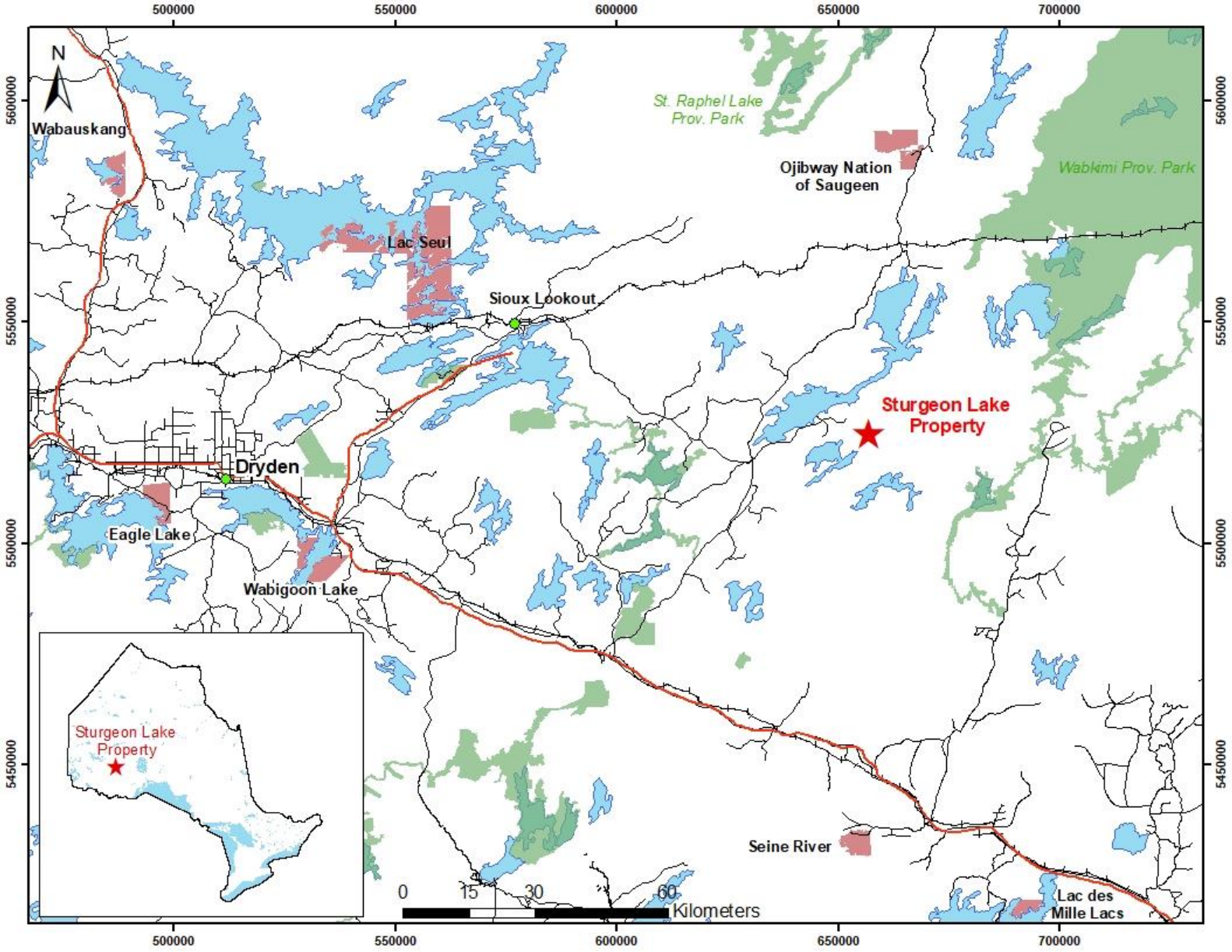

**Figure 2: Sturgeon Lake Property Claims**

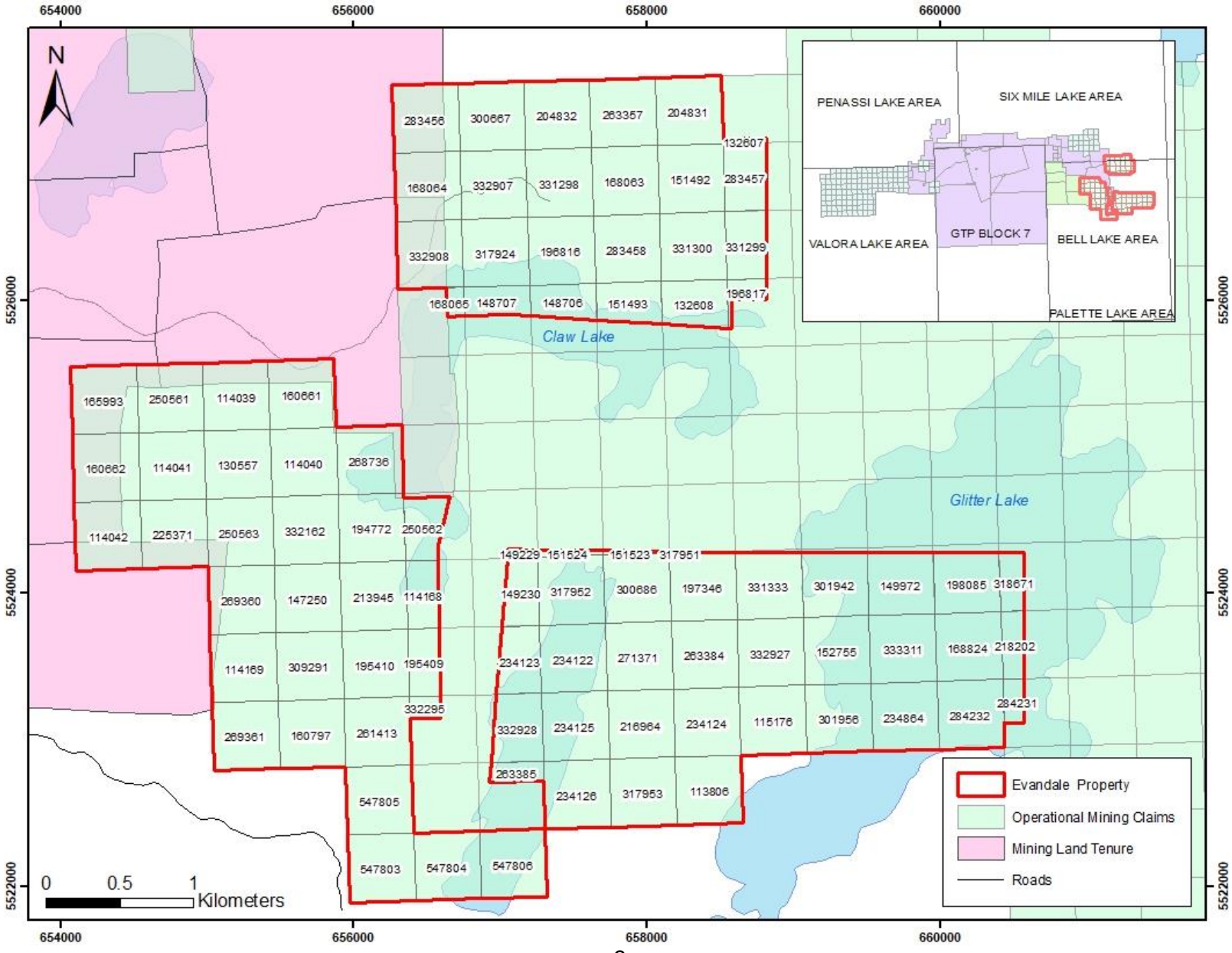

## 6.0 History

The Sturgeon Lake mining district is home to several historic VMS deposits, including the Mattabi, Lyon Lake, Sturgeon Lake, Creek Zone, and F-Group deposits. These were mined by Noranda Minerals from early 1972 to 1991. During this time, Noranda held much of the land that is currently part of the Odin Metals Ltd (Evandale) property. Several exploration holes were drilled in the Claw Lake and Hump Lake areas between 1970 and 1972 by Newconex Canadian Exploration Ltd, Mattagami Lake Mines Ltd, and Amax Exploration Ltd., some of which showed minor Zn+Cu±Pb mineralization in massive, semi-massive and stringer sulphides (Newconex Canadian Expl. Ltd, 1970a, 1970b; Mattagami Lake Mines Ltd, 1972; Amax Exploration Inc. 1972). However, these results were never followed up on during the life of the mines.

In 1990 the Ontario Geological Survey released airborne magnetic and EM survey data for the Sturgeon Lake-Savant Lake area (Ontario Geological Survey, 2003). The survey delineated extensive, subparallel conductive horizons in the Sturgeon Lake greenstone belt, as well as weak to moderate and local strong magnetic anomalies. The survey showed the conducive horizons continuing from the Noranda mines eastward past Glitter Lake and beyond.

In 1992 Noranda Exploration Company Ltd. along with Hemlo Gold Mines Ltd. conducted a geophysical and drilling program totalling 780 feet, targeting the Benderite showing at their Quill Lake property. The best drilling results were 1.65g/t Au over 1.7m and 2.05g/t Au over 1.2m (Gingerich, 1992). (OAFD File# 52G15SW0002)

In 1993 Noranda Exploration Company Ltd. undertook a mapping, sampling, and induced polarization survey program on their East Sturgeon Property, located south of Claw Lake. The mapping program identified at least three volcanic cycles which appear to be related to the volcanic cycles at the Sturgeon Lake complex. Several sulphide boulders containing up to 10- 15% Py+Po±Cpy were discovered, but significant sulphide concentrations were not identified in outcrop (Smith, 1994). (OAFD File# 52G15SW0005)

In 2003, Unitronix Corp. in conjunction with Noranda Mining and Exploration commissioned a MEGATEM survey over an area that included a portion of Odin's Sturgeon Lake claims west of Glitter Lake and extending eastward to the old Noranda Mine leases (now owned by Glencore). The survey produced a detailed airborne EM map along with a detailed airborne magnetic map that helps highlight some of the conductive structures in the area (Fugro, 2003). Unitronix (Now called Unitronix Mining and Exploration) followed up on this survey in 2006 with a high resolution horizontal magnetic gradient and XDS-VLF-EM airborne survey focusing on the Glitter Lake west, Claw Lake, and Telephone Lake areas (Barrie, 2006). The purpose of the survey was to identify additional magnetic and electromagnetic anomalies related to economic

mineralization, and to provide additional structural and geological information in the area. (OAFD File# 52G15NW2005)

In 2010 Excalibur Resources Ltd. contracted Geotech Ltd. to conduct a VTEM survey over 1069 line kms over their Sturgeon Lake east property located between Claw Lake and Dunne Lake. The VTEM survey identified several parallel horizons with laterally extensive sulphide-bearing conductors that are located along the eastern extension of the Sturgeon Lake volcanic cycles. Excalibur followed up on these results with an enzyme leech soil geochemistry survey and a soil gas hydrocarbon survey to narrow the results in preparation of a diamond drilling program. Between August 17th and October 22nd 2010, Excalibur Resources Ltd. drilled 21 holes totalling 3784m over their Sturgeon Lake properties. The holes followed up on several of the coincident SGH, enzyme leech, and VTEM anomalies identified earlier in the year. The drilling had mixed success, with favorable stratigraphy intercepted in several of the holes including several sulphide rich horizons, but minimal Cu-Zn mineralization with values up to 0.15% Zn over 9.4m and 0.1% Zn over 8.4m. In general, grades and stratigraphy became more favourable towards the west (towards the current Gossan property). However, the highest priority targets were not drilled due to summer access concerns, but these may be reached with a winter drill program. (OAFD File# 20000005531)

2010, Xstrata conducted a sampling program on their Claw Lake Property which coincides with the southern portion of Odin Metals claims.
(OAFD File# 20000005556)

In 2011 a soil gas hydrocarbon survey was undertaken by Act Labs for 3936499 Canada Inc. covering the ground just west of Claw Lake. 82 soil samples were collected and analyzed. The survey identified anomalous base metal targets with potential for copper mineralization
(Bulatovich, 2011). (OAFD File# 20000006144)

In 2012, Aur Lake Exploration Ltd. conducted a sampling assessment program on their Mattabi Claim Group covering the area south of Claw Lake and around Telephone Lake. A total of 10 samples were taken from outcrops along the south and east shores of Claw Lake, as well as along the west shore of Telephone Lake. The program encountered minimal mineralization in the outcrop samples, with values ranging from 4 – 228 ppm Cu, 5 – 111 ppm Ni, 17- 129 ppm Zn, and 0.3 - 1.2 ppm Ag. The program also located the core for S-92-01, which was a hole drilled west of Claw Lake by Noranda Exploration Company Ltd. in 1992. Aur Lake collected 39 samples from the drill core and sent them for assay to Accurassay Labs. Intersections of 1.14% Cu and 1.23% Zn over 2.05m were reported from the samples (Newton, 2012). (OAFD File# 20000007500)

2016, Gossan Resources Ltd conducted a geobotanical Alder Survey on their property east of Odins claims. The survey outlined Zn, Au and Ag anomalies trending east west across the property which roughly follow defined VTEM anomalies. (OAFD File# 20000013589)

# 7.0 Geological Setting and Mineralization

## 7.1 Regional Geology

The Sturgeon Lake property is located in the Wabigoon subprovince within the Superior geological province (Trowell, 1983). It is part of the Sturgeon Lake greenstone belt which is comprised of Neo-Archean mafic to felsic volcanic rocks, along with clastic and chemical metasediments. The Southern Sturgeon Lake greenstone belt hosts the Sturgeon Lake caldera complex, which is a 2.735 Ga mafic to intermediate to felsic submarine volcanic complex, (Franklin et al, 1977; Morton and Franklin, 1987; Morton et al, 1999; Mumin et al, 2007). To the south of the southern Sturgeon Lake belt are tonalite gneisses from the English River assemblage. The Beidelman Bay tonalite pluton intrudes the English River assemblage and the southern Sturgeon Lake greenstone belt stratigraphically below the caldera complex. To the east, the greenstone belt pinches out below the Vista Lake plutonic complex and the Quest Lake metasediments (Sanborn-Barrie et. al, 2002). Metamorphic grade varies across the region from greenschist to amphibolite facies (Figure 3).

The Sturgeon Lake caldera hosts several past producing VMS deposits, including the Mattabi, Sturgeon Lake, Lyon Lake, Creek Zone and F-group deposits. Production from these five deposits totalled 18,663,000 tonnes of ore averaging 8.5% Zn, 1.4% Cu, 0.8% Pb, and 122.3 g/t Ag. The deposits lie along an orthogonal series of graben structures defined by synvolcanic faulting (Mumin et al, 2007). They are capped by or emplaced within a series of E-W trending rhyolitic/dacitic horizons at three discrete stratigraphic levels. The eastern and western extents of the caldera complex remain poorly defined.

The following description of the regional geology is taken directly from Morton et al., 1990:

The South Sturgeon Lake area of northwestern Ontario is underlain by a well preserved, though partially eroded, Archean submarine volcanic caldera. This caldera is host to six massive sulphide deposits (Mattabi, F-Group. Sturgeon Lake Mine, Creek Zone, Lyon Lake, and Sub-Creek Zone) (Figure 3, Table 2) as well as numerous subeconomlc massive sulphide occurrences. The Sub-Creek Zone may represent the down plunge extension of the Lyon Lake. The Sturgeon Lake Mine, F-Group and Mattabi deposits were depleted of reserves in 1981, 1984 and 1988 respectively, whereas the Lyon Lake and Creek Zone deposits are currently being mined (*at the time of Morton et al.'s paper)*.

**Table 1: Grade and tonnages of the ore deposits in the South Sturgeon Lake Area (Morton et al, 1990)**

| Deposit | Tonnage ($10^6$ tons) | Zn % | Cu % | Pb % | Ag % |
|---|---|---|---|---|---|
| Mattabi | 12.55 | 8.28 | 0.74 | 0.85 | 3.31 |
| F-Group | 0.38 | 9.51 | 0.64 | 0.58 | 1.92 |
| Sturgeon Lake | 2.28 | 9.17 | 2.55 | 1.21 | 5.22 |
| Lyon Lake & Creek Zone | 3.17 | 8.67 | 1.26 | 0.99 | 4.50 |

The south Sturgeon Lake area is located within the Archean Wabigoon volcano-sedimentary greenstone belt within the Superior Province. The Wabigoon subprovince is bounded to the north by the English River Gneiss Belt and to the south by the Quetico Gneiss Belt (Trowell and Johns. 1986). The volcanic and sedimentary rocks of the area have been subjected to regional greenschist facies metamorphism with almandine-amphibolite assemblages towards both the eastern and southern extents of the Sturgeon Lake area (Trowell. 1974. 1983; Groves. 1984). The South Sturgeon Lake sequence strikes west-northwest, dips steeply (65°-75), faces north and forms the southern limb of a syncline with an axis centered through Sturgeon Lake (Trowell. 1983).

Detailed mapping of the volcanic rocks in the south Sturgeon Lake area coupled with the relogging of 200,000 m of diamond drill core, with emphasis on the physical volcanology of the rocks, has led to the recognition and description of a well preserved Archean submarine caldera complex. This complex, which has been named the Sturgeon Lake Caldera (Morton et al., 1988, 1989, 1990), is approximately 30 km in strike length and contains up to 4500 m of caldera fill material. Five separate, major ash flow tuff units have been defined, and each can be traced for kilometers across the complex with individual thicknesses ranging from 100 to more than 1200 m. Based on the stratigraphic distribution and thickness of the five ash flow tuff units and associated debris flow deposits, it is believed that the Sturgeon Lake Caldera consists of a series of smaller nested or overlapping calderas and that each ash flow unit Is associated with a collapse event. This interpretation is supported by studies of more recent caldera complexes which show that major ash flow tuff units are related to Individual collapse events and that nested or overlapping calderas are common (Cas and Wright, 1987).

Based on detailed stratigraphic mapping and core logging, numerous synvolcanic faults have been defined; those with major stratigraphic displacement (>150 m) may represent individual caldera boundaries. In general, the eastern and western margin of the complex has been located and the back (northern) bounding wall has been partially defined. A series of late, north-south-trending dip-slip faults has broken the complex into a number of blocks which allow the caldera complex to be observed at different stratigraphic levels. Individual volcanic and intrusive rock units are traceable across the faults, but thicknesses change dramatically (Figure 4). Zircon ages of the ash flow tuff

deposits and late dome lavas yield a similar age of 2,735 m.y. +/- 1.5 m.y. (Davis et al., 1985).

A large, sill-like intrusion (Beidelman Bay Complex) has a similar age to the felsic volcanics and represents, in part, the magma chamber for the eruptive material. This intrusive body can be traced along strike for 20 km and has an average width of 2.5 km; its composition varies from trondhjemite to quartz diorite with feldspar and quartz +/- feldspar porphyry phases. The Beidelman Bay Intrusive complex also hosts minor occurrences of porphyry copper-type mineralization, and the upper portions locally contain stringers of zinc-silver mineralization. A mafic (gabbroic-quartz dioritic) dyke to sill-like intrusion occurs across the length of the caldera complex (Figure 4). Trace element and rare earth analyses (Davis et al., 1985) indicate that the caldera rocks have a similar petrogenetic history and are cogenetic with the subvolcanic Beidelman Bay trondhjemite sill which intrudes the Darkwater mafic flows (Poulsen and Franklin, 1981). Metamorphosed hydrothermal alteration is widespread within the complex and in the upper part of the Beidelman Bay Intrusion. Discrete alteration assemblages form zones that are a) widespread and largely conformable to the volcanic stratigraphy, b) locally lens- or pod-like beneath sulphide occurrences and deposits and c) narrow and elongate, cross-cut stratigraphy and are associated with synvolcanic faults (Groves, 1984; Hudak, 1989; Jongewaard, 1989; Morton et al., 1988; Morton and Franklin, 1987).

The following is taken directly from Smith (2000):

The South Sturgeon Lake greenstone belt consists of a >8,800 meter thick west-northwest facing, north dipping (70-75°) sequence of mixed tholeiitic/calcalkalic volcanics forming the southern limb of a syncline. The volcanic pile rests on Archean gneissic basement, and is intruded by syn-to post-volcanic plutons, sills and dykes. The north facing, steeply dipping nature of the south Sturgeon Lake assemblage has resulted from folding about an east-west axis with the fold axis situated in the south part of Sturgeon Lake. A weaker deformation about a north-south axis produced a gradual concave arching to the east, with a change from 90" strikes in the Mattabi Mine area to 120° strikes in the Lyon Lake area.

Laterally extensive mappable units originally recognized as distinct volcanic cycles by Mattagami Exploration personnel were grouped into a number of volcanic cycles by Franklin and other GSC workers (1977), with each cycle beginning with mafic to intermediate volcanic flows and terminating with felsic pyroclastic events. A thin sedimentary layer caps each cycle. Subsequent mapping by Trowell (1983) confirmed the cyclical nature of the volcanism, although his interpretation of the belt as a simple north-facing homoclinal sequence was suggested to be an over-simplification by Morton and co-workers (1990) and that the observed thickness were probably due to thrust repetition of the stratigraphy.

Detailed re-mapping of much of the Camp along with volcanological and stratigraphic studies have been completed by Ron Morton and various graduate students over the last decade. Their work suggests the South Sturgeon Lake

assemblage represents a large submarine caldera complex, with 5 separate caldera-collapse events each marked by ash tuff horizons. They have demonstrated the importance of volcanism and synvolcanic structures in controlling the occurrence and location of VMS deposits in the Camp. The stratigraphic succession and setting of each ore body as resolved by Morton is presented in Table 2.

**Table 2: Stratigraphic and VMS Deposit Settings (Smith, 2000)**

| NORANDA 1980 | MORTON 1990 | Thickness | Deposit Location |
|---|---|---|---|
| Upper Cycle | No Name Lake Succession | 1000m to 3000m | |
| Lyon Lake Cycle | No Name Lake Succession | 1000m | |
| N.B.U | L. Succession | 1650m (+) | Lyon Lake + Sturgeon Lake |
| | Mattabi Succession | | Mattabi B, C, D |
| | Tailings Lake Succession | | Mattabi E |
| Mattabi Cycle | High Level Lake Succession | 3000m (+) | F Group |
| | Jackpot Lake Succession | | |
| | Darkwater Lake Sucession | | |

**Figure 3: Regional Geology of the Sturgeon Lake Area**

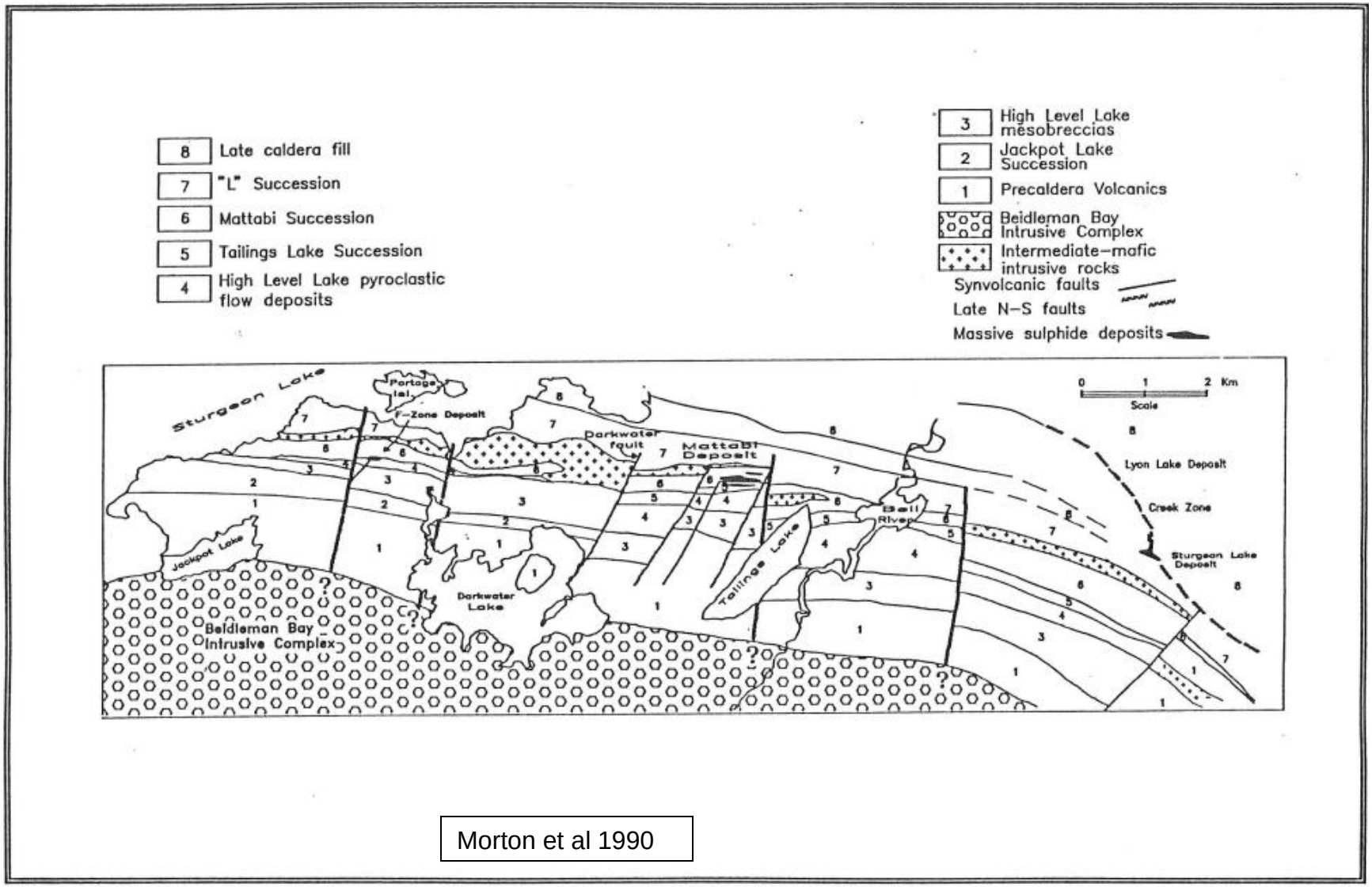


Morton et al 1990

## 7.2 Property Geology

Adapted from Newton, B. et al 2012

The property contains a series of folded felsic, intermediate and mafic volcanic rocks, pyroclastic flows, and sedimentary rocks. The units have been metamorphosed to greenschist grade and have been intruded by younger stocks of monzonite, granodiorite-trondhjemite and granite (Karrei & Morrison 2012).

The Mattabi Claim Group is situated southwest of Sturgeon Lake, on what is known as the Claw Lake cycle. According to Franklin, two formations make up the Claw Lake cycle; a mafic volcanic unit with minor tuff, and an autoclastic/hyaloclastic breccia. The mafics are located at the base of the sequence, are at least few hundred feet thick and gradually thicken to the west. This unit is composed of coarse grained, amygdaloidal, pillowed, massive basaltic and andesitic flows, with local carbonitic alteration. The pillows have a squeezed appearance, which resulted from primary deformation. This unit drastically thins out to east and pinches out west of Lyon Lake, suggesting a possible source or vent area (Trowell, 1983). A shallow water environment (less than 500m) is suggested by the pyroclastic debris and the thick appearance of the pillow selvages.

Overlaying the volcanic strata is a volcanoclastic lapilli tuff unit. This unit is laterally extensive and hosts the Mattabi Deposit (Figure. 4). This unit consists of intermediate to felsic fragmental rocks, varying in particle size from pyroclastic breccia to ash tuff. Trowell (1983) mentions that the fragmental units are composed of angular to rarely subrounded felsic clasts situated in a fine tuff matrix. This is also indicative of a shallow marine environment.

**Figure 4: Geological map of the Sturgeon Lake Volcanic Belt**

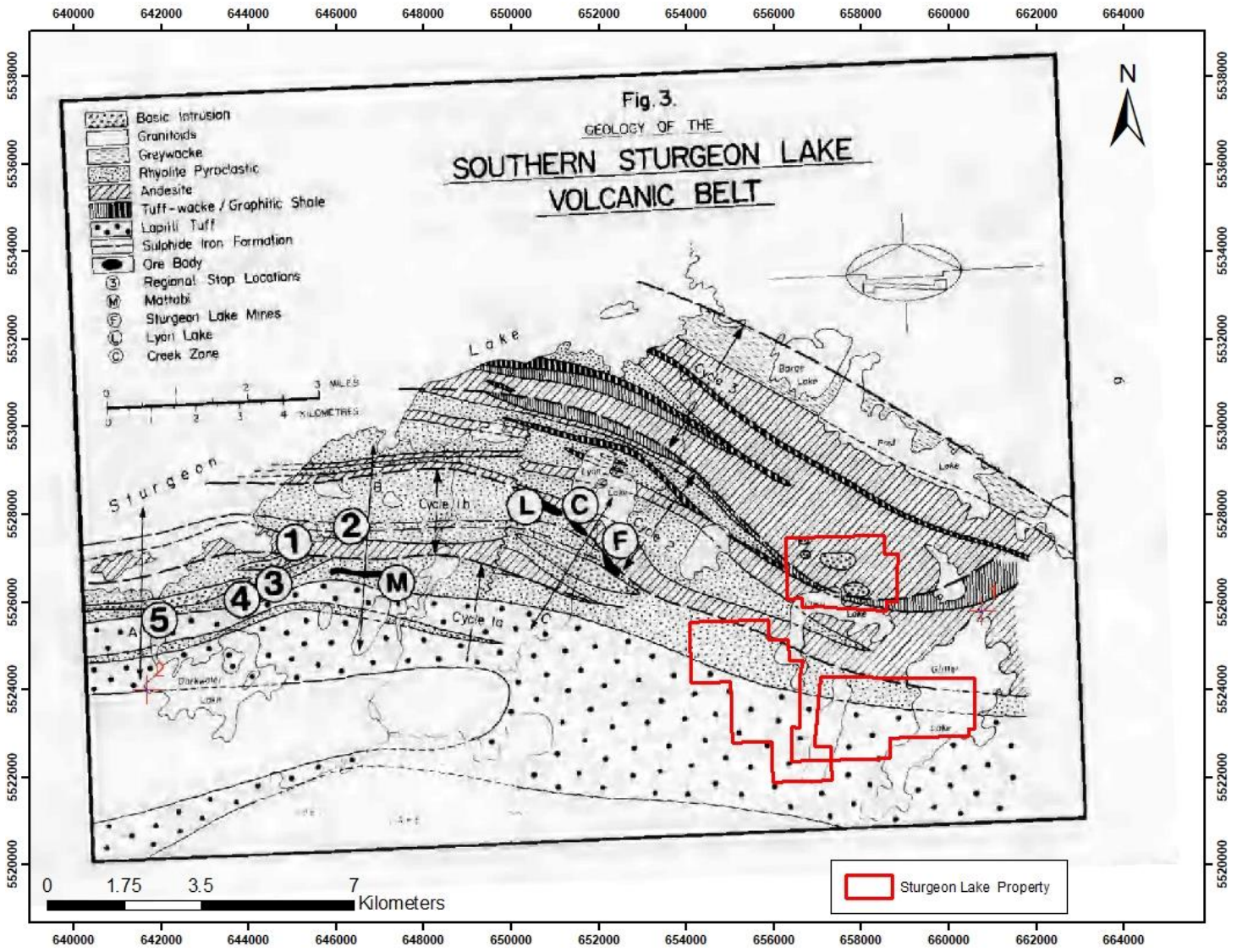

## 7.3 Property Mineralization

Two, sub-parallel, ESE-WNW striking, favorable structural-stratigraphic horizons can be projected onto and interpreted to occur within the Odin (Evandale) claim blocks near the eastern margin of the Sturgeon Lake caldera complex, surrounding Claw Lake (Cu, Au MDI Occurrence MDI52G15SW00010). These features bound the Swamp Lake trend, which include historical geophysical anomalies, BHEM targets and mineralized drill intercepts, as well as the past producing Sturgeon Lake, Creek Zone and Lyon Lake Zone Mines.

# 8.0 Deposit Types

## 8.1. Volcanogenic Massive Sulphide

Volcanogenic massive sulphide (VMS) deposits are significant producers of Zn, Cu, Pb, Ag and Au globally, and may contain a number of associated elements including Co, Sn, Cd, In, Bi, Se, Mn, Te, Ga, Ge ± As, Sb and Hg (Lydon, 1988, Misra, 2000, Galley et al., 2007). VMS deposits are a class of hydrothermal ore deposits which typically occur as lenses of polymetallic massive sulphide that form at or near the seafloor in submarine volcanic environments from metal-enriched fluids associated with seafloor hydrothermal convection (Galley et al., 2007). Deposits range in age from Archean to actively forming deposits in modern seafloor spreading and oceanic arc terranes (Lydon, 1988, Misra, 2008; Galley et al., 2007).

## 8.2. Formation

The six components required for the formation of VMS deposits in a hydrothermal system are: 1) a heat source (subvolcanic intrusion) driving the hydrothermal system; 2) a water-rock interaction zone; 3) fracture/fault zones allowing fluid flow; 4) footwall and/or hanging-wall alteration zones; 5) VMS deposit(s); and 6) distal products of chemical precipitation of sediment in the water column (Figure 6). This model also shows that at different stages in the hydrothermal system, some elements are gained while other are lost. Semi conformable alteration zones (distal to VMS deposits) show increases in Ca-Si-Fe-Na-K-Mg (epidotization-silicification, actinolite-clinozoisite-magnetite, spilitization, and chlorite-sericite±K-feldspar alteration assemblages). Stockwork vein systems (proximal alteration assemblages) show increases in Fe and Mg and depletion in Na, Ca and Si reflecting feldspar destruction (chlorite-quartz–sulphide or sericite-quartz-pyrite±aluminosilicate-rich alteration assemblages; Galley et al., 2007 and Lydon, 1988). The zone overlying subvolcanic intrusions can be altered to amphibolite-facies assemblages followed by Na-Ca-rich greenschist-facies assemblages. Subsequently and in close proximity to the seafloor zeolite-clay, carbonates and sub-greenschist mineral assemblages are found (Galley et al., 2007).

**Figure 5: Evolution of a VMS forming hydrothermal system**

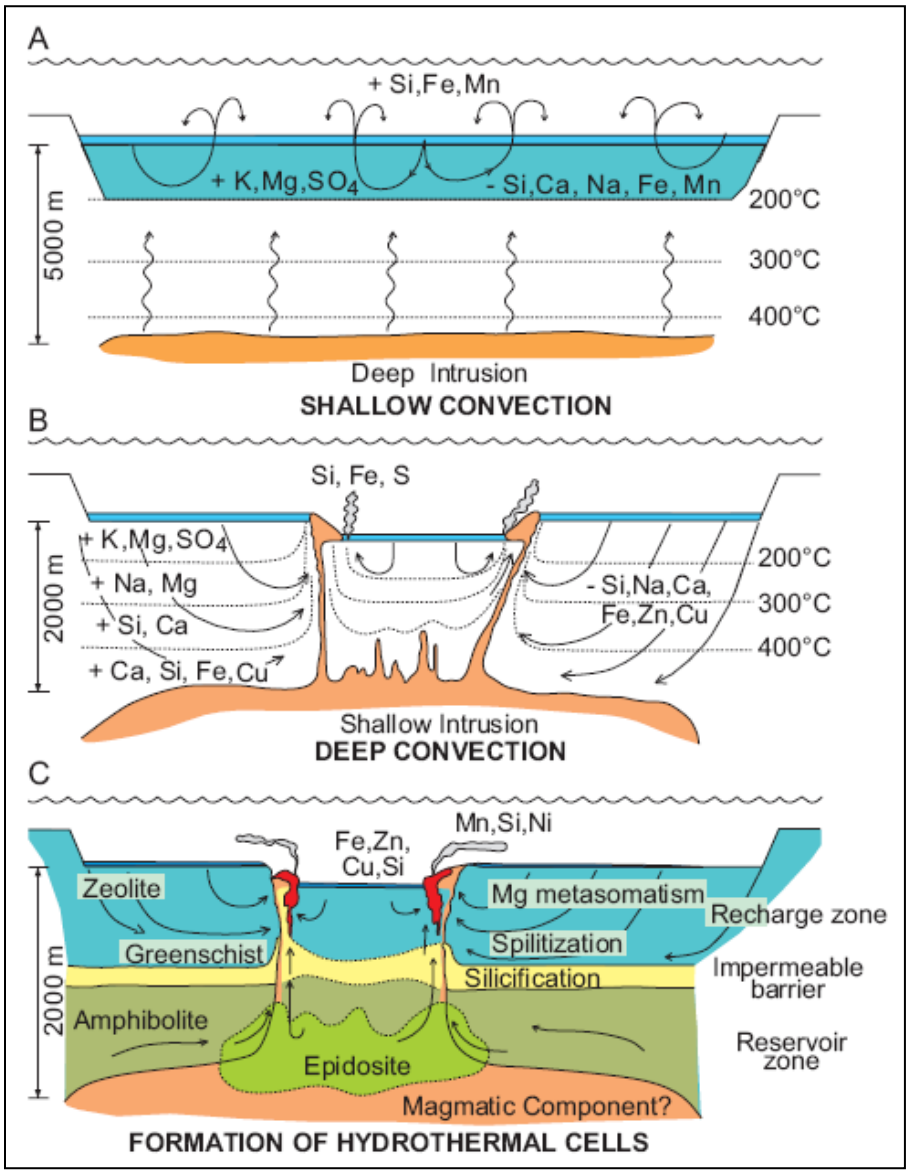


(A) Deep subvolcanic intrusion initiating a shallow convection system and initial stages of alteration. (B) Higher level intrusion subvolcanic magmas generating a deep convection system. Compositional changes illustrated by elements gained and lost from surrounding rocks controlled by temperature gradients and availability. (C) Maturation of a hydrothermal system forming hydrothermal alteration assemblages. Metal-rich fluids flow via faults/fractures and high temperature zones forming VMS deposits (from Galley, 1993; Galley et al., 2007; Franklin et al., 2005).

## 9.0 Exploration

Exploration to date includes a 414 line-kilometer helicopter-borne geophysical survey of an approximately 35 $km^2$ area covering the Sturgeon Lake Property. The survey included a versatile time domain electromagnetic (VTEM™ max) system and caesium magnetometer component.

The processed survey results are presented with the following maps:

- Electromagnetic stacked profiles of the B-field Z Component (Figure 6)
- Electromagnetic stacked profiles of dB/dt Z Components (Figure 7)
- B-Field Z Component Channel grid (Figure 8)
- Fraser Filtered dB/dt X Component Channel grid (Figure 9)
- Total Magnetic Intensity (TMI) (Figure 10)
- Calculated Time Constant (Tau) (Figure 11)
- Resistivity Depth Images (RDI) sections are presented (Figure 12)

Digital data includes all electromagnetic and magnetic products, plus ancillary data including the waveform (Appendix III).

The survey report describes the procedures for data acquisition, processing, equipment used, final image presentation and the specifications for the digital data set (Appendix III).

The work was completed between April 25 and May 15, 2019, with a total cost of $62,382.25, or $1,782.35/$km^2$ for the entire survey area.

**Figure 6: Electromagnetic stacked profiles of the B-field Z Component**

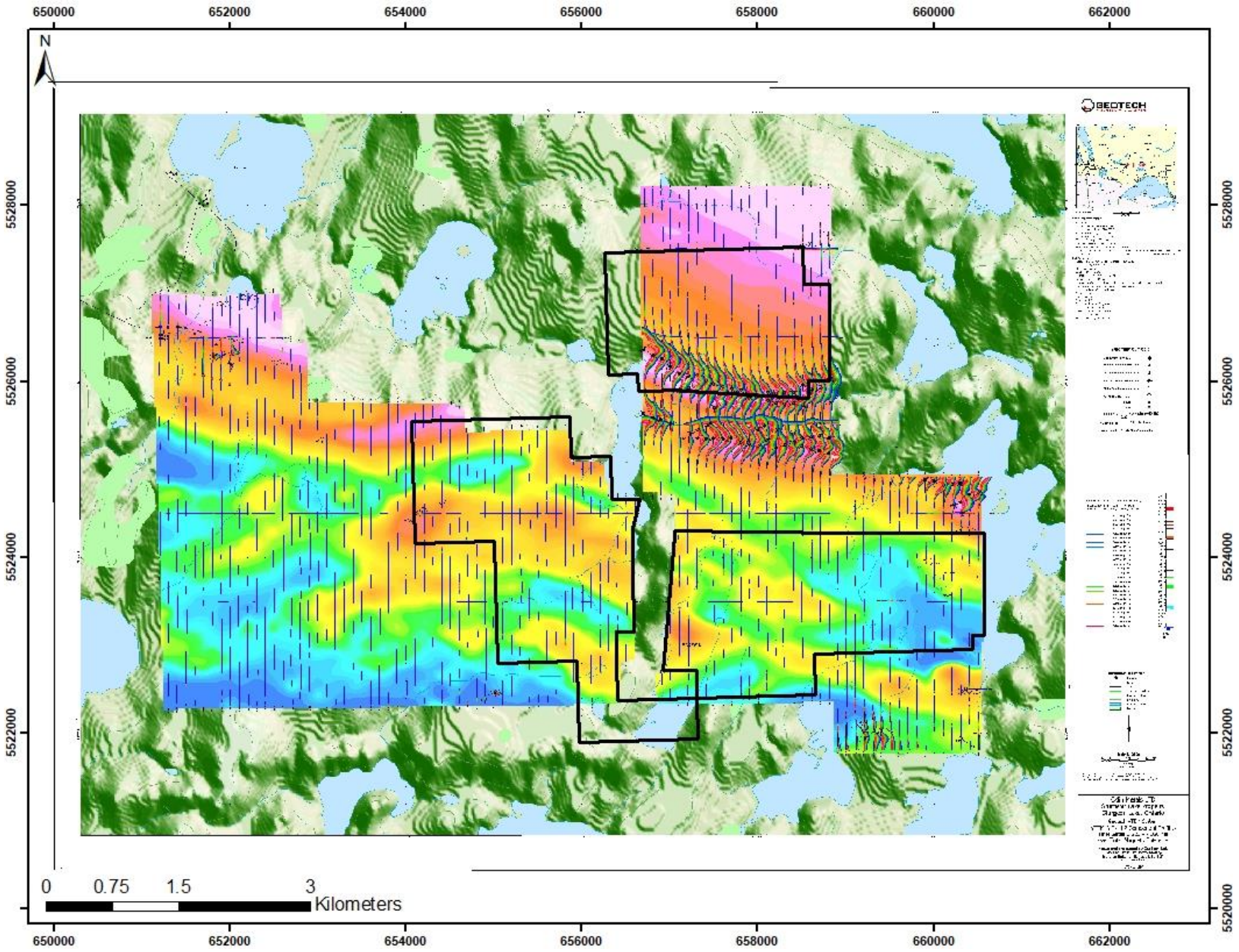

**Figure 7: Electromagnetic stacked profiles of dB/dt Z Components**

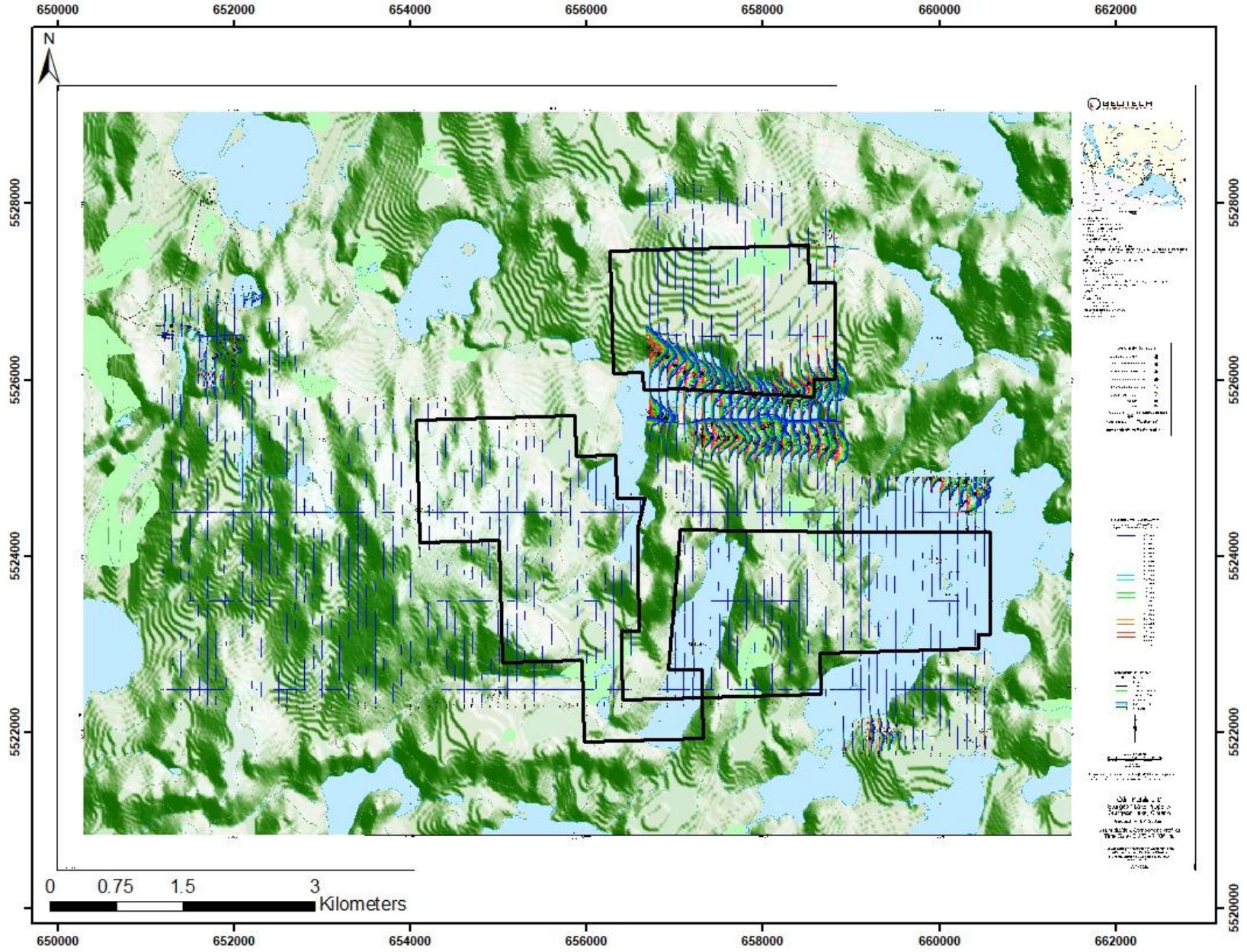

**Figure 8: B-Field Z Component Channel grid**

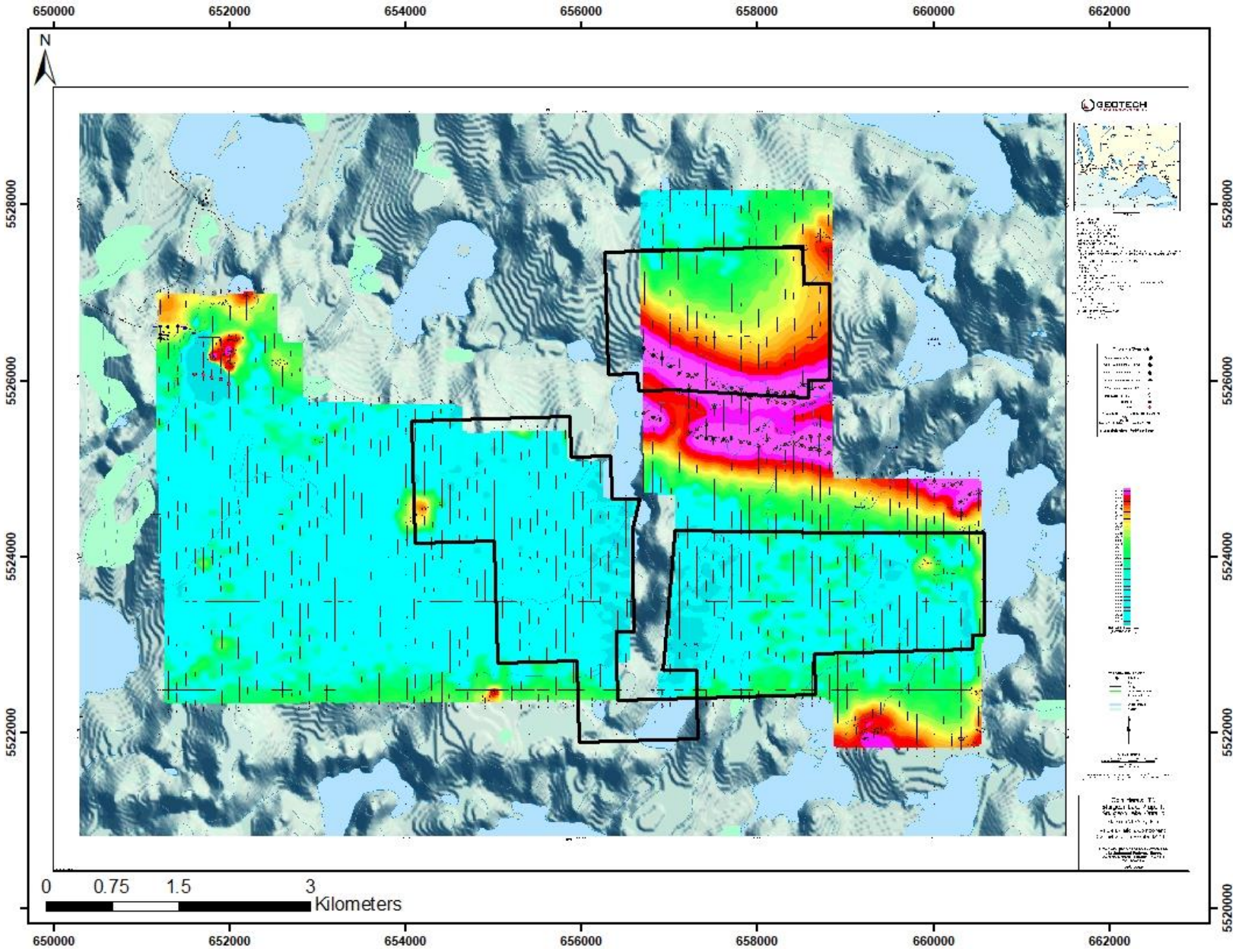

**Figure 9: Fraser Filtered dB/dt X Component Channel grid**

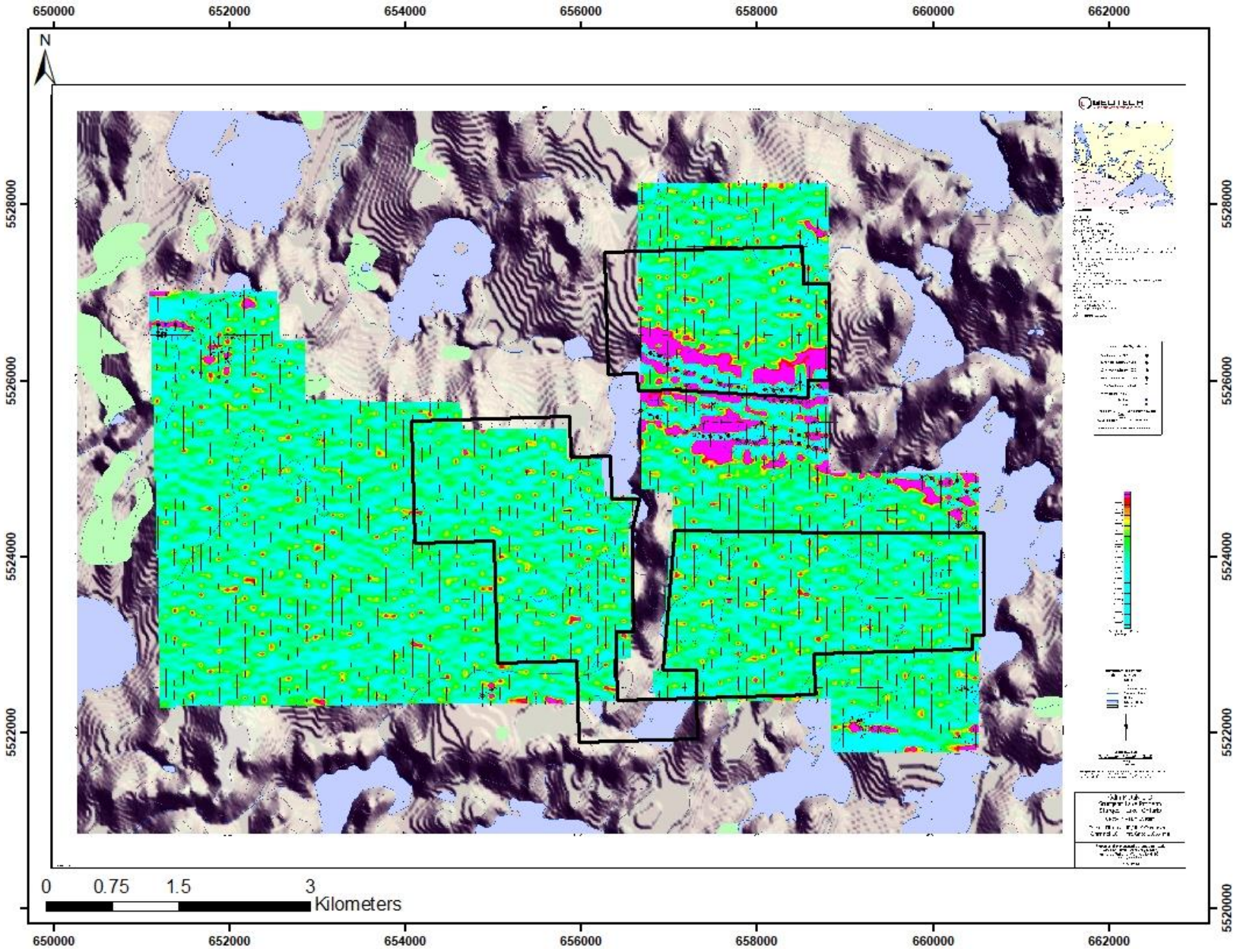

**Figure 10: Total Magnetic Intensity (TMI)**

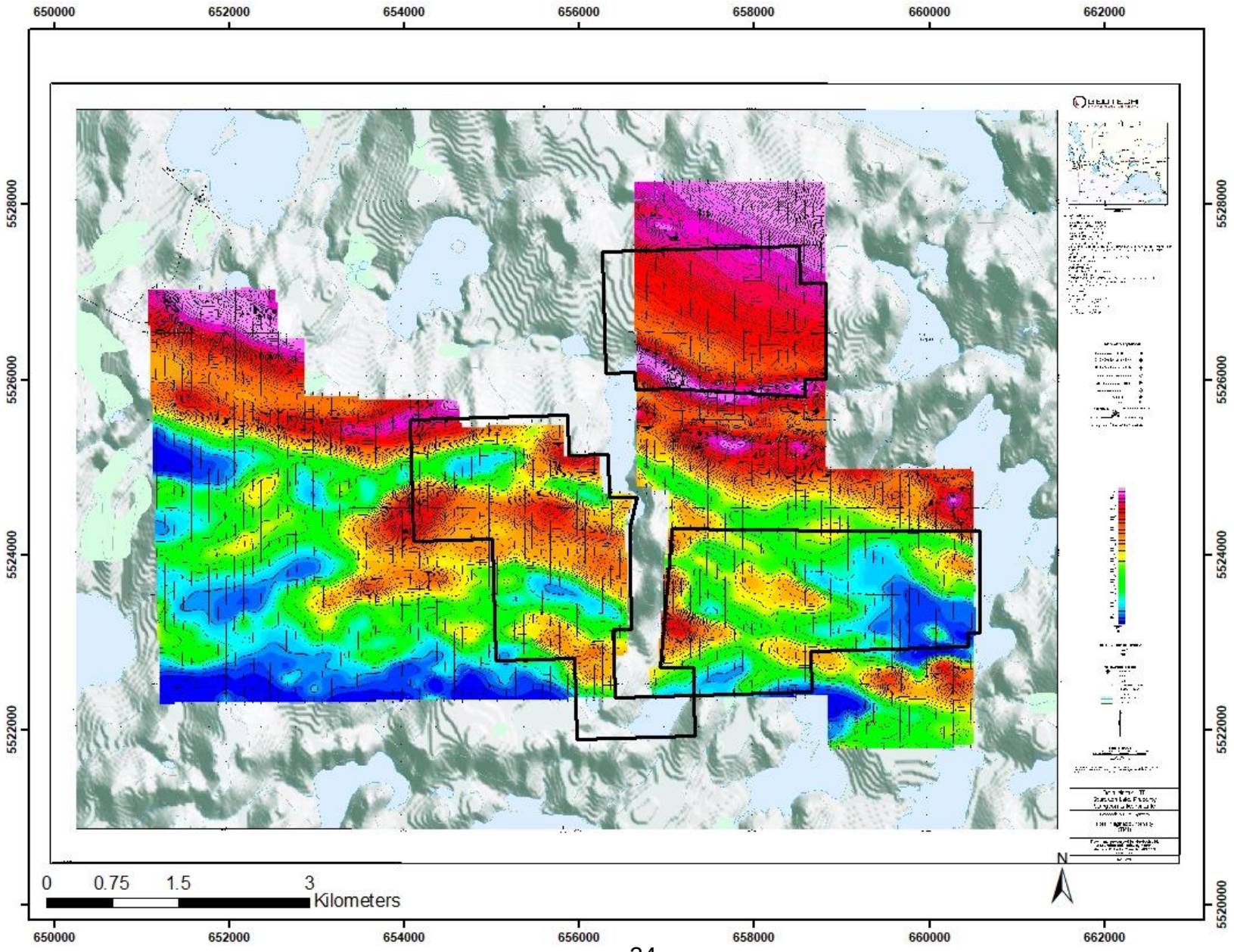

**Figure 11: Calculated Time Constant (Tau)**

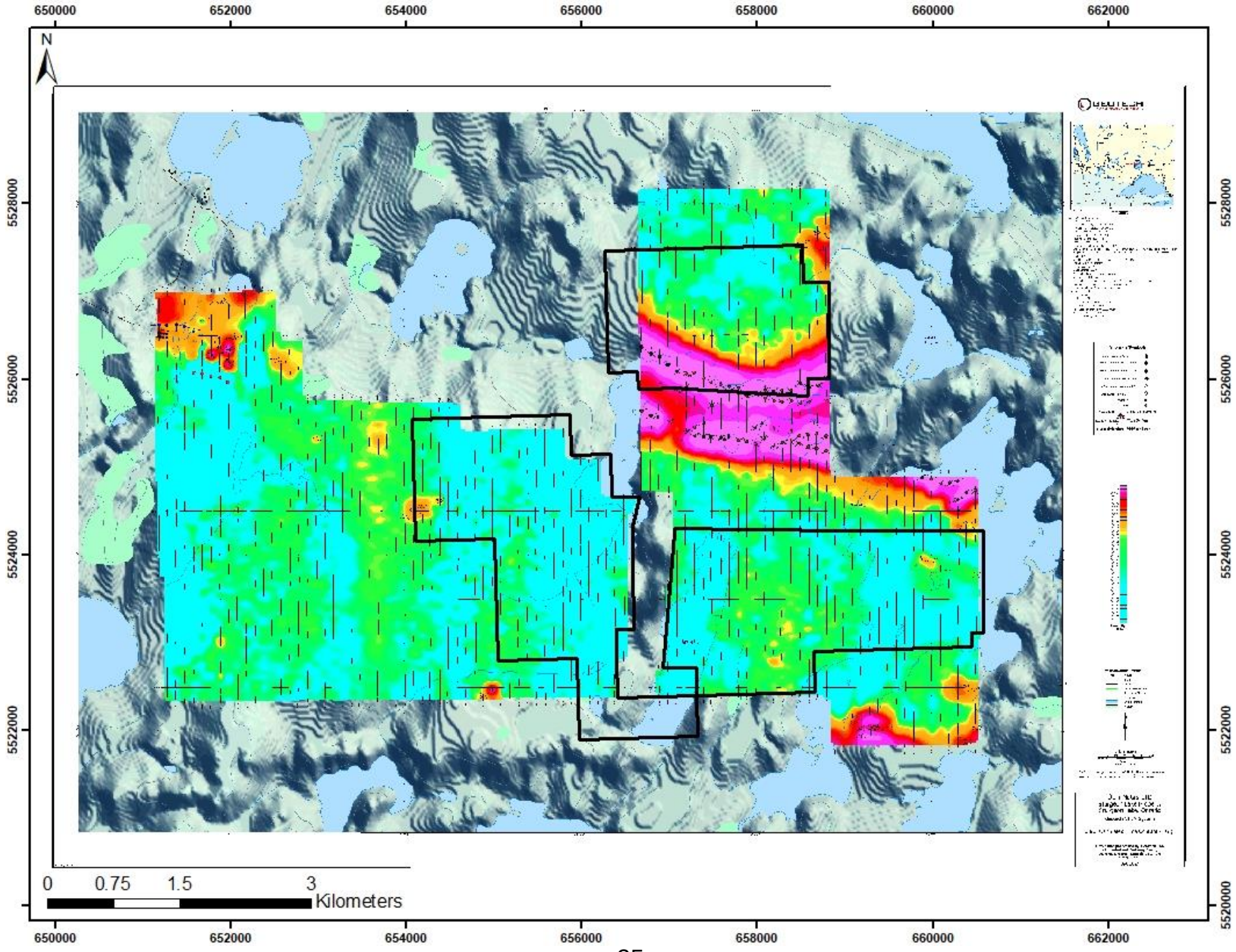

## 10.0 Interpretation and Conclusions

Geotech completed an EM anomaly picking of the VTEM data from the Sturgeon Lake property. A total of 123 single and double pick anomalies were picked in the VTEM block (Appendix II). While confirmation of these anomalies is necessary to assure no cultural influence, strong (high conductance) conductors in the EM anomalies could be potential exploration targets for VMS associated polymetallic mineralization.

**Table 3 Summary of EM time-constants and the associated conductance's of these anomalies.**

| Conductance, Siemens dB/dt Z component (min-max) | Conductance, Siemens B-field Z component (min-max) | TAU dB/dt, msec, min-max | TAU B-field, msec, min-max |
|---|---|---|---|
| 0.52- 89.71 | 0.00 - 191.26 | 0.03 - 4.82 | 0.00 - 10.28 |

**Figure 12: 3D view of VTEM Resistivity Depth Image (RDI) showing Apparent Resistivity Voxel (view looking northeast) Conductive trends within the Odin survey area**

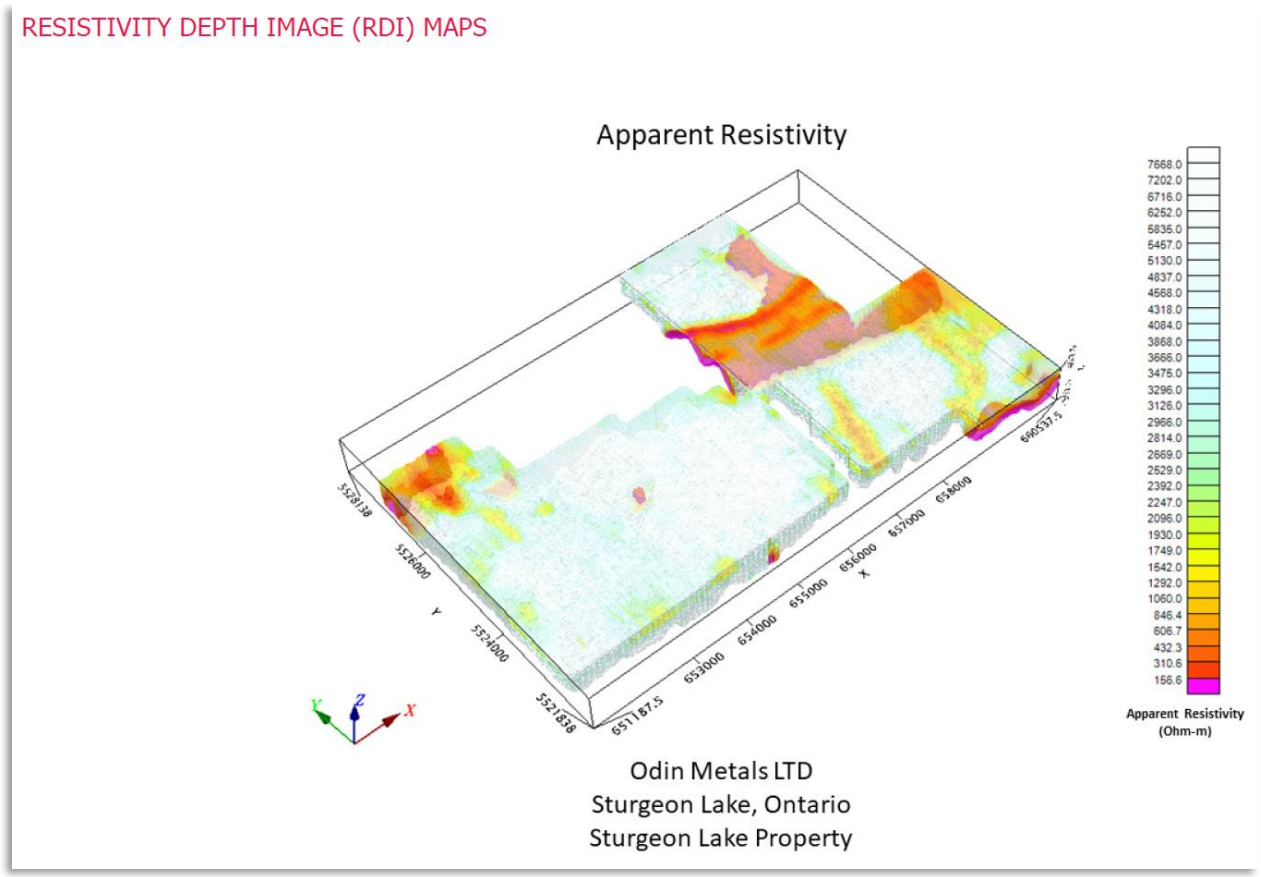


.

## 11.0 Recommendations

The airborne survey was successful in locating several anomalies across various areas of the Sturgeon Lake Property. Follow up work should be completed to further investigate the anomalies outlined in the survey.

Follow up work should involve confirmation of non-cultural EM anomalies, detailed outcrop mapping and sampling, and ground geophysical work ahead of drill testing and borehole EM of favourable targets. Geological modelling that incorporates the VTEM products is also recommended.

## 12.0 References

Amax Exploration Inc., 1972: Diamond Drilling Report #13, Area of Dunne Lake. Miscellaneous Drill Logs (52G15SE0007.PDF).

Barrie, C., 2006: Operations Report for Unitronix Mining and Exploration, High Resolution Horizontal Magnetic Gradient and XDS-VLF-EM Airborne Survey, Sturgeon Lake East Project. Report No. B-190. Ontario MNDM Assessment File 2.32811 (20002615.PDF).

Bulatovich, M., 2011: Soil Gas Hydrocarbon Geochemical Survey in the Bell Lake Area, Northwestern Ontario. Ontario MNDM Assessment File 2.49295 (20008730.PDF).

Davis, D. W. (2006) Zircon dating of polycyclic volcanism at Sturgeon Lake and Implications for Base Metal Mineralization

Galley, A.G., 1993. Semi-conformable alteration zones in volcanogenic massive sulphide districts, Journal of Geochemical Exploration, v. 48, p. 175-200.

Galley, A.G., Hannington, M.D., and Jonasson, I.R., 2007. Volcanogenic massive sulphide deposits. *In* Goodfellow, W.D., ed., Mineral Deposits of Canada: A Synthesis of Major Deposit-Types, District Metallogeny, the Evolution of Geological Provinces, and Exploration Methods, Geological Association of Canada, Mineral Deposits Division, Special Publication No. 5, p. 141-161.

Gingerich, J., 1992: Report on Geophysical Surveying and Diamond Drilling 1992, Group 51 – Simax Option; Noranda Exploration Company Ltd; Ontario MNDM Assessment File (52G15SW0002.PDF).

Franklin, J.M., Gibson, H.L., Jonasson, I.R., and Galley, A.G., 2005. Volcanogenic massive sulfide deposits. *In* Hedenquist, J.W., Thompson, J.F.H., Goldfarb, R.J., and Richards, J.P., eds., Economic Geology 100th Anniversary Volume, The Economic Geology Publishing Company, p. 523-560.

Franklin, J.M., Gibb, W., Poulsen, K.H., and Severin, P., 1977: Archean metallogeny and stratigraphy of the South Sturgeon Lake area; Institute of Lake Superior Geology, 23rd Annual Meeting; Mattabi field trip guide-book, 75 p.

Fugro Airborne Surveys, 2003: Logistics and Processing Report, Airborne Magnetic and MEGATEM Survey, Sturgeon Lake Survey Area, Thunder Bay, Ontario, Canada; Job No. 03-438. Ontario MNDM Assessment File 2.27992 (52G15NW2005.PDF).

Karrei, L., and Morrison, R. (2012). Due Diligence Review of Sturgeon Lake Projects in Northwestern Ontario, pp 80

Morton, R.L., Franklin, J.M., 1987: Two-fold classification of Archean volcanic-associated massive sulfide deposits; Economic Geology, Vol 82, p. 1057-1063.

Morton, R.L., Hudak, G., Franklin, J.M., 1999: Geology, south Sturgeon Lake area, Ontario; Geological Survey of Canada; Open File 3642, scale 1:15,000

Mumin, A.H., Scott, S.D., Somarin A.K, Oran, K.S., 2007: Structural Controls on Massive Sulfide Deposition and Hydrothermal Alteration in the South Sturgeon Lake Caldera, Northwestern Ontario; Exploration and Mining Geology, Vol 16, Nos 1-2, p. 83-107, 2007.

Mumin, A.H, Mumin, A. 2017: Geobotanical Alder Survey Assessment Report on the Sturgeon Lake Property, Thunder Bay Mining Division. (OAFD File 20000013589)

Newton, B., 2012: Mattabi Claim Group Assessment Report for Aur Lake Exploration Ltd.; Ontario MNDM Assessment File 2.53119 (20011004.PDF, 20011005.PDF, 20011006.PDF).

Ontario Geological Survey, 2003: Sturgeon Lake-Savant Lake Area, Ontario airborne magnetic and electromagnetic surveys, processed data and derivative products, Archean and Proterozoic “greenstone” belts; Geophysical Data Set 1033 – Revised; Ontario Geological Survey, Sudbury.

Ontario Geological Survey, 2011: 1:250,000 scale bedrock geology of Ontario; Ontario Geological Survey, Miscellaneous Release-Data 126 – Revision 1.

Severin, P. W. A. (1982) *Geology of the Sturgeon Lake copper-zinc-lead-silver-gold deposit*, in CIM Bulletin, October 1982, 75, No. 846, 107-123.

Smith, A., 1994: Report on 1993 Geological Mapping and Lithogeochemical Sampling, East Sturgeon Lake Property, West Precambrian District; Ontario MNDM Assessment File 2.15502 (52G15SW0005.PDF).

Smith, A. (2000) *Report on 1999-2000 Borehole Physical Property Surveying on Block 7 and Group 55 Properties*, Noranda Inc., MNDM&F Assessment File Research Imaging (AFRI), AFRI#52G15NW2003

Trowell, N.F., 1983: Geology of the Sturgeon Lake Area, Districts of Thunder Bay and Kenora; Ontario Geological Survey Report 221 (R221.PDF).

Trowell, N. F. and Johns, G. W. (1986) *Stratigraphic correlation of the western Wabigoon subprovince, northwestern Ontario*, in J. Wood and H. Wallace (eds.), Volcanology and Mineral Deposits, Ontario Geological Survey Miscellaneous Paper 129, 50-61.

## 13.0 Certificate of Qualifications

Brent Clark
941 Cobalt Crescent
Thunder Bay, Ontario
Canada, P7B 5Z4
Telephone: 807-622-3284, Fax: 807-622-4156

CERTIFICATE OF QUALIFIED PERSON

I, Brent Clark, do hereby certify that:

1. I graduated with the degree of Honours Bachelor of Science (Earth Sciences) from Carleton University, Ottawa, Ontario in 2014.

2. "Assessment Report" refers to the report titled "Assessment Report on the Sturgeon Lake Property"

3. I am a registered Geologist in Training (G.I.T) the Professional Geoscientists of Ontario (#10506).

4. I have worked as a Geologist for 5 years since my graduation from university.

5. I have had no other prior involvement with the mineral Property that forms the subject of this Assessment Report.

6. As of the date of this certificate, and to the best of my knowledge, information and belief, the Assessment Report contains all scientific and technical information that is required to be disclosed to make the Assessment Report not misleading.

Dated this 15th day of August 2019.

SIGNED

"Brent Clark"

_____
Brent Clark, G.I.T

# Appendix I

Sturgeon Lake Property Claims

The Sturgeon Lake Property consists of 90 claims totalling 1547 hectares. The claims are listed below with the “Legacy Claims” being the original staked claims, and the “Tenure ID” being the new cell claim under the new MLAS system.

| Legacy Claim Id | Township / Area | Tenure ID | Anniversary Date | Tenure Status | Work Required |
|---|---|---|---|---|---|
| 4281448 | BELL LAKE AREA | 114039 | 2019-05-01 | Active | 200 |
| 4281448 | BELL LAKE AREA | 114040 | 2019-05-01 | Active | 200 |
| 4281448 | BELL LAKE AREA | 114041 | 2019-05-01 | Active | 400 |
| 4281448 | BELL LAKE AREA | 114042 | 2019-05-01 | Active | 200 |
| 4281448 | BELL LAKE AREA | 130557 | 2019-05-01 | Active | 400 |
| 4281448 | BELL LAKE AREA | 160661 | 2019-05-01 | Active | 200 |
| 4281448 | BELL LAKE AREA | 160662 | 2019-05-01 | Active | 200 |
| 4281448 | BELL LAKE AREA | 165993 | 2019-05-01 | Active | 200 |
| 4281448 | BELL LAKE AREA | 194772 | 2019-05-01 | Active | 200 |
| 4281448 | BELL LAKE AREA | 225371 | 2019-05-01 | Active | 200 |
| 4281448 | BELL LAKE AREA | 250561 | 2019-05-01 | Active | 200 |
| 4281448 | BELL LAKE AREA | 250562 | 2019-05-01 | Active | 200 |
| 4281448 | BELL LAKE AREA | 250563 | 2019-05-01 | Active | 200 |
| 4281448 | BELL LAKE AREA | 268736 | 2019-05-01 | Active | 200 |
| 4281448 | BELL LAKE AREA | 332162 | 2019-05-01 | Active | 400 |
| 4281449 | BELL LAKE AREA | 114168 | 2019-05-01 | Active | 200 |
| 4281449 | BELL LAKE AREA | 114169 | 2019-05-01 | Active | 200 |
| 4281449 | BELL LAKE AREA | 147250 | 2019-05-01 | Active | 400 |
| 4281449 | BELL LAKE AREA | 160797 | 2019-05-01 | Active | 400 |
| 4281449 | BELL LAKE AREA | 195409 | 2019-05-01 | Active | 200 |
| 4281449 | BELL LAKE AREA | 195410 | 2019-05-01 | Active | 400 |
| 4281449 | BELL LAKE AREA | 213945 | 2019-05-01 | Active | 400 |
| 4281449 | BELL LAKE AREA | 261413 | 2019-05-01 | Active | 400 |
| 4281449 | BELL LAKE AREA | 269360 | 2019-05-01 | Active | 200 |
| 4281449 | BELL LAKE AREA | 269361 | 2019-05-01 | Active | 200 |
| 4281449 | BELL LAKE AREA | 309291 | 2019-05-01 | Active | 400 |
| 4281449 | BELL LAKE AREA | 332295 | 2019-05-01 | Active | 200 |
| 4281450 | BELL LAKE AREA | 113806 | 2019-05-01 | Active | 400 |
| 4281450 | BELL LAKE AREA | 149229 | 2019-05-01 | Active | 200 |
| 4281450 | BELL LAKE AREA | 149230 | 2019-05-01 | Active | 200 |
| 4281450 | BELL LAKE AREA | 151523 | 2019-05-01 | Active | 200 |
| 4281450 | BELL LAKE AREA | 151524 | 2019-05-01 | Active | 200 |
| 4281450 | BELL LAKE AREA | 197346 | 2019-05-01 | Active | 200 |
| 4281450 | BELL LAKE AREA | 216964 | 2019-05-01 | Active | 400 |
| 4281450 | BELL LAKE AREA | 234122 | 2019-05-01 | Active | 400 |
| 4281450 | BELL LAKE AREA | 234123 | 2019-05-01 | Active | 200 |

| Legacy Claim Id | Township / Area | Tenure ID | Anniversary Date | Tenure Status | Work Required |
|---|---|---|---|---|---|
| 4281450 | BELL LAKE AREA | 234124 | 2019-05-01 | Active | 400 |
| 4281450 | BELL LAKE AREA | 234125 | 2019-05-01 | Active | 400 |
| 4281450 | BELL LAKE AREA | 234126 | 2019-05-01 | Active | 400 |
| 4281450 | BELL LAKE AREA | 263384 | 2019-05-01 | Active | 400 |
| 4281450 | BELL LAKE AREA | 263385 | 2019-05-01 | Active | 200 |
| 4281450 | BELL LAKE AREA | 271371 | 2019-05-01 | Active | 400 |
| 4281450 | BELL LAKE AREA | 300686 | 2019-05-01 | Active | 400 |
| 4281450 | BELL LAKE AREA | 317951 | 2019-05-01 | Active | 200 |
| 4281450 | BELL LAKE AREA | 317952 | 2019-05-01 | Active | 400 |
| 4281450 | BELL LAKE AREA | 317953 | 2019-05-01 | Active | 400 |
| 4281450 | BELL LAKE AREA | 331333 | 2019-05-01 | Active | 200 |
| 4281450 | BELL LAKE AREA | 332927 | 2019-05-01 | Active | 400 |
| 4281450 | BELL LAKE AREA | 332928 | 2019-05-01 | Active | 200 |
| 4281451 | BELL LAKE AREA | 115176 | 2019-05-01 | Active | 400 |
| 4281451 | BELL LAKE AREA | 149972 | 2019-05-01 | Active | 200 |
| 4281451 | BELL LAKE AREA | 152755 | 2019-05-01 | Active | 400 |
| 4281451 | BELL LAKE AREA | 168824 | 2019-05-01 | Active | 400 |
| 4281451 | BELL LAKE AREA | 198085 | 2019-05-01 | Active | 200 |
| 4281451 | BELL LAKE AREA | 218202 | 2019-05-01 | Active | 200 |
| 4281451 | BELL LAKE AREA | 234864 | 2019-05-01 | Active | 400 |
| 4281451 | BELL LAKE AREA | 284231 | 2019-05-01 | Active | 200 |
| 4281451 | BELL LAKE AREA | 284232 | 2019-05-01 | Active | 400 |
| 4281451 | BELL LAKE AREA | 301942 | 2019-05-01 | Active | 200 |
| 4281451 | BELL LAKE AREA | 301956 | 2019-05-01 | Active | 400 |
| 4281451 | BELL LAKE AREA | 318671 | 2019-05-01 | Active | 200 |
| 4281451 | BELL LAKE AREA | 333311 | 2019-05-01 | Active | 400 |
| 4281452 | BELL LAKE AREA | 132608 | 2019-05-01 | Active | 200 |
| 4281452 | SIX MILE LAKE AREA | 300667 | 2019-05-01 | Active | 400 |
| 4281452 | SIX MILE LAKE AREA | 283456 | 2019-05-01 | Active | 200 |
| 4281452 | SIX MILE LAKE AREA | 263357 | 2019-05-01 | Active | 400 |
| 4281452 | SIX MILE LAKE AREA | 204832 | 2019-05-01 | Active | 400 |
| 4281452 | SIX MILE LAKE AREA | 204831 | 2019-05-01 | Active | 400 |
| 4281452 | SIX MILE LAKE AREA | 132607 | 2019-05-01 | Active | 200 |
| 4281452 | BELL LAKE AREA,SIX MILE LAKE AREA | 332907 | 2019-05-01 | Active | 400 |
| 4281452 | BELL LAKE AREA, SIX MILE LAKE AREA | 331298 | 2019-05-01 | Active | 400 |
| 4281452 | BELL LAKE AREA, SIX MILE LAKE AREA | 283457 | 2019-05-01 | Active | 200 |

| Legacy Claim Id | Township / Area | Tenure ID | Anniversary Date | Tenure Status | Work Required |
|---|---|---|---|---|---|
| 4281452 | BELL LAKE AREA, SIX MILE LAKE AREA | 168064 | 2019-05-01 | Active | 200 |
| 4281452 | BELL LAKE AREA, SIX MILE LAKE AREA | 168063 | 2019-05-01 | Active | 400 |
| 4281452 | BELL LAKE AREA, SIX MILE LAKE AREA | 151492 | 2019-05-01 | Active | 400 |
| 4281452 | BELL LAKE AREA | 148706 | 2019-05-01 | Active | 200 |
| 4281452 | BELL LAKE AREA | 148707 | 2019-05-01 | Active | 200 |
| 4281452 | BELL LAKE AREA | 151493 | 2019-05-01 | Active | 200 |
| 4281452 | BELL LAKE AREA | 168065 | 2019-05-01 | Active | 200 |
| 4281452 | BELL LAKE AREA | 196816 | 2019-05-01 | Active | 400 |
| 4281452 | BELL LAKE AREA | 196817 | 2019-05-01 | Active | 200 |
| 4281452 | BELL LAKE AREA | 283458 | 2019-05-01 | Active | 400 |
| 4281452 | BELL LAKE AREA | 317924 | 2019-05-01 | Active | 400 |
| 4281452 | BELL LAKE AREA | 331299 | 2019-05-01 | Active | 200 |
| 4281452 | BELL LAKE AREA | 331300 | 2019-05-01 | Active | 400 |
| 4281452 | BELL LAKE AREA | 332908 | 2019-05-01 | Active | 200 |
| | BELL LAKE AREA | 547803 | 2021-04-08 | Active | 400 |
| | BELL LAKE AREA | 547804 | 2021-04-08 | Active | 400 |
| | BELL LAKE AREA | 547805 | 2021-04-08 | Active | 400 |
| | BELL LAKE AREA | 547806 | 2021-04-08 | Active | 400 |

# Appendix II

EM Anomaly Summary

| Line | x | y | z | radarb | Culture | AIIP | Grade | Anom_ID | Anom_Labels | AnConBF | AnConSF | AnTAUBF | AnTAUSF |
|---|---|---|---|---|---|---|---|---|---|---|---|---|---|
| 2550 | 651214.6 | 5526619 | 562.8 | 60.1 | 7 | * | * | | | * | * | * | * |
| 2560 | 651295.6 | 5526613.4 | 553 | 51.3 | 7 | * | * | | | * | * | * | * |
| 2570 | 651411.4 | 5526618.1 | 546.4 | 50.5 | 7 | * | * | | | * | * | * | * |
| 2580 | 651495.4 | 5526602.3 | 550.3 | 56.6 | 7 | * | * | | | * | * | * | * |
| 2590 | 651605.1 | 5526077.9 | 550.2 | 49.5 | * | 5 | * | | | * | * | * | * |
| 2590 | 651601.8 | 5526545.6 | 540.9 | 41.2 | 7 | * | * | | | * | * | * | * |
| 2600 | 651710.2 | 5526669.4 | 540.8 | 44.8 | * | * | 1 | N | A | 0.7 | 1.16 | 0.04 | 0.06 |
| 2600 | 651701.3 | 5526068.8 | 544.8 | 42 | * | 5 | * | | | * | * | * | * |
| 2610 | 651800.6 | 5526036.6 | 544.8 | 39.3 | * | 5 | * | | | * | * | * | * |
| 2610 | 651804.3 | 5526277.9 | 551 | 47.2 | * | * | 4 | K | A | 104.68 | 33.37 | 5.63 | 1.79 |
| 2610 | 651808.3 | 5526863.2 | 551.3 | 56.8 | * | * | 1 | N | B | 2.74 | 2.4 | 0.15 | 0.13 |
| 2620 | 651907.5 | 5526886.5 | 559 | 62.6 | * | * | 1 | N | A | 2.29 | 0.77 | 0.12 | 0.04 |
| 2620 | 651896.5 | 5526365.8 | 556.7 | 51.2 | * | * | 2 | N | B | 46.71 | 6.93 | 2.51 | 0.37 |
| 2620 | 651900.8 | 5526018.3 | 548.2 | 42.1 | * | 5 | * | | | * | * | * | * |
| 2630 | 651996.3 | 5525967.9 | 551.6 | 46.2 | * | 5 | * | | | * | * | * | * |
| 2630 | 652000.3 | 5526187.8 | 549.7 | 40.6 | * | * | 3 | K | A | 97.53 | 16.43 | 5.24 | 0.88 |
| 2630 | 652006.2 | 5526337.5 | 552.3 | 42.9 | * | * | 4 | K | B | 124.39 | 30.29 | 6.69 | 1.63 |
| 2630 | 652007.4 | 5526489.9 | 560.4 | 51 | * | * | 1 | K | C | 106.51 | 3.48 | 5.73 | 0.19 |
| 2640 | 652105.5 | 5526959.2 | 532.1 | 44 | * | * | 1 | K | A | 9.06 | 3.08 | 0.49 | 0.17 |
| 2640 | 652106.4 | 5526464.8 | 564.2 | 44.4 | * | * | 1 | K | B | 53.93 | 1.2 | 2.9 | 0.06 |
| 2650 | 652194.3 | 5526958.3 | 539.1 | 51.6 | * | * | 1 | K | A | 6.46 | 3.97 | 0.35 | 0.21 |
| 2660 | 652303.2 | 5526956.8 | 544.8 | 55.1 | * | * | 1 | K | A | 6 | 3.24 | 0.32 | 0.17 |
| 2680 | 652507.5 | 5526214.3 | 568.7 | 62.6 | * | * | 1 | K | A | 0 | 0.67 | 0 | 0.04 |
| 2690 | 652601 | 5526222.4 | 567 | 58.7 | * | * | 1 | K | A | 1.23 | 1.02 | 0.07 | 0.05 |
| 2730 | 652993.7 | 5525335.2 | 560.8 | 54.1 | * | * | 1 | K | A | 0 | 0.68 | 0 | 0.04 |
| 2830 | 654009.8 | 5524437.5 | 608.6 | 63.1 | * | * | 1 | K | A | 0 | 0.54 | 0 | 0.03 |
| 2840 | 654095.5 | 5524512.4 | 604.9 | 65.8 | * | * | 1 | K | A | 2.99 | 0.87 | 0.16 | 0.05 |

| Line | x | y | z | radarb | Culture | AIIP | Grade | Anom_ID | Anom_Labels | AnConBF | AnConSF | AnTAUBF | AnTAUSF |
|---|---|---|---|---|---|---|---|---|---|---|---|---|---|
| 2850 | 654206.9 | 5524550.5 | 590.5 | 56.7 | * | * | 1 | K | A | 26.63 | 1.73 | 1.43 | 0.09 |
| 2870 | 654407.1 | 5524618.3 | 590.6 | 56.4 | * | * | 1 | K | A | 0 | 0.69 | 0 | 0.04 |
| 2920 | 654903.2 | 5522402.6 | 562.9 | 51.2 | * | * | 1 | K | A | 15.15 | 0.63 | 0.81 | 0.03 |
| 2930 | 654999.4 | 5522465.9 | 552.9 | 39 | * | * | 4 | K | A | 191.26 | 30.85 | 10.28 | 1.66 |
| 3100 | 656703.3 | 5525637.7 | 551.3 | 51.6 | * | * | 6 | N | A | 104.32 | 52.54 | 5.61 | 2.82 |
| 3100 | 656701.6 | 5526370.1 | 556 | 53.6 | * | * | 5 | K | B | 65.31 | 48.89 | 3.51 | 2.63 |
| 3110 | 656810.7 | 5526291.6 | 557.9 | 56.1 | * | * | 6 | K | A | 74.46 | 54.34 | 4 | 2.92 |
| 3110 | 656810.3 | 5525587.6 | 563.6 | 54.5 | * | * | 6 | K | B | 119.3 | 61.5 | 6.41 | 3.31 |
| 3120 | 656892.4 | 5525563.1 | 554.1 | 45.1 | * | * | 6 | K | A | 147.22 | 57.53 | 7.91 | 3.09 |
| 3120 | 656911.4 | 5526257.9 | 548.1 | 43.9 | * | * | 6 | K | B | 83.05 | 62.97 | 4.46 | 3.39 |
| 3130 | 657006.2 | 5526167.2 | 545.4 | 45.2 | * | * | 6 | K | A | 75.37 | 54.3 | 4.05 | 2.92 |
| 3130 | 657006.2 | 5525513.5 | 568.2 | 49.4 | * | * | 3 | K | B | 124.82 | 16.5 | 6.71 | 0.89 |
| 3140 | 657105.4 | 5525332.2 | 566.5 | 55.4 | * | * | 2 | K | A | 41.43 | 5.72 | 2.23 | 0.31 |
| 3140 | 657101.2 | 5525878.9 | 539.7 | 40.8 | * | * | 4 | N | B | 131.59 | 26.48 | 7.07 | 1.42 |
| 3140 | 657106.2 | 5526089.4 | 539.6 | 37.2 | * | * | 6 | K | C | 97.05 | 51.49 | 5.22 | 2.77 |
| 3150 | 657212.8 | 5526066.3 | 534.3 | 32.6 | * | * | 5 | N | A | 77.13 | 44.39 | 4.15 | 2.39 |
| 3150 | 657214.4 | 5525925.2 | 533.3 | 31.7 | * | * | 5 | N | B | 73.63 | 43.85 | 3.96 | 2.36 |
| 3150 | 657213.5 | 5525401.6 | 562.5 | 49.7 | * | * | 4 | N | C | 65.73 | 20.82 | 3.53 | 1.12 |
| 3160 | 657312 | 5525359.6 | 568.1 | 60.2 | * | * | 5 | K | A | 94.48 | 42.83 | 5.08 | 2.3 |
| 3160 | 657311.2 | 5525454.1 | 569.1 | 59.9 | * | * | 5 | N | B | 94.76 | 40.33 | 5.09 | 2.17 |
| 3160 | 657303.8 | 5526075.7 | 539.6 | 38.8 | * | * | 5 | N | C | 83.39 | 40.49 | 4.48 | 2.18 |
| 3170 | 657413.4 | 5526012.5 | 538.3 | 36 | * | * | 5 | N | A | 103.01 | 42.83 | 5.54 | 2.3 |
| 3170 | 657411 | 5525348.4 | 564.9 | 59.3 | * | * | 6 | K | B | 111.11 | 76.4 | 5.97 | 4.11 |
| 3180 | 657492.2 | 5525346.6 | 563.2 | 57.6 | * | * | 6 | K | A | 135.26 | 82.6 | 7.27 | 4.44 |
| 3180 | 657505.1 | 5525701.9 | 545.7 | 46.4 | * | * | 4 | N | B | 105.18 | 34.31 | 5.65 | 1.84 |
| 3180 | 657495.9 | 5525965.8 | 536.5 | 36 | * | * | 5 | N | C | 100.91 | 49.69 | 5.43 | 2.67 |
| 3190 | 657605.2 | 5525943.3 | 549.7 | 48.9 | * | * | 6 | N | A | 96.66 | 59.82 | 5.2 | 3.22 |
| 3190 | 657607 | 5525340.3 | 563 | 58.1 | * | * | 6 | K | B | 131.78 | 83.38 | 7.08 | 4.48 |
| 3200 | 657695.1 | 5525354.9 | 558.5 | 54.5 | * | * | 6 | K | A | 120.03 | 72.8 | 6.45 | 3.91 |
| 3200 | 657704.7 | 5525918.2 | 553.6 | 50.5 | * | * | 6 | N | B | 94.17 | 53.31 | 5.06 | 2.87 |
| 3210 | 657806.8 | 5525904.2 | 540.8 | 40.3 | * | * | 6 | N | A | 103.79 | 66.85 | 5.58 | 3.59 |
| 3210 | 657804.9 | 5525306.9 | 558.2 | 55.1 | * | * | 6 | N | B | 99.89 | 69.28 | 5.37 | 3.72 |

| Line | x | y | z | radarb | Culture | AIIP | Grade | Anom_ID | Anom_Labels | AnConBF | AnConSF | AnTAUBF | AnTAUSF |
|---|---|---|---|---|---|---|---|---|---|---|---|---|---|
| 3220 | 657902.7 | 5525291.6 | 552.9 | 52.8 | * | * | 6 | N | A | 85.11 | 57.95 | 4.58 | 3.12 |
| 3220 | 657902.1 | 5525811.1 | 542.9 | 39.8 | * | * | 6 | N | B | 101.32 | 57.54 | 5.45 | 3.09 |
| 3230 | 658000.4 | 5525828.9 | 542.8 | 42.1 | * | * | 6 | K | A | 114.82 | 65.47 | 6.17 | 3.52 |
| 3230 | 657998.3 | 5525451 | 551.6 | 46.9 | * | * | 5 | K | B | 102.98 | 38.6 | 5.54 | 2.08 |
| 3230 | 658004 | 5525265.6 | 566.7 | 59.6 | * | * | 5 | N | C | 104.9 | 37.28 | 5.64 | 2 |
| 3240 | 658096.6 | 5525331.8 | 561.5 | 55.4 | * | * | 5 | N | A | 126.07 | 40.09 | 6.78 | 2.16 |
| 3240 | 658109.1 | 5525786 | 549.9 | 47.1 | * | * | 6 | N | B | 98.76 | 59.01 | 5.31 | 3.17 |
| 3240 | 658110.2 | 5525877.3 | 555 | 51.1 | * | * | 6 | N | C | 123.4 | 76.75 | 6.63 | 4.13 |
| 3250 | 658208.8 | 5525864.4 | 551.7 | 51.6 | * | * | 6 | N | A | 139.66 | 80.01 | 7.51 | 4.3 |
| 3250 | 658211.6 | 5525755.8 | 551.2 | 48.6 | * | * | 6 | N | B | 124.11 | 69.95 | 6.67 | 3.76 |
| 3250 | 658206.5 | 5525442.4 | 573.1 | 57.9 | * | * | 4 | N | C | 132.29 | 33.51 | 7.11 | 1.8 |
| 3250 | 658205.1 | 5525250.1 | 567.9 | 61.8 | * | * | 5 | K | D | 96.7 | 35.65 | 5.2 | 1.92 |
| 3260 | 658306 | 5525283.7 | 562.3 | 55 | * | * | 6 | N | A | 142.09 | 50.72 | 7.64 | 2.73 |
| 3260 | 658298.6 | 5525744.8 | 543.4 | 41.5 | * | * | 6 | N | B | 108.93 | 73.18 | 5.86 | 3.93 |
| 3260 | 658300.4 | 5525868.4 | 555.6 | 51.1 | * | * | 6 | N | C | 109.74 | 72.95 | 5.9 | 3.92 |
| 3270 | 658407.2 | 5525868.7 | 548.7 | 49 | * | * | 6 | N | A | 121.88 | 80.41 | 6.55 | 4.32 |
| 3270 | 658408.9 | 5525756.2 | 544.7 | 43.7 | * | * | 6 | N | B | 116.25 | 68.72 | 6.25 | 3.69 |
| 3270 | 658407.6 | 5525408.1 | 556 | 51.3 | * | * | 4 | N | C | 132.31 | 31.22 | 7.11 | 1.68 |
| 3270 | 658400.5 | 5525287.9 | 554.9 | 51.8 | * | * | 4 | N | D | 132.31 | 31.22 | 7.11 | 1.68 |
| 3280 | 658501.3 | 5525272 | 545.9 | 43.9 | * | * | 6 | N | A | 116.4 | 57.25 | 6.26 | 3.08 |
| 3280 | 658500.3 | 5525356.1 | 543 | 41.2 | * | * | 6 | N | B | 116.4 | 57.25 | 6.26 | 3.08 |
| 3280 | 658511.8 | 5525734.8 | 559.5 | 54.2 | * | * | 5 | N | C | 125.21 | 48.91 | 6.73 | 2.63 |
| 3280 | 658508.4 | 5525959.3 | 565.8 | 61.5 | * | * | 6 | K | D | 117.17 | 65.72 | 6.3 | 3.53 |
| 3280 | 658509.4 | 5527518.5 | 559.9 | 49.6 | * | * | 1 | K | E | 4.3 | 0.63 | 0.23 | 0.03 |
| 3290 | 658605.2 | 5527555.8 | 559.6 | 48.2 | * | * | 1 | K | A | 31.14 | 1.56 | 1.67 | 0.08 |
| 3290 | 658611.1 | 5525907.4 | 561.4 | 59.2 | * | * | 5 | K | B | 92.79 | 46.82 | 4.99 | 2.52 |
| 3290 | 658607.9 | 5525744.1 | 559.5 | 55.5 | * | * | 4 | N | C | 109.52 | 34.7 | 5.89 | 1.87 |
| 3290 | 658599.5 | 5525367.5 | 548.4 | 46.2 | * | * | 6 | N | D | 116.82 | 63.89 | 6.28 | 3.43 |
| 3290 | 658601.9 | 5525234.4 | 552.9 | 49.3 | * | * | 6 | N | E | 133.06 | 89.71 | 7.15 | 4.82 |
| 3300 | 658703.7 | 5527667.1 | 558 | 52.8 | * | * | 1 | N | A | 65.83 | 4.26 | 3.54 | 0.23 |
| 3300 | 658714.8 | 5525931.2 | 554.2 | 53.3 | * | * | 5 | N | B | 85.99 | 38.69 | 4.62 | 2.08 |
| 3300 | 658697.6 | 5525379.8 | 554.8 | 51 | * | * | 5 | N | C | 120.2 | 46.47 | 6.46 | 2.5 |
| 3300 | 658698.3 | 5525217.6 | 566 | 59.7 | * | * | 6 | N | D | 109.86 | 62.02 | 5.91 | 3.33 |
| 3310 | 658805.1 | 5525183.8 | 555.5 | 49.2 | * | * | 6 | N | A | 103.93 | 68.32 | 5.59 | 3.67 |

| Line | x | y | z | radarb | Culture | AIIP | Grade | Anom_ID | Anom_Labels | AnConBF | AnConSF | AnTAUBF | AnTAUSF |
|---|---|---|---|---|---|---|---|---|---|---|---|---|---|
| 3310 | 658805.1 | 5525352.9 | 565.6 | 58.7 | * | * | 6 | N | B | 103.3 | 54.09 | 5.55 | 2.91 |
| 3310 | 658807 | 5525757.5 | 557.2 | 53.4 | * | * | 3 | N | C | 60.1 | 18.63 | 3.23 | 1 |
| 3310 | 658808 | 5526025.4 | 563.3 | 60.4 | * | * | 4 | K | D | 64.47 | 34.35 | 3.47 | 1.85 |
| 3310 | 658798.5 | 5527634.7 | 543.7 | 37.7 | * | * | 2 | N | E | 68.93 | 6.98 | 3.71 | 0.38 |
| 3340 | 659110.5 | 5522098.7 | 555.2 | 55.8 | * | * | 1 | N | A | 11.65 | 3.96 | 0.63 | 0.21 |
| 3350 | 659202.7 | 5521942.2 | 557.7 | 57.1 | * | * | 4 | K | A | 71.2 | 30.71 | 3.83 | 1.65 |
| 3350 | 659204.5 | 5522036.7 | 555 | 56.7 | * | * | 3 | N | B | 55.08 | 14.45 | 2.96 | 0.78 |
| 3350 | 659206.6 | 5522115.6 | 549.2 | 50.4 | * | * | 3 | N | C | 55.08 | 14.45 | 2.96 | 0.78 |
| 3360 | 659315.8 | 5522034.9 | 559.6 | 56.1 | * | * | 4 | N | A | 71.46 | 28.84 | 3.84 | 1.55 |
| 3370 | 659397 | 5522035.6 | 560.4 | 61.8 | * | * | 4 | N | A | 80.57 | 32.47 | 4.33 | 1.75 |
| 3380 | 659508.8 | 5522027.7 | 557.6 | 60.6 | * | * | 2 | N | A | 63 | 8.98 | 3.39 | 0.48 |
| 3420 | 659896.9 | 5524885.3 | 552.7 | 61.4 | * | * | 6 | K | A | 156.39 | 63.79 | 8.41 | 3.43 |
| 3420 | 659913.3 | 5523954.1 | 532.4 | 38.9 | * | * | 1 | K | B | 2.47 | 0.67 | 0.13 | 0.04 |
| 3430 | 660004.4 | 5523948.4 | 534.6 | 41.1 | * | * | 1 | K | A | 0.67 | 0.64 | 0.04 | 0.03 |
| 3430 | 659999 | 5524864.7 | 537.5 | 41.6 | * | * | 6 | N | B | 153.62 | 69.6 | 8.26 | 3.74 |
| 3440 | 660109.3 | 5524821 | 542.9 | 49.7 | * | * | 5 | N | A | 125.58 | 49.24 | 6.75 | 2.65 |
| 3450 | 660206 | 5524589.3 | 526 | 32.1 | * | * | 3 | K | A | 60.89 | 13.88 | 3.27 | 0.75 |
| 3450 | 660208.5 | 5524824.1 | 527.1 | 33.5 | * | * | 6 | N | B | 137.34 | 52.04 | 7.38 | 2.8 |
| 3460 | 660294.7 | 5524844.1 | 531.2 | 38.7 | * | * | 5 | K | A | 135.1 | 42.65 | 7.26 | 2.29 |
| 3460 | 660300 | 5524633.7 | 526.1 | 33.2 | * | * | 5 | K | B | 75.43 | 42.01 | 4.06 | 2.26 |
| 3460 | 660308.8 | 5524326.5 | 526.3 | 32.7 | * | * | 1 | K | C | 2.15 | 2.53 | 0.12 | 0.14 |
| 3460 | 660304.6 | 5522476.6 | 553.3 | 58.5 | * | * | 1 | K | D | 1.48 | 1.85 | 0.08 | 0.1 |
| 3460 | 660303.6 | 5521942.2 | 560.2 | 57.1 | * | * | 1 | N | E | 21.14 | 3.08 | 1.14 | 0.17 |
| 3470 | 660403.6 | 5521880.2 | 554.5 | 51.3 | * | * | 1 | K | A | 33.85 | 3.82 | 1.82 | 0.21 |
| 3470 | 660400.4 | 5522482.3 | 552.3 | 57.9 | * | * | 1 | K | B | 1.61 | 1.17 | 0.09 | 0.06 |
| 3470 | 660396.5 | 5524355.4 | 529.5 | 35.5 | * | * | 1 | N | C | 1.33 | 0.82 | 0.07 | 0.04 |
| 3470 | 660401.6 | 5524716.3 | 526.5 | 32.6 | * | * | 6 | K | D | 112.81 | 61.86 | 6.07 | 3.33 |
| 3480 | 660501.9 | 5524735.8 | 533.6 | 40.3 | * | * | 5 | N | A | 146.56 | 37.49 | 7.88 | 2.02 |
| 3480 | 660503.6 | 5524290.4 | 529.1 | 35.2 | * | * | 1 | N | B | 0.96 | 0.7 | 0.05 | 0.04 |
| 3480 | 660510.1 | 5523774.3 | 528.2 | 34.8 | * | * | 1 | K | C | 0.55 | 0.52 | 0.03 | 0.03 |
| 3480 | 660499 | 5522471.3 | 548.3 | 55.2 | * | * | 1 | K | D | 3.35 | 1.14 | 0.18 | 0.06 |
| 3480 | 660504 | 5522033.9 | 557.1 | 58.1 | * | * | 2 | N | E | 60.83 | 9.51 | 3.27 | 0.51 |
| 5030 | 658775.4 | 5527494.4 | 548.6 | 46.5 | * | * | 2 | K | A | 86.31 | 8.87 | 4.64 | 0.48 |
| 5040 | 652025.3 | 5526499 | 570.8 | 59.9 | * | * | 1 | K | A | 82.04 | 2.67 | 4.41 | 0.14 |

| Line | x | y | z | radarb | Culture | AIIP | Grade | Anom_ID | Anom_Labels | AnConBF | AnConSF | AnTAUBF | AnTAUSF |
|---|---|---|---|---|---|---|---|---|---|---|---|---|---|
| 5050 | 658659.1 | 5525502.5 | 547.9 | 49.9 | * | * | 4 | K | A | 122.51 | 29.49 | 6.59 | 1.59 |
| 5050 | 658071.3 | 5525498.7 | 560.3 | 58.4 | * | * | 5 | K | B | 107.04 | 41.58 | 5.75 | 2.24 |
| 5050 | 657417.6 | 5525500.5 | 569.7 | 59.4 | * | * | 4 | K | C | 144.67 | 33.11 | 7.78 | 1.78 |
| 5060 | 660312.4 | 5524497.2 | 554.9 | 67 | * | * | 3 | K | A | 43.68 | 10.11 | 2.35 | 0.54 |
| 5060 | 654138.8 | 5524499.1 | 603.7 | 67.9 | * | * | 1 | K | B | 14.74 | 1.32 | 0.79 | 0.07 |
| 5070 | 657378.5 | 5523502.3 | 556.3 | 55.1 | * | 5 | * | | | * | * | * | * |
| 5080 | 660380 | 5522499.3 | 558.1 | 61.5 | * | * | 1 | N | A | 3.04 | 1.85 | 0.16 | 0.1 |
| 5080 | 659432.7 | 5522495.3 | 530.9 | 38 | * | 5 | * | | | * | * | * | * |
| 5080 | 657057.8 | 5522499.7 | 557.4 | 53.3 | * | 5 | * | | | * | * | * | * |
| 5080 | 656175.3 | 5522502 | 565.2 | 60.5 | * | 5 | * | | | * | * | * | * |

# Appendix III

Geotech VTEM Report

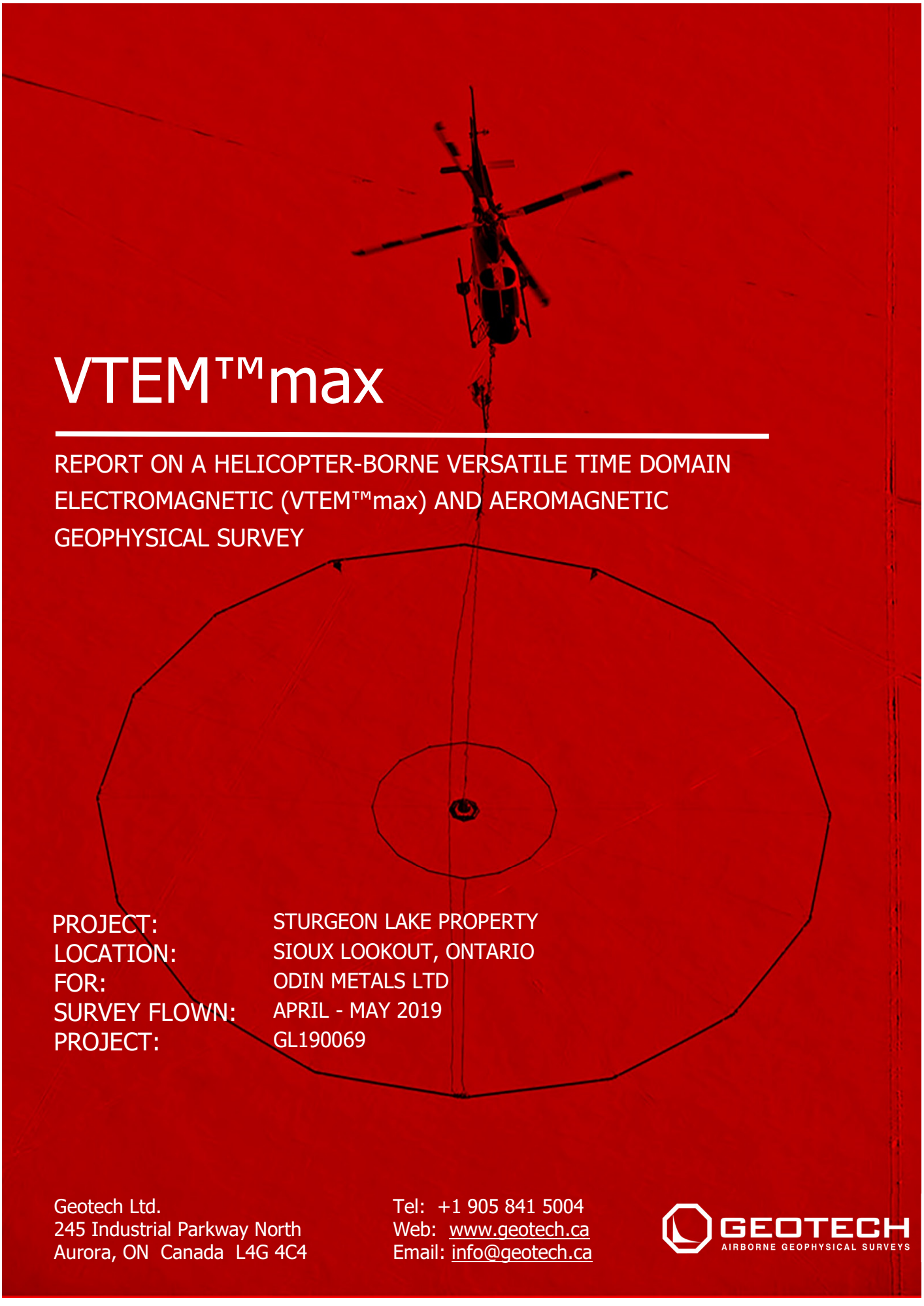

# VTEM™max

REPORT ON A HELICOPTER-BORNE VERSATILE TIME DOMAIN ELECTROMAGNETIC (VTEM™max) AND AEROMAGNETIC GEOPHYSICAL SURVEY

| | |
|---|---|
| PROJECT: | STURGEON LAKE PROPERTY |
| LOCATION: | SIOUX LOOKOUT, ONTARIO |
| FOR: | ODIN METALS LTD |
| SURVEY FLOWN: | APRIL - MAY 2019 |
| PROJECT: | GL190069 |

Geotech Ltd.
245 Industrial Parkway North
Aurora, ON Canada L4G 4C4

Tel: +1 905 841 5004
Web: www.geotech.ca
Email: info@geotech.ca

GEOTECH
AIRBORNE GEOPHYSICAL SURVEYS

# TABLE OF CONTENTS



# LIST OF FIGURES

# LIST OF TABLES



# APPENDICES

# EXECUTIVE SUMMARY

## STURGEON LAKE PROPERTY
## STURGEON LAKE, ONTARIO

During April 25th to May 15th, 2019 Geotech Ltd. carried out a helicopter-borne geophysical survey over the Sturgeon Lake Property situated near Sioux Lookout, Ontario.

Principal geophysical sensors included a versatile time domain electromagnetic (VTEM™max) system and a caesium magnetometer. Ancillary equipment included a GPS navigation system and a radar altimeter. A total of 414 line-kilometres of geophysical data were acquired during the survey.

In-field data quality assurance and preliminary processing were carried out on a daily basis during the acquisition phase. Preliminary and final data processing, including generation of final digital data and map products were undertaken from the office of Geotech Ltd. in Aurora, Ontario.

The processed survey results are presented as the following maps:

- Electromagnetic stacked profiles of the B-field Z Component
- Electromagnetic stacked profiles of dB/dt Z Components
- B-Field Z Component Channel grid
- Fraser Filtered dB/dt X Component Channel grid
- Total Magnetic Intensity (TMI)
- Calculated Time Constant (Tau)
- Resistivity Depth Images (RDI) sections are presented

Digital data includes all electromagnetic and magnetic products, plus ancillary data including the waveform.

The survey report describes the procedures for data acquisition, processing, equipment used, final image presentation and the specifications for the digital data set.

# 1. INTRODUCTION

## 1.1 GENERAL CONSIDERATIONS

Geotech Ltd. performed a helicopter-borne geophysical survey over the Sturgeon Lake Property situated near Sioux Lookout, Ontario (Figure 1 & Figure 2).

Michel Allard represented Odin Metals LTD during the data acquisition and data processing phases of this project.

The geophysical surveys consisted of helicopter borne EM using the versatile time-domain electromagnetic (VTEM™) max system with Full-Waveform processing. Measurements consisted of Vertical (Z) and In-line Horizontal (X) components of the EM fields using an induction coil and the aeromagnetic total field using a caesium magnetometer. A total of 414 line-km of geophysical data were acquired during the survey.

The crew was based out of Sioux Lookout, Ontario for the acquisition phase of the survey.

Data quality control and quality assurance, and preliminary data processing were carried out on a daily basis during the acquisition phase of the project. Final data processing followed immediately after the end of the survey. Final reporting, data presentation and archiving were completed from the Aurora office of Geotech Ltd. in July, 2019.


Figure 1: Survey location

## 1.2 SURVEY AND SYSTEM SPECIFICATIONS

The survey area is located near Sioux Lookout, Ontario (Figure 2).

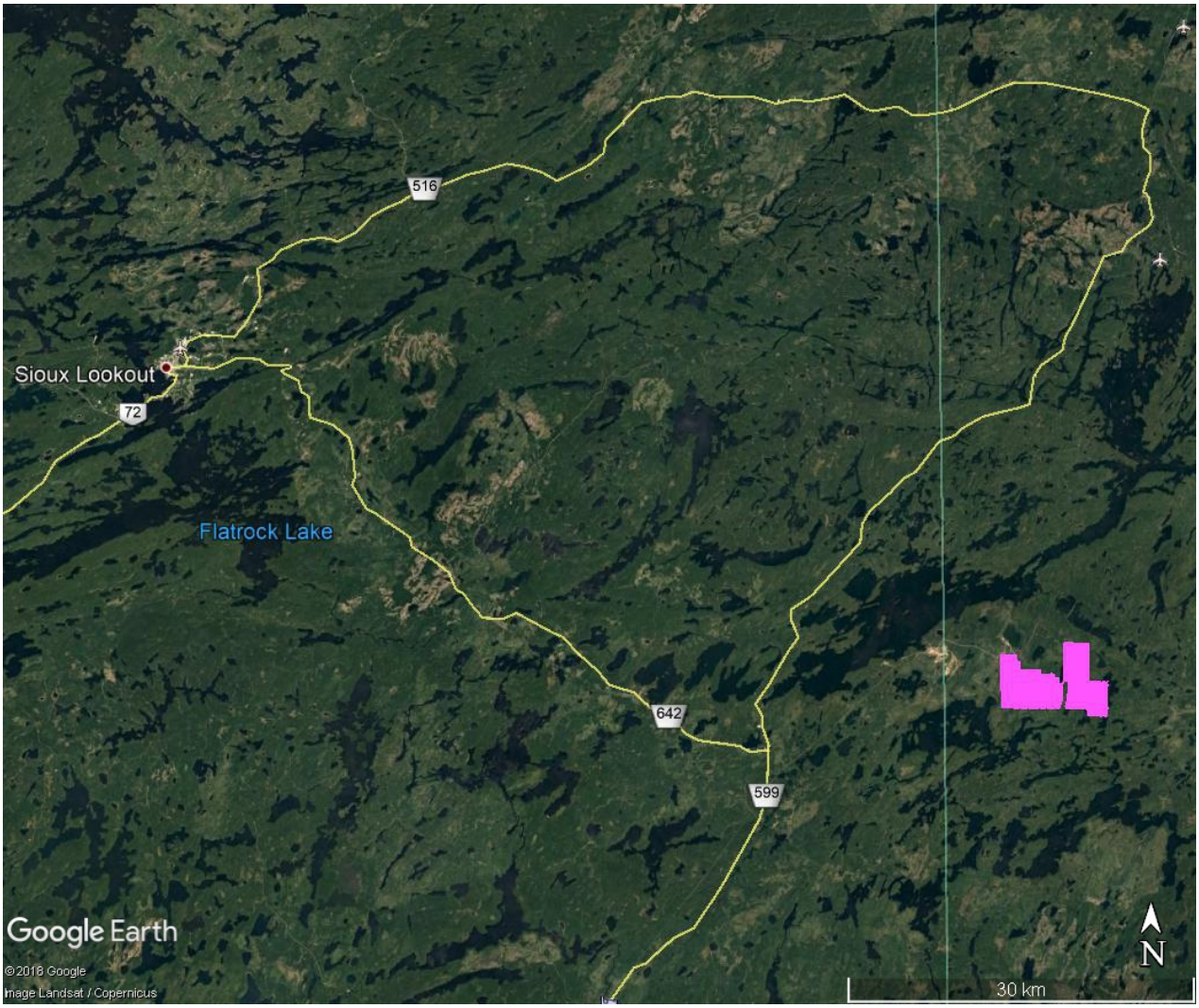


Figure 2: Survey area location on Google Earth.

The survey area was flown in a north to south (N 0°E) line direction at 100 metre line spacings as depicted in Figure 3. Tie lines were flown perdendicular at 1000 metre spacings. For more detailed information on the flight spacing and direction see Table 1.

## 1.3 TOPOGRAPHIC RELIEF AND CULTURAL FEATURES

Topographically, the survey area exhibit minimal relief with elevations ranging from 437 to 498 metres above mean sea level over an area of 35 square kilometres (Figure 3).

There are various rivers and streams running through the survey area which connect various small lakes and wetlands. There are also a number of small roads/trails throughout the survey areas as well as powerlines and mining ares.

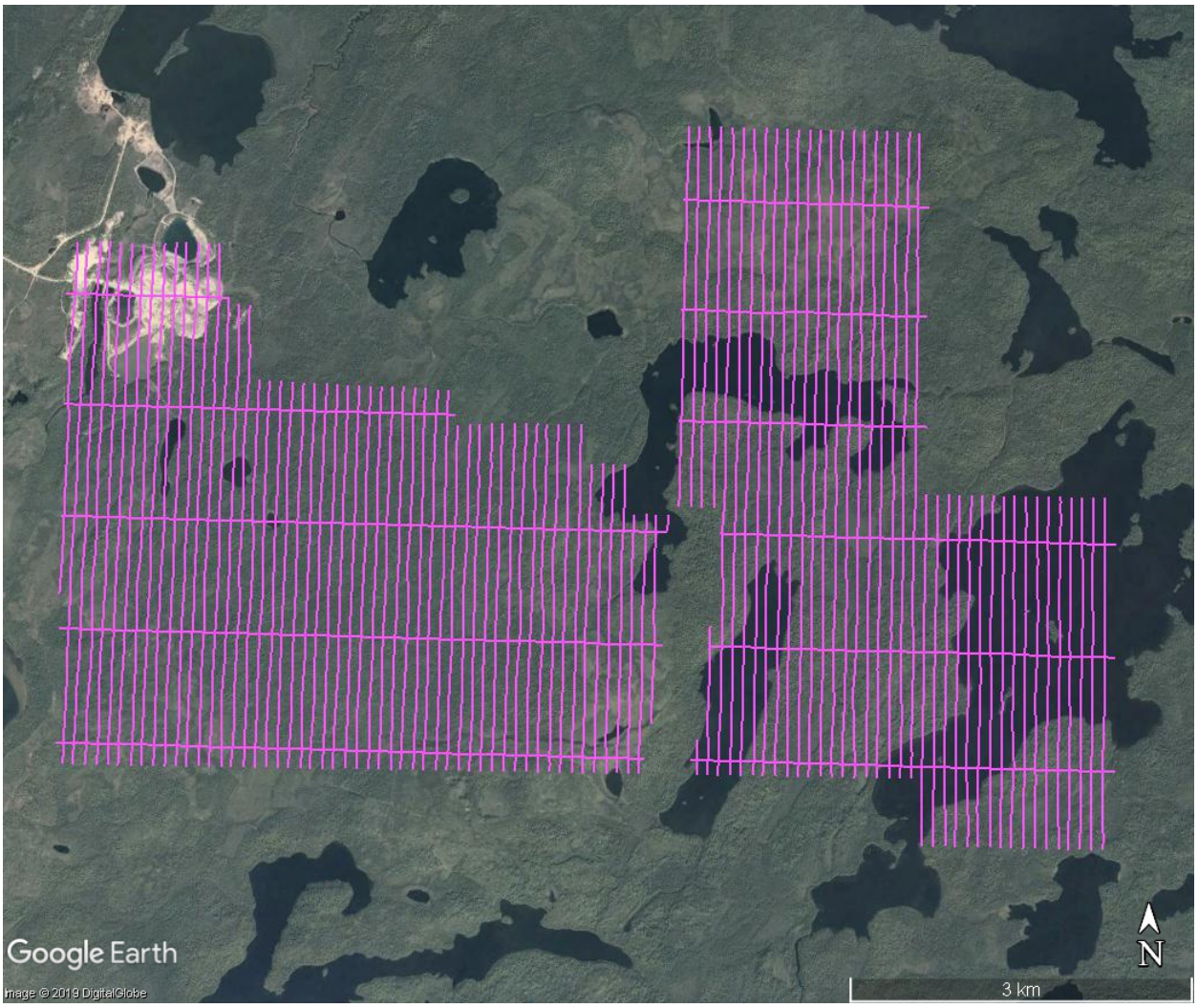


Figure 3: Flight path over a Google Earth Image

# 2. DATA ACQUISITION

## 2.1 SURVEY AREA

The survey area (see Figure 3 and Appendix A) and general flight specifications are as follows:

Table 1: Survey Specifications

| Survey block | Line spacing (m) | Area ($Km^2$) | Planned[1] Line-km | Actual Line-km | Flight direction | Line numbers |
|---|---|---|---|---|---|---|
| Sturgeon Lake | Traverse: 100 | 35 | 396 | 414 | N0°E - N180°E | 2560 - 3480 |
| | Tie: 1000 | | | | N90°E - N270°E | 5030 - 5080 |
| TOTAL | | 35 | 396 | 414 | | |

Survey area boundaries co-ordinates are provided in Appendix B.

## 2.2 SURVEY OPERATIONS

Survey operations were based out of Sioux Lookout, Ontario from April 25th to May 15th, 2019. The following table shows the timing of the flying.

Table 2: Survey schedule

| Date | Comments |
|---|---|
| 25-Apr-19 | Crew and equipment arrive in Sioux Lookout |
| 26-Apr-19 | System assembly |
| 27-Apr-19 | System assembly |
| 28-Apr-19 | System testing |
| 29-Apr-19 | System testing |
| 30-Apr-19 | Production |
| 1-May-19 | Production |
| 2-May-19 | No production due to weather |
| 3-May-19 | Production |
| 4-May-19 | No production due to weather |
| 5-May-19 | No production due to weather |
| 6-May-19 | Production |
| 7-May-19 | Production |
| 8-May-19 | Production |
| 9-May-19 | No production due to weather |
| 10-May-19 | Production |
| 11-May-19 | Production |
| 12-May-19 | No production due to weather |
| 13-May-19 | Production |
| 14-May-19 | Production |
| 15-May-19 | Production - flight path complete |

[1] Note: Actual Line kilometres represent the total line kilometres in the final database. These line-km normally exceed the Planned Line-km, as indicated in the survey NAV files.

## 2.3 FLIGHT SPECIFICATIONS

During the survey the helicopter was maintained at a mean altitude of 101 metres above the ground with an average survey speed of 80 km/hour. This allowed for an actual average Transmitter-receiver loop terrain clearance of 53 metres and a magnetic sensor clearance of 91 metres.

The on board operator was responsible for monitoring the system integrity. He also maintained a detailed flight log during the survey, tracking the times of the flight as well as any unusual geophysical or topographic features.

On return of the aircrew to the base camp the survey data was transferred from a compact flash card (PCMCIA) to the data processing computer. The data were then uploaded via ftp to the Geotech office in Aurora for daily quality assurance and quality control by qualified personnel.

## 2.4 AIRCRAFT AND EQUIPMENT

### 2.4.1 SURVEY AIRCRAFT

The survey was flown using a Eurocopter Aerospatiale (A-star) 350 B3 helicopter. The helicopter was owned and operated by Geotech Aviation. Installation of the geophysical and ancillary equipment was carried out by a Geotech Ltd crew.

### 2.4.2 ELECTROMAGNETIC SYSTEM

The electromagnetic system was a Geotech Time Domain EM (VTEM™max) full receiver-waveform streamed data recorded system. The "full waveform VTEM system" uses the streamed half-cycle recording of transmitter and receiver waveforms to obtain a complete system response calibration throughout the entire survey flight. The VTEM™ transmitter current waveform is shown diagrammatically in Figure 4.

The VTEM™ Receiver and transmitter coils were in concentric-coplanar and Z-direction oriented configuration. The receiver system for the project also included a coincident-coaxial X-direction coil to measure the in-line dB/dt and calculate B-Field responses. The Transmitter-receiver loop was towed at a mean distance of 48 metres below the aircraft as shown in Figure 5.

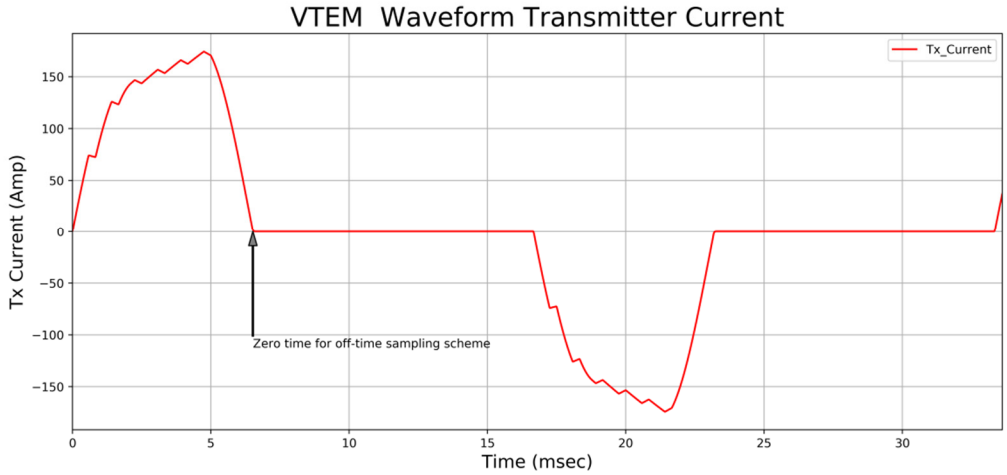


Figure 4: VTEM™ Transmitter Current Waveform

The VTEM™ decay sampling scheme is shown in Table 3 below. Forty-three time measurement gates were used for the final data processing in the range from 0.021 to 8.083 msec. Zero time for the off-time sampling scheme is equal to the current pulse width and is defined as the time near the end of the turn-off ramp where the dI/dt waveform falls to 1/2 of its peak value.

Table 3: Off-Time Decay Sampling Scheme

| VTEM™ Decay Sampling Scheme | | | | |
|---|---|---|---|---|
| Index | Start | End | Middle | Width |
| Milliseconds | | | | |
| 4 | 0.018 | 0.023 | 0.021 | 0.005 |
| 5 | 0.023 | 0.029 | 0.026 | 0.005 |
| 6 | 0.029 | 0.034 | 0.031 | 0.005 |
| 7 | 0.034 | 0.039 | 0.036 | 0.005 |
| 8 | 0.039 | 0.045 | 0.042 | 0.006 |
| 9 | 0.045 | 0.051 | 0.048 | 0.007 |
| 10 | 0.051 | 0.059 | 0.055 | 0.008 |
| 11 | 0.059 | 0.068 | 0.063 | 0.009 |
| 12 | 0.068 | 0.078 | 0.073 | 0.010 |
| 13 | 0.078 | 0.090 | 0.083 | 0.012 |
| 14 | 0.090 | 0.103 | 0.096 | 0.013 |
| 15 | 0.103 | 0.118 | 0.110 | 0.015 |
| 16 | 0.118 | 0.136 | 0.126 | 0.018 |
| 17 | 0.136 | 0.156 | 0.145 | 0.020 |
| 18 | 0.156 | 0.179 | 0.167 | 0.023 |
| 19 | 0.179 | 0.206 | 0.192 | 0.027 |
| 20 | 0.206 | 0.236 | 0.220 | 0.030 |
| 21 | 0.236 | 0.271 | 0.253 | 0.035 |
| 22 | 0.271 | 0.312 | 0.290 | 0.040 |
| 23 | 0.312 | 0.358 | 0.333 | 0.046 |
| 24 | 0.358 | 0.411 | 0.383 | 0.053 |
| 25 | 0.411 | 0.472 | 0.440 | 0.061 |
| 26 | 0.472 | 0.543 | 0.505 | 0.070 |
| 27 | 0.543 | 0.623 | 0.580 | 0.081 |
| 28 | 0.623 | 0.716 | 0.667 | 0.093 |
| 29 | 0.716 | 0.823 | 0.766 | 0.107 |
| 30 | 0.823 | 0.945 | 0.880 | 0.122 |
| 31 | 0.945 | 1.086 | 1.010 | 0.141 |
| 32 | 1.086 | 1.247 | 1.161 | 0.161 |
| 33 | 1.247 | 1.432 | 1.333 | 0.185 |
| 34 | 1.432 | 1.646 | 1.531 | 0.214 |
| 35 | 1.646 | 1.891 | 1.760 | 0.245 |
| 36 | 1.891 | 2.172 | 2.021 | 0.281 |
| 37 | 2.172 | 2.495 | 2.323 | 0.323 |
| 38 | 2.495 | 2.865 | 2.667 | 0.370 |

| VTEM™ Decay Sampling Scheme | | | | |
|---|---|---|---|---|
| Index | Start | End | Middle | Width |
| Milliseconds | | | | |
| 39 | 2.865 | 3.292 | 3.063 | 0.427 |
| 40 | 3.292 | 3.781 | 3.521 | 0.490 |
| 41 | 3.781 | 4.341 | 4.042 | 0.560 |
| 42 | 4.341 | 4.987 | 4.641 | 0.646 |
| 43 | 4.987 | 5.729 | 5.333 | 0.742 |
| 44 | 5.729 | 6.581 | 6.125 | 0.852 |
| 45 | 6.581 | 7.560 | 7.036 | 0.979 |
| 46 | 7.560 | 8.685 | 8.083 | 1.125 |

Z Component: 4 - 46 time gates
X Component: 20 - 46 time gates

VTEM™ system specifications:

| Transmitter | Receiver |
|---|---|
| • Transmitter loop diameter: 34.6 m<br>• Number of turns: 4<br>• Effective Transmitter loop area: 3761 $m^2$<br>• Transmitter base frequency: 30 Hz<br>• Peak current: 174<br>• Pulse width: 6.52 Waveform shape: Bi-polar trapezoid<br>• Peak dipole moment: 654,994 nIA<br>• Average transmitter-receiver loop terrain clearance: 51 metres above the ground | • X Coil diameter: 0.32 m<br>• Number of turns: 245<br>• Effective coil area: 19.69 $m^2$<br>• Z-Coil diameter: 1.2 m<br>• Number of turns: 100<br>• Effective coil area: 113.04 $m^2$ |

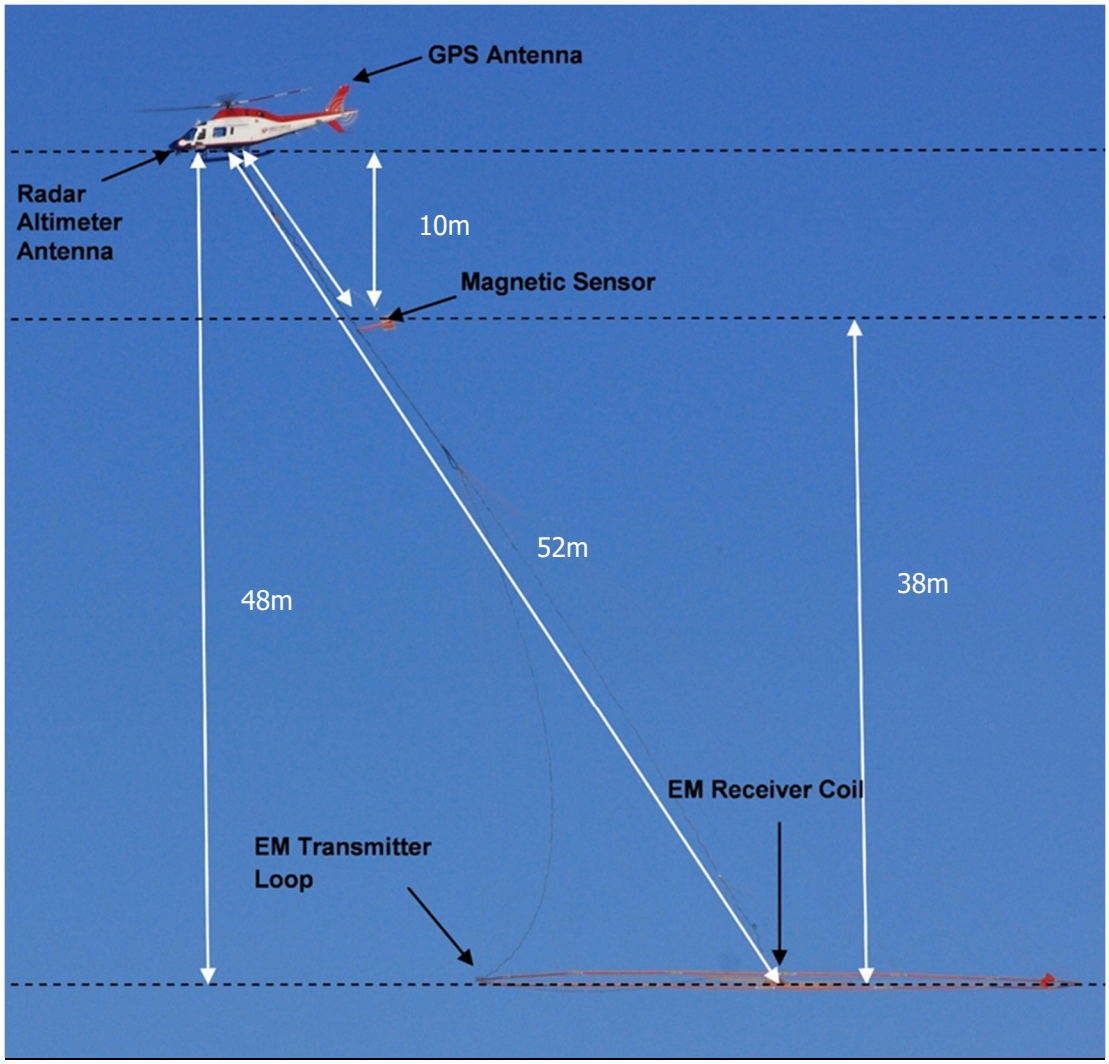


Figure 5: VTEM™max System Configuration.

### 2.4.3 AIRBORNE MAGNETOMETER

The magnetic sensor utilized for the survey was Geometrics optically pumped caesium vapour magnetic field sensor mounted 10 metres below the helicopter, as shown in Figure 5. The sensitivity of the magnetic sensor is 0.02 nanoTesla (nT) at a sampling interval of 0.1 seconds.

### 2.4.4 FULL WAVEFORM VTEM™ SENSOR CALIBRATION

The calibration is performed on the complete VTEM™ system installed in and connected to the helicopter, using special calibration equipment. This calibration takes place on the ground at the start of the project prior to surveying.

The procedure takes half-cycle files acquired and calculates a calibration file consisting of a single stacked half-cycle waveform. The purpose of the stacking is to attenuate natural and man-made magnetic signals, leaving only the response to the calibration signal.

This calibration allows the transfer function between the EM receiver and data acquisition system and also the transfer function of the current monitor and data acquisition system to be determined. These calibration results are then used in VTEM full waveform processing.

### 2.4.5 RADAR ALTIMETER

A Terra TRA 3000/TRI 40 radar altimeter was used to record terrain clearance. The antenna was mounted beneath the bubble of the helicopter cockpit (Figure 5).

### 2.4.6 GPS NAVIGATION SYSTEM

The navigation system used was a Geotech PC104 based navigation system utilizing a NovAtel's WAAS (Wide Area Augmentation System) enabled GPS receiver, Geotech navigate software, a full screen display with controls in front of the pilot to direct the flight and a NovAtel GPS antenna mounted on the helicopter tail (Figure 5). As many as 11 GPS and two WAAS satellites may be monitored at any one time. The positional accuracy or circular error probability (CEP) is 1.8 m, with WAAS active, it is 1.0 m. The co-ordinates of the survey area were set-up prior to the survey and the information was fed into the airborne navigation system.

### 2.4.7 DIGITAL ACQUISITION SYSTEM

A Geotech data acquisition system recorded the digital survey data on an internal compact flash card. Data is displayed on an LCD screen as traces to allow the operator to monitor the integrity of the system. The data type and sampling interval as provided in Table 4

Table 4: Acquisition Sampling Rates

| Data Type | Sampling |
|---|---|
| TDEM | 0.1 sec |
| Magnetometer | 0.1 sec |
| GPS Position | 0.2 sec |
| Radar Altimeter | 0.2 sec |
| Inclinometer | 0.1 sec |

## 2.5 BASE STATION

A combined magnetometer/GPS base station was utilized on this project. A Geometrics Caesium vapour magnetometer was used as a magnetic sensor with a sensitivity of 0.001 nT. The base station was recording the magnetic field together with the GPS time at 1 Hz on a base station computer.

The first base station magnetometer sensor was installed in a secured location away from culture and electric transmission lines and moving ferrous objects such as motor vehicles. The base station data were backed-up to the data processing computer at the end of each survey day.

# 3. PERSONNEL

The following Geotech Ltd. personnel were involved in the project.

FIELD:

| | |
|---|---|
| Project Manager: | Shauna-Lee Hewitt (Office) |
| Data QC: | Neil Fiset (Office) |
| Crew chief: | Colin Lennox |
| Operator: | Kenneth Wessels |

The survey pilot and the mechanical engineer were employed directly by the helicopter operator – Geotech Aviation.

| | |
|---|---|
| Pilot: | Damien Calichon |
| Mechanical Engineer: | Rachel Trottier |

OFFICE:

| | |
|---|---|
| Preliminary Data Processing: | Neil Fiset |
| Final Data Processing: | Julian Boada |
| Final Data QA/QC: | Kanita Khaled |
| Reporting/Mapping: | Kyle Orlowski |

Processing and reporting were carried out under the supervision of Kanita Khaled, P.Geo. The customer relations were looked after by David Hitz.

# 4. DATA PROCESSING AND PRESENTATION

Data compilation and processing were carried out by the application of Geosoft OASIS Montaj and programs proprietary to Geotech Ltd.

## 4.1 FLIGHT PATH

The flight path, recorded by the acquisition program as WGS 84 latitude/longitude, was converted into the WGS84 Datum, UTM Zone 15 North coordinate system in Oasis Montaj.

The flight path was drawn using linear interpolation between x, y positions from the navigation system. Positions are updated every second and expressed as UTM easting's (x) and UTM northing's (y).

## 4.2 ELECTROMAGNETIC DATA

The Full Waveform EM specific data processing operations included:

- Half cycle stacking (performed at time of acquisition);
- System response correction;
- Parasitic and drift removal.

A three stage digital filtering process was used to reject major sferic events and to reduce noise levels. Local sferic activity can produce sharp, large amplitude events that cannot be removed by conventional filtering procedures. Smoothing or stacking will reduce their amplitude but leave a broader residual response that can be confused with geological phenomena. To avoid this possibility, a computer algorithm searches out and rejects the major sferic events.

The signal to noise ratio was further improved by the application of a low pass linear digital filter. This filter has zero phase shift which prevents any lag or peak displacement from occurring, and it suppresses only variations with a wavelength less than about 1 second or 15 metres. This filter is a symmetrical 1 sec linear filter.

The results are presented as stacked profiles of EM voltages for the time gates, in linear - logarithmic scale for the B-field Z component and dB/dt responses in the Z and X components. B-field Z component time channel recorded at 0.440 milliseconds after the termination of the impulse is also presented as a colour image. Calculated Time Constant (TAU) with Calculated Vertical Derivative contours is presented in Appendix C and E. Resistivity Depth Image (RDI) is also presented in Appendix F and G.

VTEM™ has two receiver coil orientations. Z-axis coil is oriented parallel to the transmitter coil axis and both are horizontal to the ground. The X-axis coil is oriented parallel to the ground and along the line-of-flight. This combined two coil configuration provides information on the position, depth, dip and thickness of a conductor. Generalized modeling results of VTEM data, are shown in Appendix D.

In general X-component data produce cross-over type anomalies: from "+ to – "in flight direction of flight for "thin" sub vertical targets and from "- to +" in direction of flight for "thick" targets. Z component data produce double peak type anomalies for "thin" sub vertical targets and single peak for "thick" targets.

The limits and change-over of "thin-thick" depends on dimensions of a TEM system (Appendix D, Figure D-16).

Because of X component polarity is under line-of-flight, convolution Fraser Filter (Figure 6) is applied to X component data to represent axes of conductors in the form of grid map. In this case positive FF anomalies always correspond to "plus-to-minus" X data crossovers independent of the flight direction.

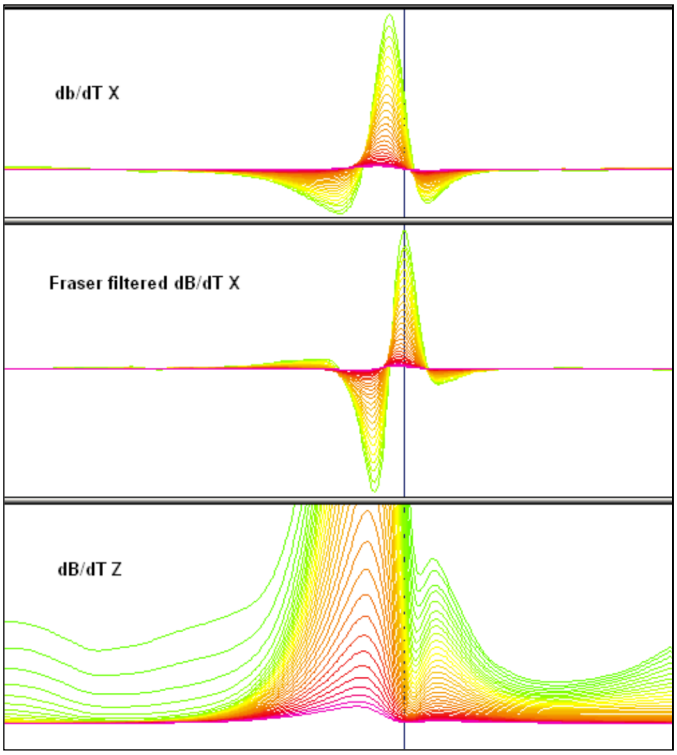


Figure 6: Z, X and Fraser filtered X (FFx) components for "thin" target.

## 4.3 MAGNETIC DATA

The processing of the magnetic data involved the correction for diurnal variations by using the digitally recorded ground base station magnetic values. The base station magnetometer data was edited and merged into the Geosoft GDB database on a daily basis. The aeromagnetic data was corrected for diurnal variations by subtracting the observed magnetic base station deviations.

Tie line levelling was carried out by adjusting intersection points along traverse lines. A micro-levelling procedure was applied to remove persistent low-amplitude components of flight-line noise remaining in the data.

The corrected magnetic data was interpolated between survey lines using a random point gridding method to yield x-y grid values for a standard grid cell size of approximately 25 metres at the mapping scale. The Minimum Curvature algorithm was used to interpolate values onto a rectangular regular spaced grid.

## 4.4 EM ANOMALIES

The objective of picking EM anomalies in the VTEM data from the Sturgeon Lake Property is to identify local and discrete EM anomalies.

The EM data were examined for anomalous responses using all time domain EM channels for the dB/dt and B-Field profiles. The resulting EM anomaly picks are presented as overlays in a Geosoft map and approximately correspond to the position of the target's center projected onto surface.

Each individual conductor pick is represented by an anomaly symbol classified according to calculated conductance[2].

Identified anomalies were classified into one of six categories, as shown in Figure 7. The anomaly symbol is accompanied by postings denoting the calculated dB/dt conductance, calculated dB/dt and B-field decay constant (Tau). Each symbol is also accompanied by an anomaly identification letter, e.g., A, B, C...etc., uniquely defined for each flight line. Double peak anomalies in the dB/dt data (sub-vertical and thin conductors) are distinguished by an orange dot inside the anomaly symbol. The anomalous responses are picked, reviewed and edited on a line by line basis to discriminate between bedrock, overburden and culture conductors.

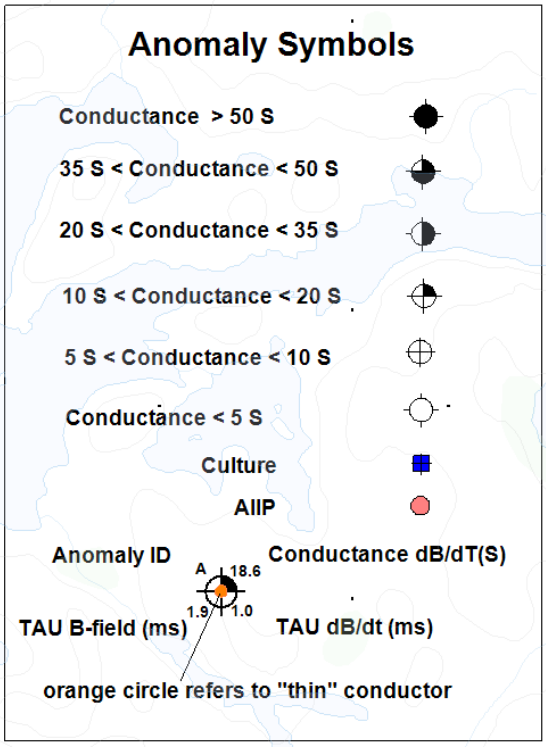


Figure 7: EM anomaly legends.

[1] Note: Conductance values were obtained from the dB/dt and B-Field EM time constants (Tau) whose relationships to Tau were calculated using the oblate spheroid model of McNeill (1980, TN-7, "Applications of Transient EM Techniques").

# 5. DELIVERABLES

## 5.1 SURVEY REPORT

The survey report describes the data acquisition, processing, and final presentation of the survey results. The survey report is provided in two paper copies and digitally in PDF format.

## 5.2 MAPS

Final maps were produced at scale of 1:10,000 for best representation of the survey size and line spacing. The coordinate/projection system used was WGS84 Datum, UTM Zone 15 North. All maps show the flight path trace and topographic data; latitude and longitude are also noted on maps.

The preliminary and final results of the survey are presented as EM profiles, a late-time gate gridded EM channel, and a colour magnetic TMI contour map.

- Maps at 1:10,000 in Geosoft MAP format, as follows:

| | |
|---|---|
| GL190069_10k_dBdt: | dB/dt profiles Z Component, Time Gates 0.220 – 7.036 ms in linear – logarithmic scale. |
| GL190069_10k_Bfield: | B-field profiles Z Component, Time Gates 0.220 – 7.036 ms in linear – logarithmic scale. |
| GL190069_10k _BFz25: | B-field late time Z Component Channel 25, Time Gate 0.440 ms colour image. |
| GL190069_10k _SFxFF28: | Fraser Filtered dB/dt X Component Channel 28, Time Gate 0.667 ms colour image. |
| GL190069_10k _TMI: | Total magnetic intensity (TMI) colour image and contours. |
| GL190069_10k _TauSF: | dB/dt Calculated Time Constant (Tau) |

- Maps are also presented in PDF format.
- The topographic data base was derived from CANVEC data (http://maps.canada.ca)
- Background shading is derived from ASTER GDEM (https://gdex.cr.usgs.gov/gdex/)
- Inset data derived from Geocommunities (www.geocomm.com)
- A Google Earth file *GL190069_Odin.kmz* showing the flight path of the block is included. Free versions of Google Earth software from: http://earth.google.com/download-earth.html

## 5.3 DIGITAL DATA

Two copies of the data and maps on DVD were prepared to accompany the report. Each DVD contains a digital file of the line data in GDB Geosoft Montaj format as well as the maps in Geosoft Montaj Map and PDF format.

- DVD structure.

  Data contains databases, grids and maps, as described below.
  Report contains a copy of the report and appendices in PDF format.

Databases in Geosoft GDB format, containing the channels listed in Table 5.

Table 5: Geosoft GDB Data Format

| Channel name | Units | Description |
|---|---|---|
| X: | metres | UTM Easting WGS84 Zone 15 North |
| Y: | metres | UTM Northing WGS84 Zone 15 North |
| Longitude: | Decimal Degrees | WGS 84 Longitude data |
| Latitude: | Decimal Degrees | WGS 84 Latitude data |
| Z: | metres | GPS antenna elevation (above Geoid) |
| Zb: | metres | EM bird elevation (above Geoid) |
| Radar: | metres | helicopter terrain clearance from radar altimeter |
| Radarb: | metres | Calculated EM transmitter-receiver loop terrain clearance from radar altimeter |
| DEM: | metres | Digital Elevation Model |
| Gtime: | Seconds of the day | GPS time |
| Basemag: | nT | Magnetic diurnal variation data |
| MAG1 | nT | Raw Total Magnetic field data |
| MAG2 | nT | Diurnal corrected Total Magnetic field data |
| MAG3 | nT | Levelled Total Magnetic field data |
| CVG | nT/m | Calculated Magnetic Vertical Gradient |
| SFz[4]: | pV/(A*m4) | Z dB/dt 0.021 millisecond time channel |
| SFz[5]: | pV/(A*m4) | Z dB/dt 0.026 millisecond time channel |
| SFz[6]: | pV/(A*$m^4$) | Z dB/dt 0.031 millisecond time channel |
| SFz[7]: | pV/(A*$m^4$) | Z dB/dt 0.036 millisecond time channel |
| SFz[8]: | pV/(A*$m^4$) | Z dB/dt 0.042 millisecond time channel |
| SFz[9]: | pV/(A*$m^4$) | Z dB/dt 0.048 millisecond time channel |
| SFz[10]: | pV/(A*$m^4$) | Z dB/dt 0.055 millisecond time channel |
| SFz[11]: | pV/(A*$m^4$) | Z dB/dt 0.063 millisecond time channel |
| SFz[12]: | pV/(A*$m^4$) | Z dB/dt 0.073 millisecond time channel |
| SFz[13]: | pV/(A*$m^4$) | Z dB/dt 0.083 millisecond time channel |
| SFz[14]: | pV/(A*$m^4$) | Z dB/dt 0.096 millisecond time channel |
| SFz[15]: | pV/(A*$m^4$) | Z dB/dt 0.110 millisecond time channel |
| SFz[16]: | pV/(A*$m^4$) | Z dB/dt 0.126 millisecond time channel |
| SFz[17]: | pV/(A*$m^4$) | Z dB/dt 0.145 millisecond time channel |
| SFz[18]: | pV/(A*$m^4$) | Z dB/dt 0.167 millisecond time channel |
| SFz[19]: | pV/(A*$m^4$) | Z dB/dt 0.192 millisecond time channel |
| SFz[20]: | pV/(A*$m^4$) | Z dB/dt 0.220 millisecond time channel |
| SFz[21]: | pV/(A*$m^4$) | Z dB/dt 0.253 millisecond time channel |
| SFz[22]: | pV/(A*$m^4$) | Z dB/dt 0.290 millisecond time channel |
| SFz[23]: | pV/(A*$m^4$) | Z dB/dt 0.333 millisecond time channel |

| Channel name | Units | Description |
|---|---|---|
| SFz[24]: | pV/(A*m$^4$) | Z dB/dt 0.383 millisecond time channel |
| SFz[25]: | pV/(A*m$^4$) | Z dB/dt 0.440 millisecond time channel |
| SFz[26]: | pV/(A*m$^4$) | Z dB/dt 0.505 millisecond time channel |
| SFz[27]: | pV/(A*m$^4$) | Z dB/dt 0.580 millisecond time channel |
| SFz[28]: | pV/(A*m$^4$) | Z dB/dt 0.667 millisecond time channel |
| SFz[29]: | pV/(A*m$^4$) | Z dB/dt 0.766 millisecond time channel |
| SFz[30]: | pV/(A*m$^4$) | Z dB/dt 0.880 millisecond time channel |
| SFz[31]: | pV/(A*m$^4$) | Z dB/dt 1.010 millisecond time channel |
| SFz[32]: | pV/(A*m$^4$) | Z dB/dt 1.161 millisecond time channel |
| SFz[33]: | pV/(A*m$^4$) | Z dB/dt 1.333 millisecond time channel |
| SFz[34]: | pV/(A*m$^4$) | Z dB/dt 1.531 millisecond time channel |
| SFz[35]: | pV/(A*m$^4$) | Z dB/dt 1.760 millisecond time channel |
| SFz[36]: | pV/(A*m$^4$) | Z dB/dt 2.021 millisecond time channel |
| SFz[37]: | pV/(A*m$^4$) | Z dB/dt 2.323 millisecond time channel |
| SFz[38]: | pV/(A*m$^4$) | Z dB/dt 2.667 millisecond time channel |
| SFz[39]: | pV/(A*m$^4$) | Z dB/dt 3.063 millisecond time channel |
| SFz[40]: | pV/(A*m$^4$) | Z dB/dt 3.521 millisecond time channel |
| SFz[41]: | pV/(A*m$^4$) | Z dB/dt 4.042 millisecond time channel |
| SFz[42]: | pV/(A*m$^4$) | Z dB/dt 4.641 millisecond time channel |
| SFz[43]: | pV/(A*m$^4$) | Z dB/dt 5.333 millisecond time channel |
| SFz[44]: | pV/(A*m$^4$) | Z dB/dt 6.125 millisecond time channel |
| SFz[45]: | pV/(A*m$^4$) | Z dB/dt 7.036 millisecond time channel |
| SFz[46]: | pV/(A*m$^4$) | Z dB/dt 8.083 millisecond time channel |
| SFx[20]: | pV/(A*m$^4$) | X dB/dt 0.220 millisecond time channel |
| SFx[21]: | pV/(A*m$^4$) | X dB/dt 0.253 millisecond time channel |
| SFx[22]: | pV/(A*m$^4$) | X dB/dt 0.290 millisecond time channel |
| SFx[23]: | pV/(A*m$^4$) | X dB/dt 0.333 millisecond time channel |
| SFx[24]: | pV/(A*m$^4$) | X dB/dt 0.383 millisecond time channel |
| SFx[25]: | pV/(A*m$^4$) | X dB/dt 0.440 millisecond time channel |
| SFx[26]: | pV/(A*m$^4$) | X dB/dt 0.505 millisecond time channel |
| SFx[27]: | pV/(A*m$^4$) | X dB/dt 0.580 millisecond time channel |
| SFx[28]: | pV/(A*m$^4$) | X dB/dt 0.667 millisecond time channel |
| SFx[29]: | pV/(A*m$^4$) | X dB/dt 0.766 millisecond time channel |
| SFx[30]: | pV/(A*m$^4$) | X dB/dt 0.880 millisecond time channel |
| SFx[31]: | pV/(A*m$^4$) | X dB/dt 1.010 millisecond time channel |
| SFx[32]: | pV/(A*m$^4$) | X dB/dt 1.161 millisecond time channel |
| SFx[33]: | pV/(A*m$^4$) | X dB/dt 1.333 millisecond time channel |
| SFx[34]: | pV/(A*m$^4$) | X dB/dt 1.531 millisecond time channel |
| SFx[35]: | pV/(A*m$^4$) | X dB/dt 1.760 millisecond time channel |
| SFx[36]: | pV/(A*m$^4$) | X dB/dt 2.021 millisecond time channel |
| SFx[37]: | pV/(A*m$^4$) | X dB/dt 2.323 millisecond time channel |
| SFx[38]: | pV/(A*m$^4$) | X dB/dt 2.667 millisecond time channel |
| SFx[39]: | pV/(A*m$^4$) | X dB/dt 3.063 millisecond time channel |
| SFx[40]: | pV/(A*m$^4$) | X dB/dt 3.521 millisecond time channel |
| SFx[41]: | pV/(A*m$^4$) | X dB/dt 4.042 millisecond time channel |
| SFx[42]: | pV/(A*m$^4$) | X dB/dt 4.641 millisecond time channel |
| SFx[43]: | pV/(A*m$^4$) | X dB/dt 5.333 millisecond time channel |
| SFx[44]: | pV/(A*m$^4$) | X dB/dt 6.125 millisecond time channel |
| SFx[45]: | pV/(A*m$^4$) | X dB/dt 7.036 millisecond time channel |
| SFx[46]: | pV/(A*m$^4$) | X dB/dt 8.083 millisecond time channel |

| Channel name | Units | Description |
|---|---|---|
| BFz | (pV*ms)/(A*m$^4$) | Z B-Field data for time channels 4 to 46 |
| BFx | (pV*ms)/(A*m$^4$) | X B-Field data for time channels 20 to 46 |
| SFxFF | pV/(A*m$^4$) | Fraser Filtered X dB/dt |
| NchanBF | | Latest time channels of TAU calculation |
| TauBF | ms | Time constant B-Field |
| NchanSF | | Latest time channels of TAU calculation |
| TauSF | ms | Time constant dB/dt |
| PLM: | | 60 Hz power line monitor |

Electromagnetic B-field and dB/dt Z component data is found in array channel format between indexes 4 – 46, and X component data from 20 – 46, as described above.

- Database of the Resistivity Depth Images in Geosoft GDB format, containing the following channels:

Table 6: Geosoft Resistivity Depth Image GDB Data Format

| Channel name | Units | Description |
|---|---|---|
| Xg | metres | UTM Easting WGS84 Zone 15 North |
| Yg | metres | UTM Northing WGS84 Zone 15 North |
| Dist: | meters | Distance from the beginning of the line |
| Depth: | meters | array channel, depth from the surface |
| Z: | meters | array channel, depth from sea level |
| AppRes: | Ohm-m | array channel, Apparent Resistivity |
| TR: | meters | EM system height from sea level |
| Topo: | meters | digital elevation model |
| Radarb: | metres | Calculated EM transmitter-receiver loop terrain clearance from radar altimeter |
| SF: | pV/(A*m^4) | array channel, dB/dT |
| MAG: | nT | TMI data |
| CVG: | nT/m | CVG data |
| DOI: | metres | Depth of Investigation: a measure of VTEM depth effectiveness |
| PLM: | | 60Hz Power Line Monitor |

- Database of the VTEM Waveform "GL190069_waveform.gdb" in Geosoft GDB format, containing the following channels:

Table 7: Geosoft database for the VTEM waveform

| Channel name | Units | Description |
|---|---|---|
| Time: | milliseconds | Sampling rate interval, 5.2083 microseconds |
| Tx_Current: | amps | Output current of the transmitter |

- Geosoft Resistivity Depth Image Products:

  | | |
  |---|---|
  | Sections: | Apparent resistivity sections along each line in .GRD and .PDF format |
  | Slices: | Apparent resistivity slices at selected depths from 25m to depth of investigation, at an increment of 25m in .GRD and .PDF format |
  | Voxel: | 3D Voxel imaging of apparent resistivity data clipped by digital elevation and depth of investigation |

- Grids in Geosoft GRD and GeoTIFF format, as follows:

  | | |
  |---|---|
  | BFz25: | B-Field Z Component Channel 25 (Time Gate 0.440 ms) |
  | DEM: | Digital Elevation Model (metres) |
  | CVG: | Calculated Vertical Derivative (nT/m) |
  | SFxFF28: | Fraser Filtered dB/dt X Component Channel 28 (Time Gate 0.667 ms) |
  | TauBF: | B-Field Z Component, Calculated Time Constant (ms) |
  | TauSF: | dB/dt Z Component, Calculated Time Constant (ms) |
  | Mag3: | Total Magnetic Intensity (nT) |
  | SFz15: | dB/dt Z Component Channel 15 (Time Gate 0.110 ms) |
  | SFz25: | dB/dt Z Component Channel 25 (Time Gate 0.440 ms) |
  | SFz35: | dB/dt Z Component Channel 35 (Time Gate 1.760 ms) |

  A Geosoft .GRD file has a .GI metadata file associated with it, containing grid projection information. A grid cell size of 25 metres was used.

# 6. CONCLUSIONS AND RECOMMENDATIONS

A helicopter-borne versatile time domain electromagnetic (VTEM™max) and magnetic geophysical survey has been completed over the Sturgeon Lake Property situated near Sioux Lookout, Ontario.

The total area coverage is 35 km$^2$. Total survey line coverage 414 line kilometres. The principal sensors included a Time Domain EM system and a caesium magnetometer. Results have been presented as stacked profiles, and contour colour images at a scale of 1:10,000. A formal Interpretation has not been included or requested.

Based on geophysical observation, the $dB_Z/dt$ time constant tau and all dB/dt and B-field decay channel results show a major conductive anomaly trend located at the north end of the block trending East-West, as well as several smaller/shorter strike length conductive bodies scattered throughout the southern part of the block. The Northern anomaly has high magnetic association and average apparent resistivity values ranging from 1-3 Ohm- m.

EM anomaly picking and EM Maxwell plate modeling was performed in support of the results, further information regarding the interpretation can be found in the accompanying document GL190069_Odin_Interpretation.pdf.

Respectfully submitted[3],

Kanita Khaled
**Geotech Ltd.**

Julian Boada
**Geotech Ltd.**

PROFESSIONAL GEOSCIENTIST
KANITA KHALED
PRACTISING MEMBER
2995
ONTARIO

Kyle Orlowski
**Geotech Ltd.**

July 2019

[3] Final data processing of the EM and magnetic data were carried out by Julian Boada from the office of Geotech Ltd. in Aurora, Ontario, under the supervision of Kanita Khaled, P.Geo.

# APPENDIX A

## SURVEY AREA LOCATION MAP

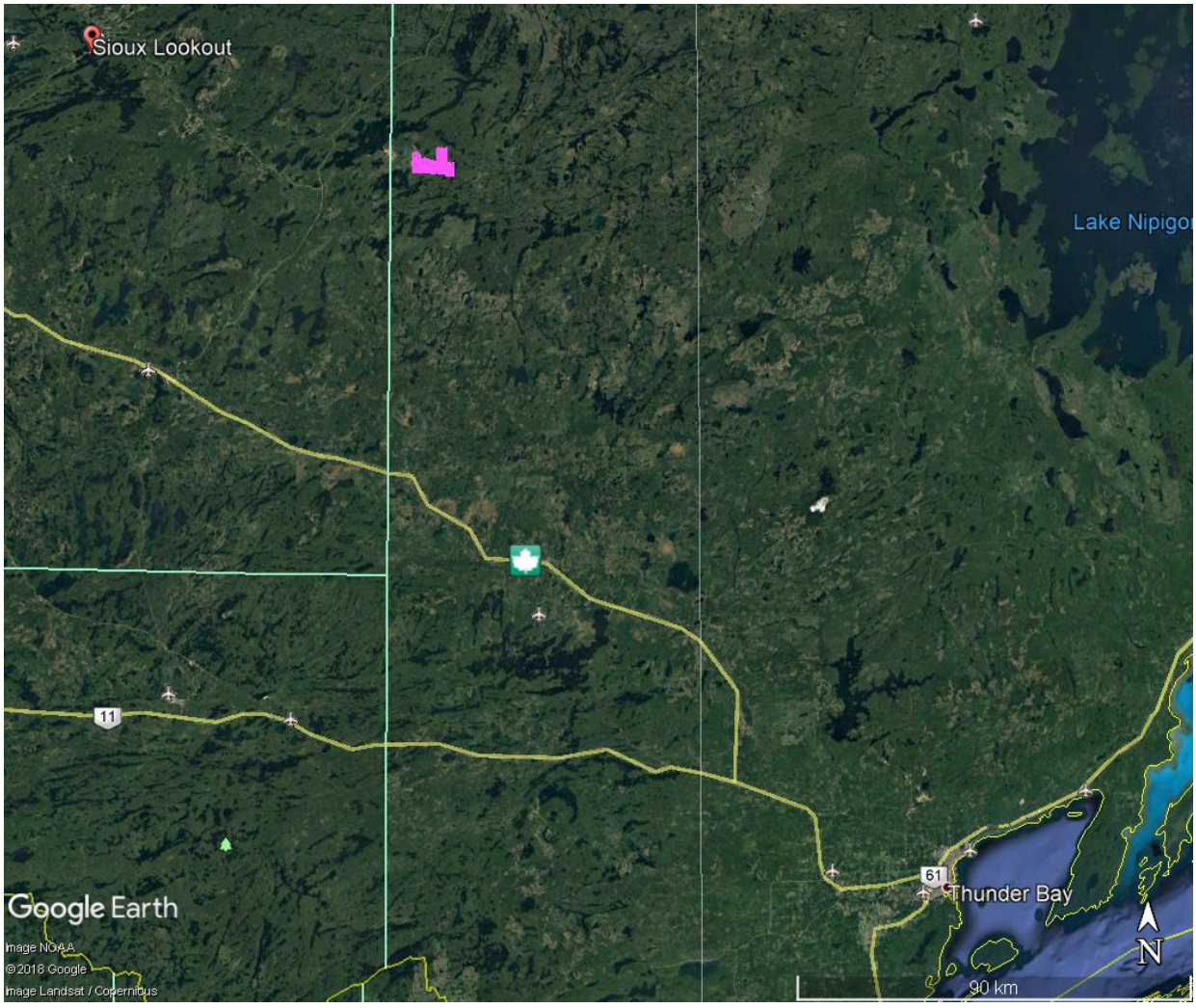


Overview of the Survey Area

# APPENDIX B

## SURVEY AREA COORDINATES

(WGS 84, UTM Zone 15 North)

| WGS84 UTM Zone 15N | |
|---|---|
| X | Y |
| 658805 | 5528130 |
| 656605 | 5528130 |
| 656652 | 5525498 |
| 656673 | 5524748 |
| 656650 | 5524662 |
| 656281 | 5524652 |
| 656269 | 5525096 |
| 655859 | 5525094 |
| 655851 | 5525445 |
| 655137 | 5525438 |
| 654683 | 5525405 |
| 654644 | 5525723 |
| 652892 | 5525765 |
| 652876 | 5526438 |
| 652603 | 5526441 |
| 652565 | 5526976 |
| 652231 | 5527009 |
| 651831 | 5526960 |
| 651492 | 5526989 |
| 651114 | 5526975 |
| 651210 | 5523281 |
| 651243 | 5522361 |
| 656405 | 5522416 |
| 656394 | 5522833 |
| 656595 | 5522838 |
| 656568 | 5524380 |
| 657053 | 5524303 |
| 656923 | 5522678 |
| 656848 | 5522684 |
| 656905 | 5522421 |
| 658805 | 5522441 |
| 658905 | 5521854 |
| 660505 | 5521862 |
| 660510 | 5524786 |
| 660505 | 5524862 |
| 658905 | 5524854 |
| 658833 | 5525500 |
| 658805 | 5528130 |

# APPENDIX C

## GEOPHYSICAL MAPS[1]

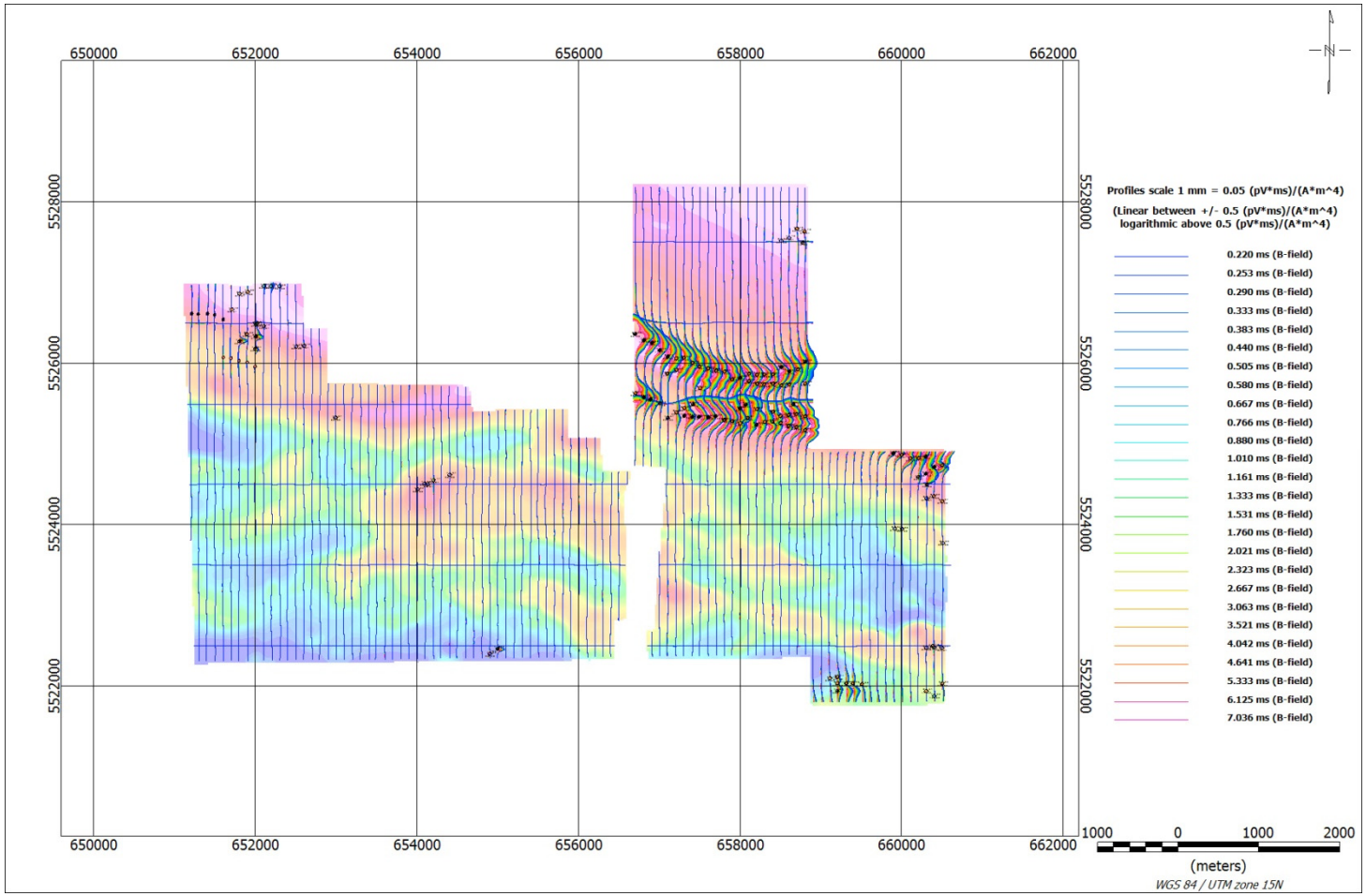


B-field profiles Z Component, Time Gates 0.220 – 7.036 ms, over Total Magnetic Intensity grid

[1] Complete full size geophysical maps are also available in PDF format located in the final data maps folder

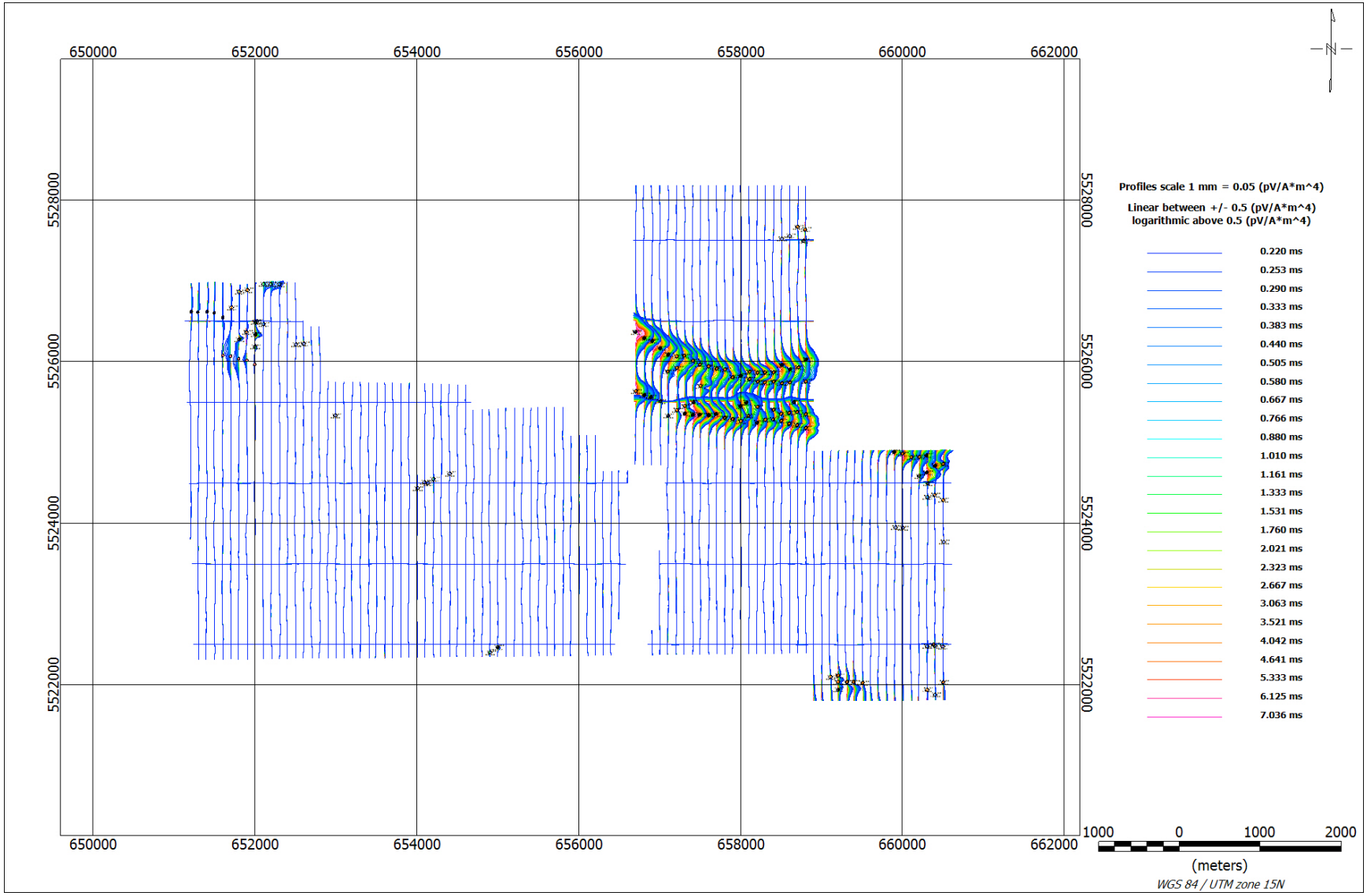


dB/dt profiles Z Component, Time Gates 0.220 – 7.036 ms

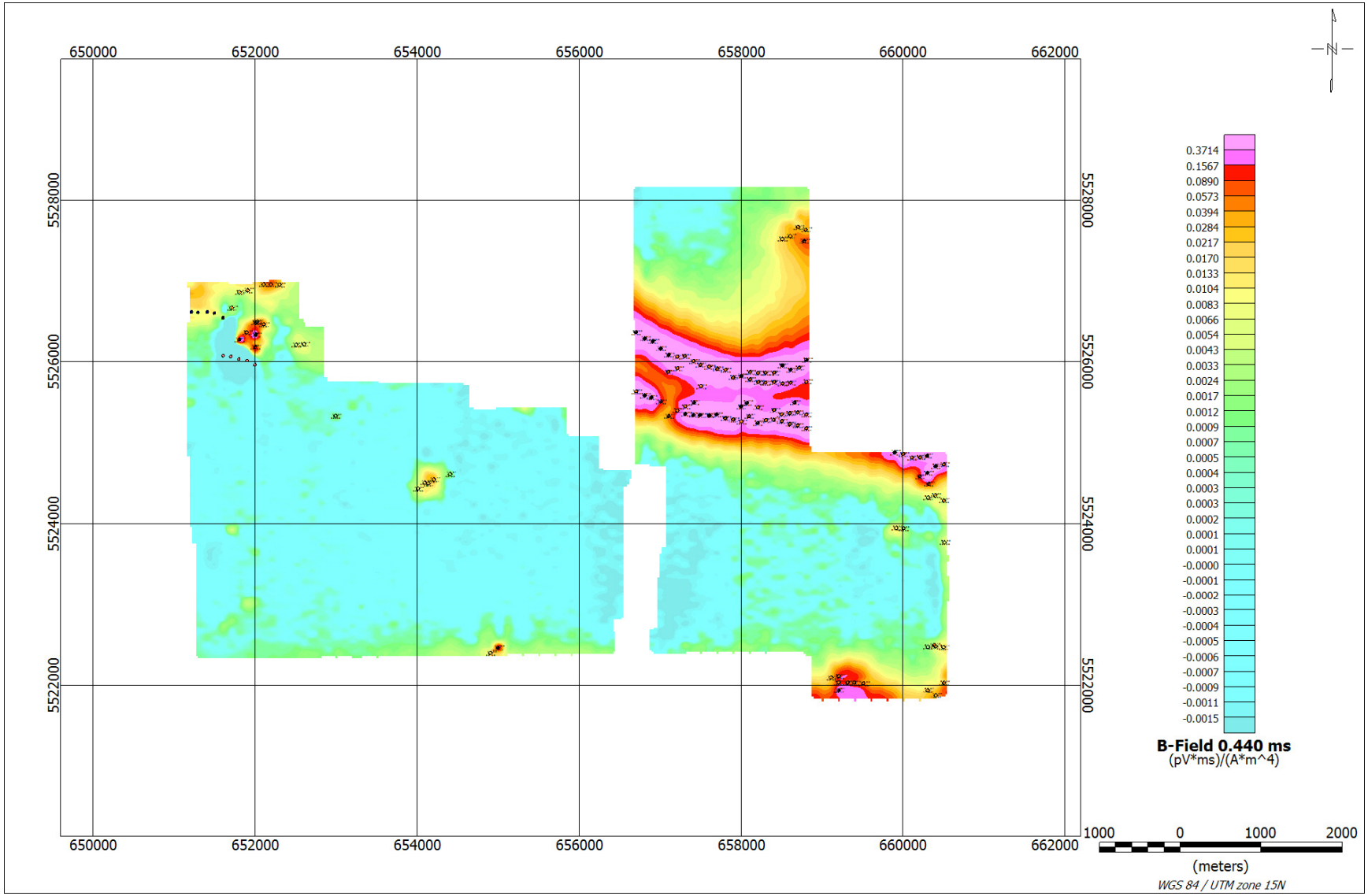


B-Field late time Z Component Channel 25, Time Gate 0.440 ms

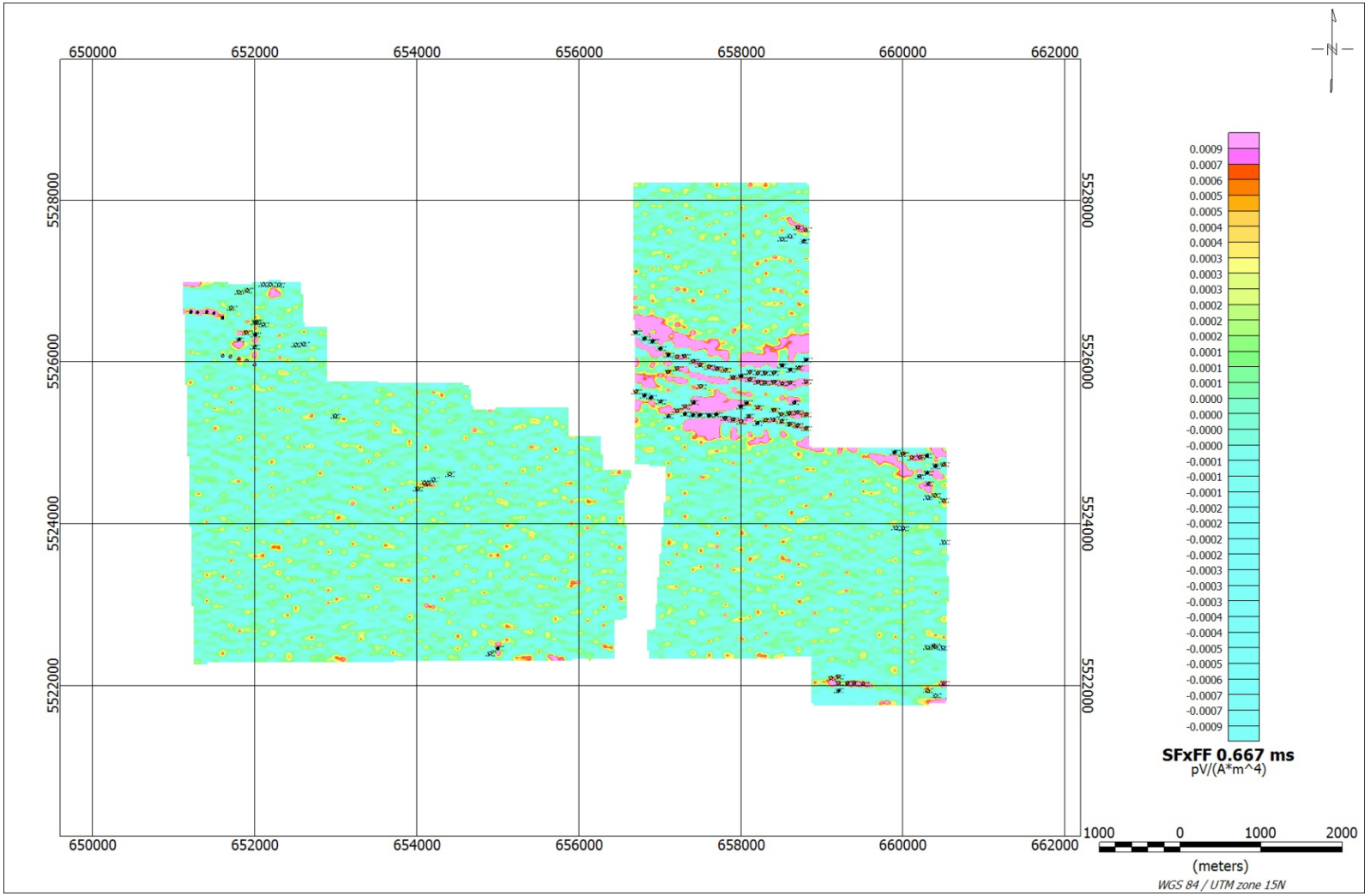


Fraser Filtered dB/dt X Component Channel 28, Time Gate 0.667 ms

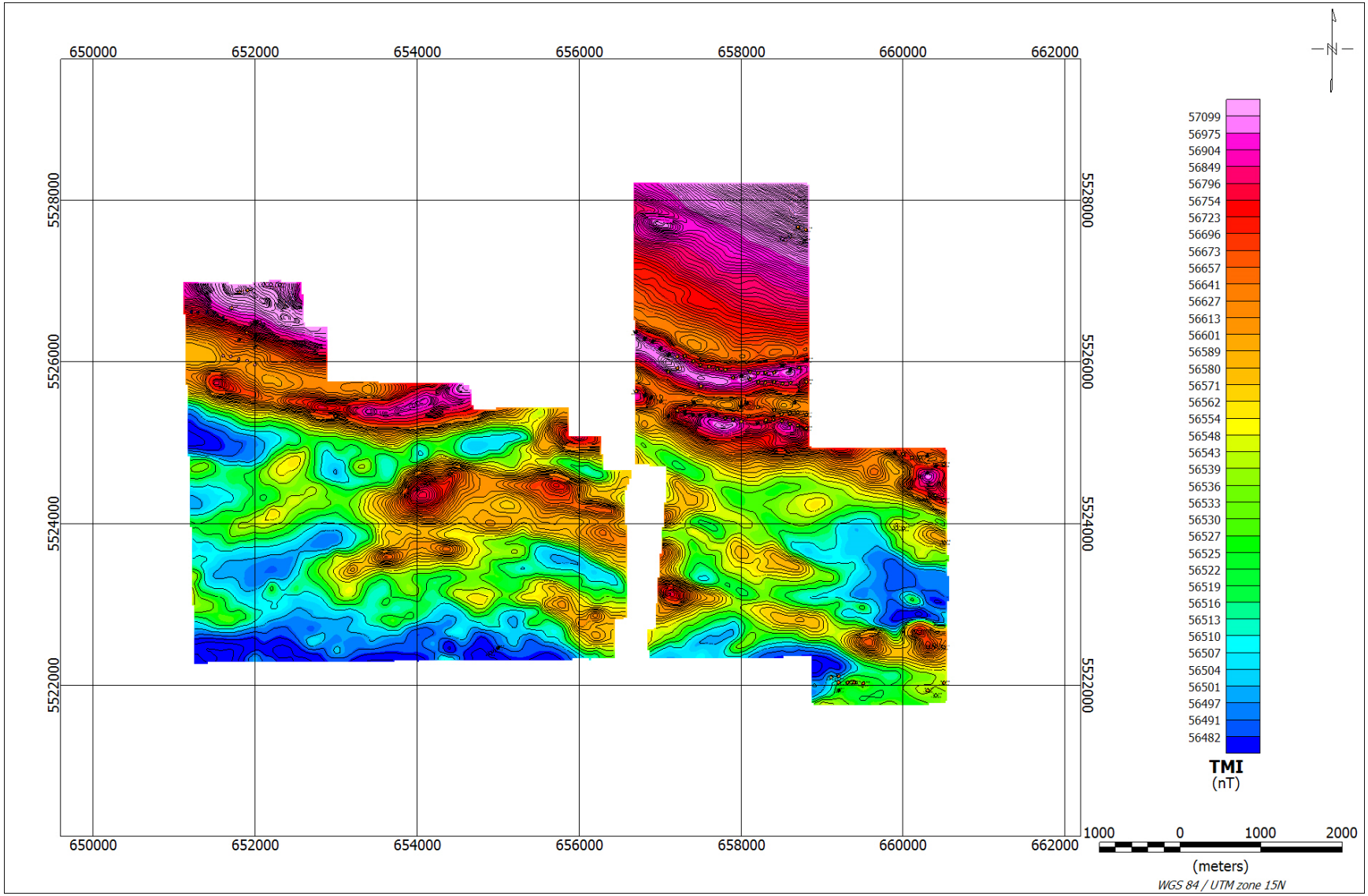


Total Magnetic intensity (TMI), with contours

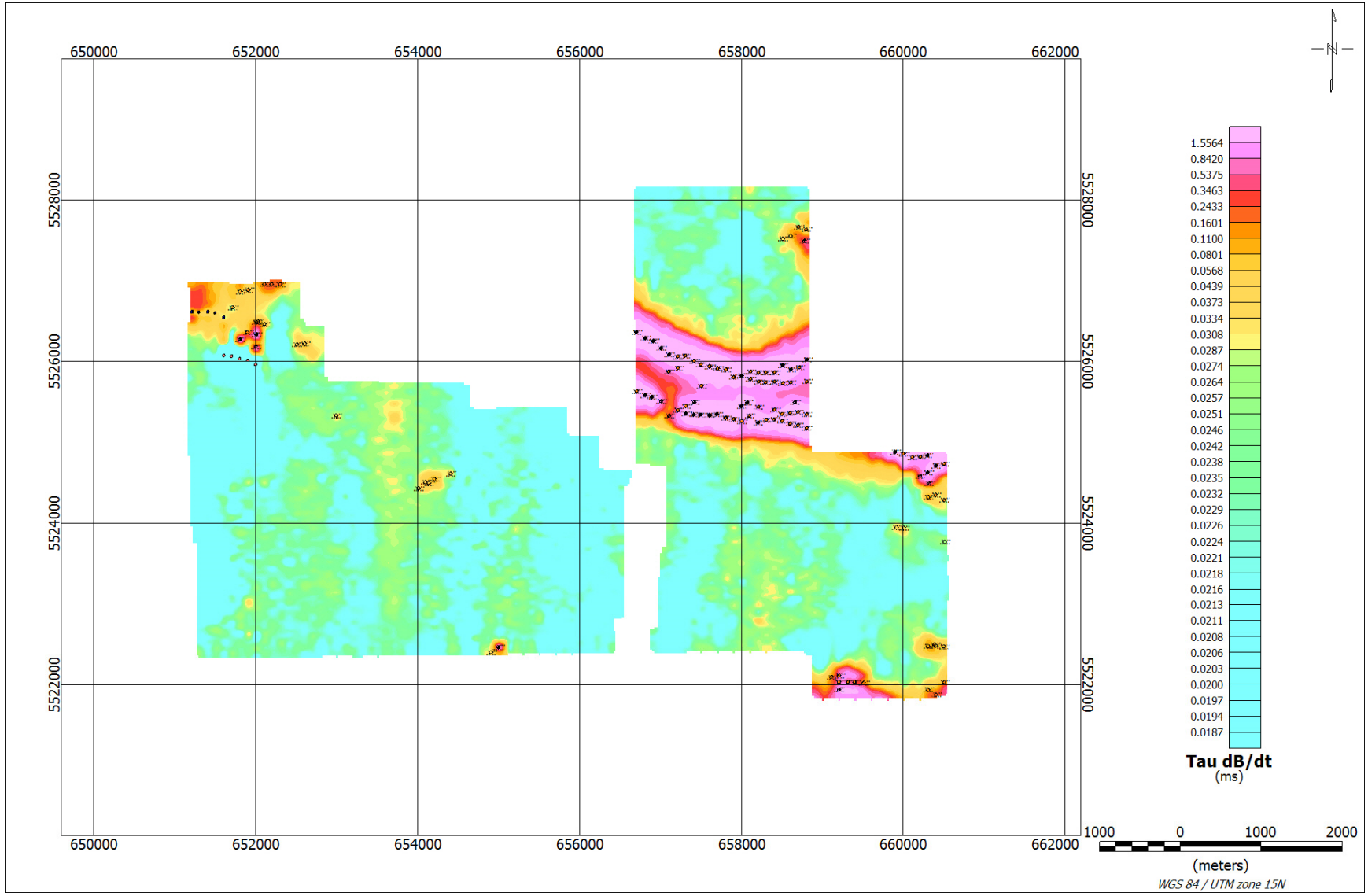


dB/dt Calculated Time Constant (Tau)

## RESISTIVITY DEPTH IMAGE (RDI) MAPS

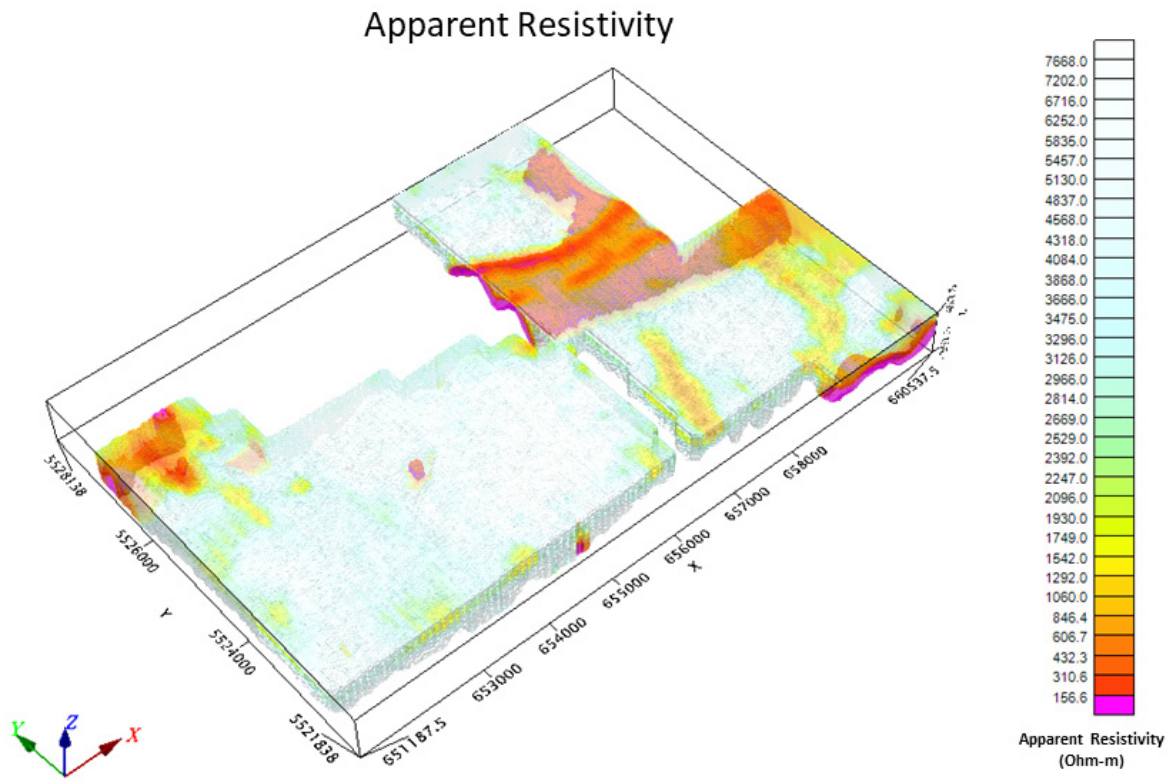


3D view of VTEM RDI Apparent Resistivity Voxel (view looking northeast)

# APPENDIX D

## GENERALIZED MODELING RESULTS OF THE VTEM SYSTEM
## INTRODUCTION

The VTEM system is based on a concentric or central loop design, whereby, the receiver is positioned at the centre of a transmitter loop that produces a primary field. The wave form is a bi-polar, modified square wave with a turn-on and turn-off at each end.

During turn-on and turn-off, a time varying field is produced (dB/dt) and an electro-motive force (emf) is created as a finite impulse response. A current ring around the transmitter loop moves outward and downward as time progresses. When conductive rocks and mineralization are encountered, a secondary field is created by mutual induction and measured by the receiver at the centre of the transmitter loop.

Efficient modeling of the results can be carried out on regularly shaped geometries, thus yielding close approximations to the parameters of the measured targets. The following is a description of a series of common models made for the purpose of promoting a general understanding of the measured results.

A set of models has been produced for the Geotech VTEM™ system dB/dT Z and X components (see models D1 to D15). The Maxwell ™ modeling program (EMIT Technology Pty. Ltd. Midland, WA, AU) used to generate the following responses assumes a resistive half-space. The reader is encouraged to review these models, so as to get a general understanding of the responses as they apply to survey results. While these models do not begin to cover all possibilities, they give a general perspective on the simple and most commonly encountered anomalies.

As the plate dips and departs from the vertical position, the peaks become asymmetrical.

As the dip increases, the aspect ratio (Min/Max) decreases and this aspect ratio can be used as an empirical guide to dip angles from near 90º to about 30º. The method is not sensitive enough where dips are less than about 30º.

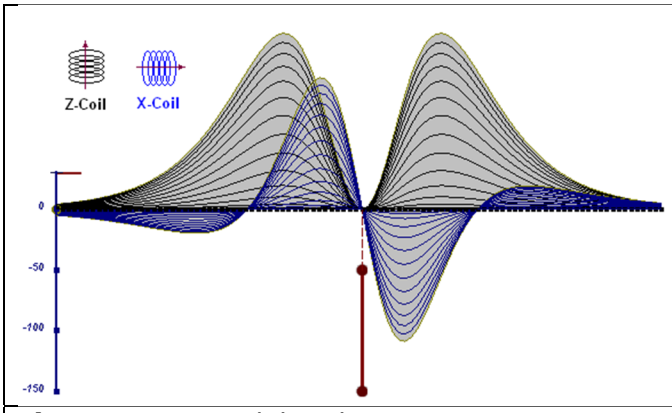


**Figure D-1**: vertical thin plate

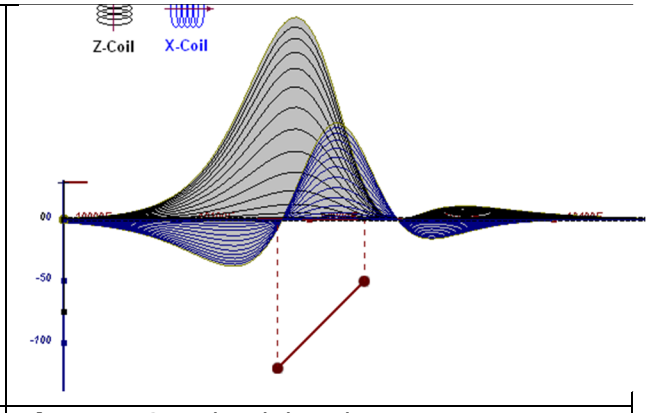


**Figure D-2**: inclined thin plate

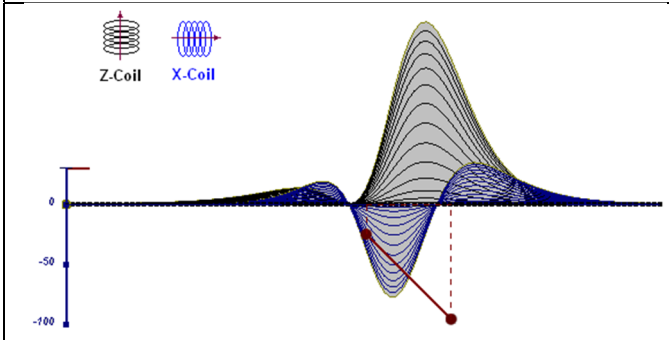


**Figure D-3**: inclined thin plate

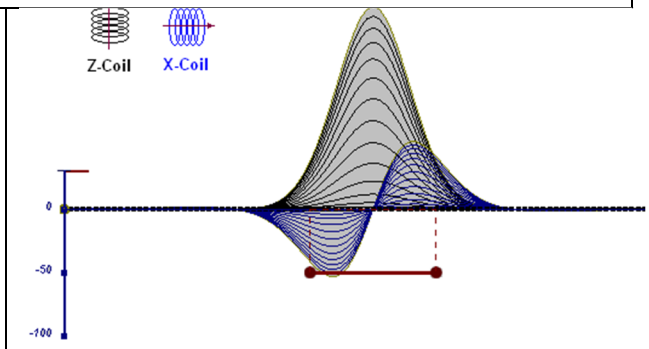


**Figure D-4**: horizontal thin plate

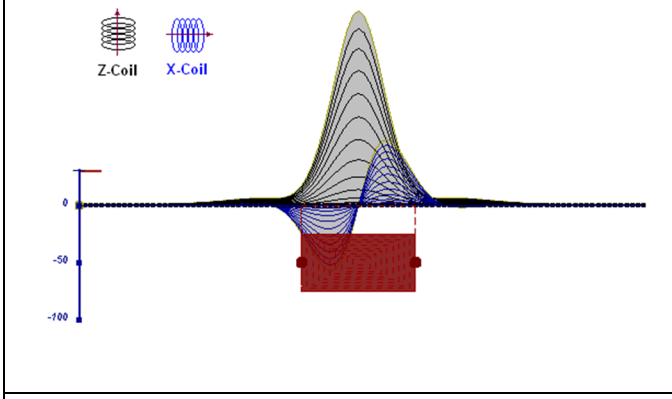


**Figure D-5**: horizontal thick plate (linear scale of the response)

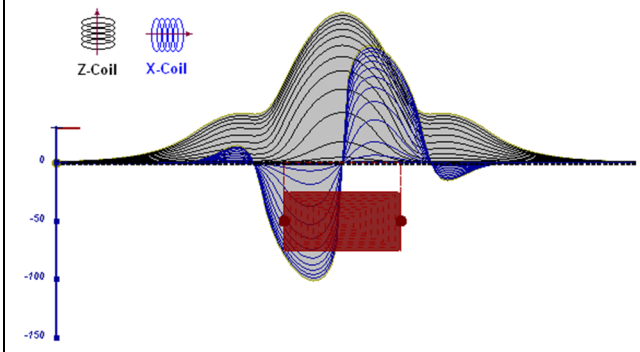


**Figure D-6**: horizontal thick plate (log scale of the response)

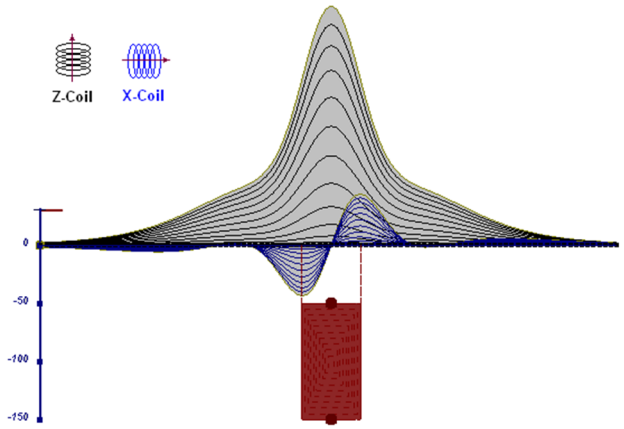


**Figure D-7**: vertical thick plate (linear scale of the response). 50 m depth

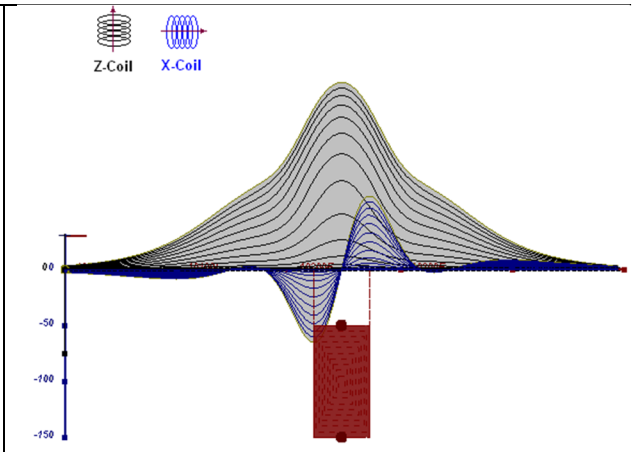


**Figure D-8**: vertical thick plate (log scale of the response). 50 m depth

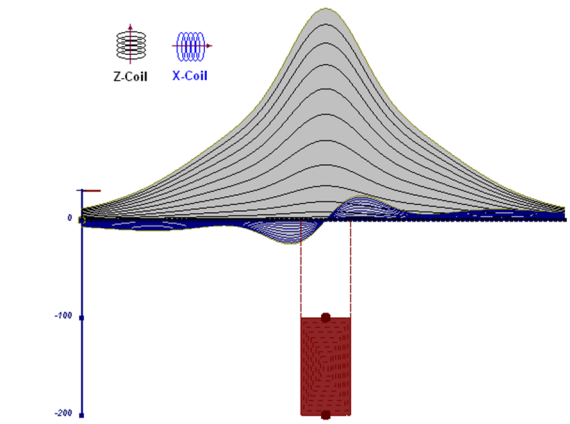


**Figure D-9**: vertical thick plate (linear scale of the response). 100 m depth

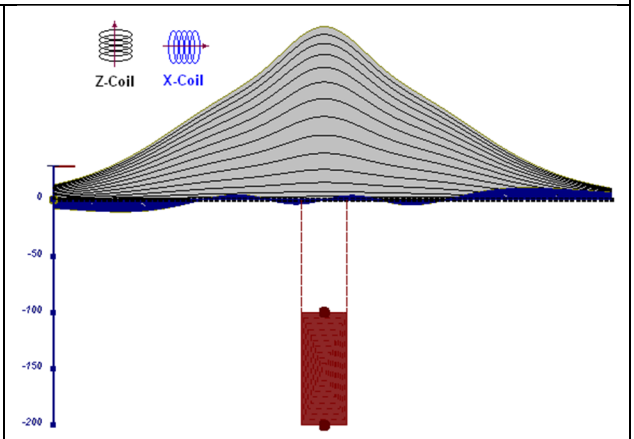


**Figure D-10**: vertical thick plate (linear scale of the response). Depth / horizontal thickness=2.5

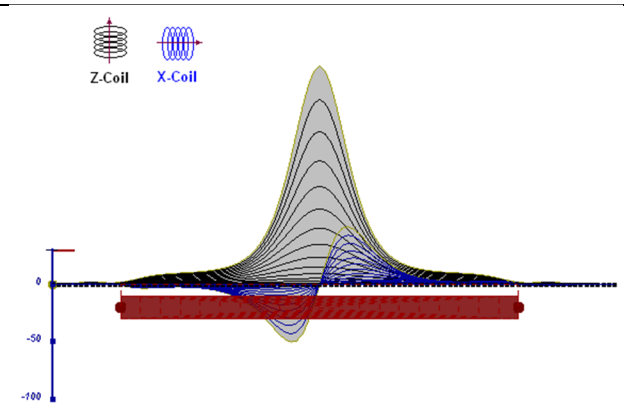


**Figure D-11**: horizontal thick plate (linear scale of the response)

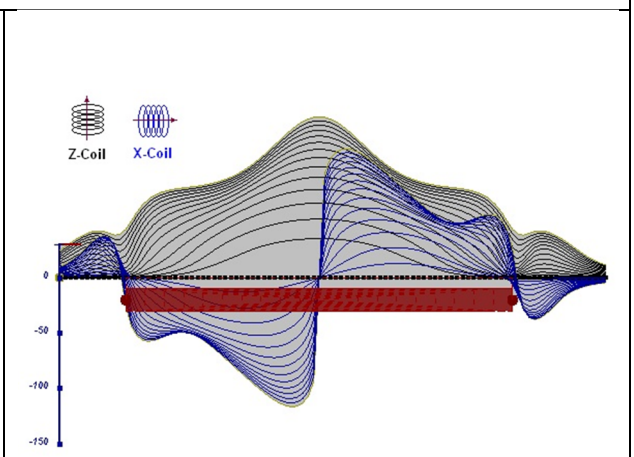


**Figure D-12**: horizontal thick plate (log scale of the response)

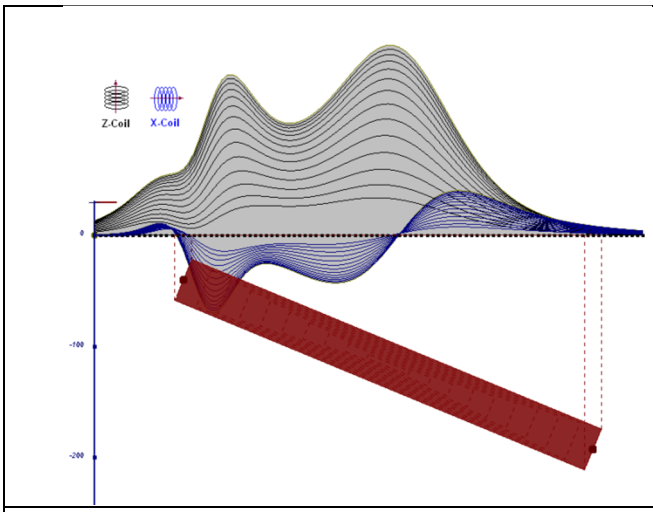


**Figure D-13**: inclined long thick plate

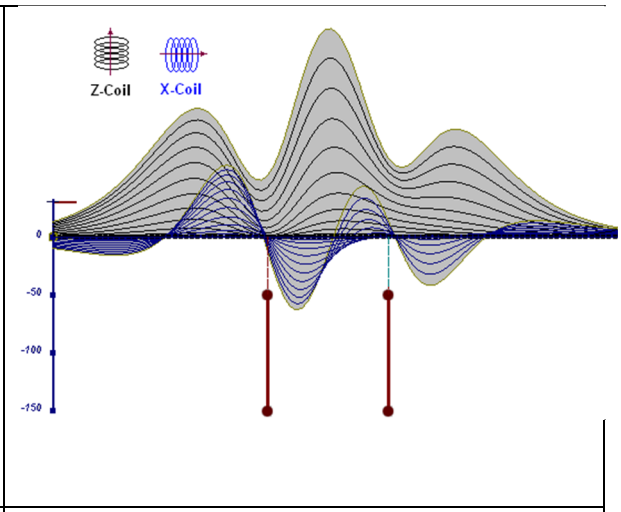


**Figure D-14**: two vertical thin plates

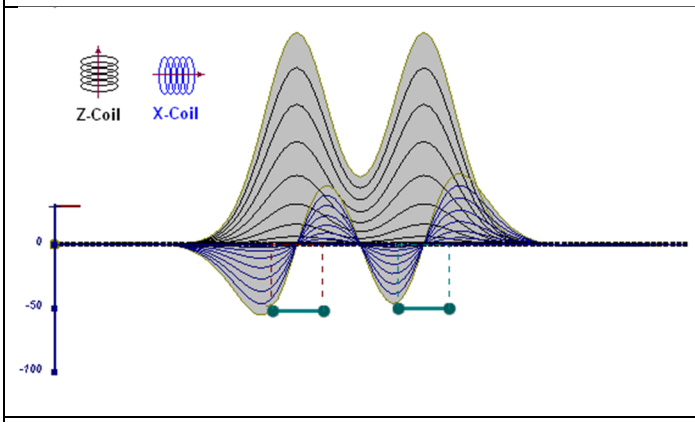


**Figure D-15**: two horizontal thin plates

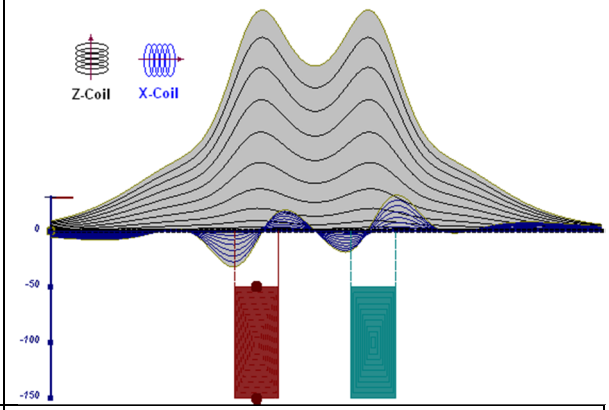


**Figure D-16**: two vertical thick plates

The same type of target but with different thickness, for example, creates different form of the response:

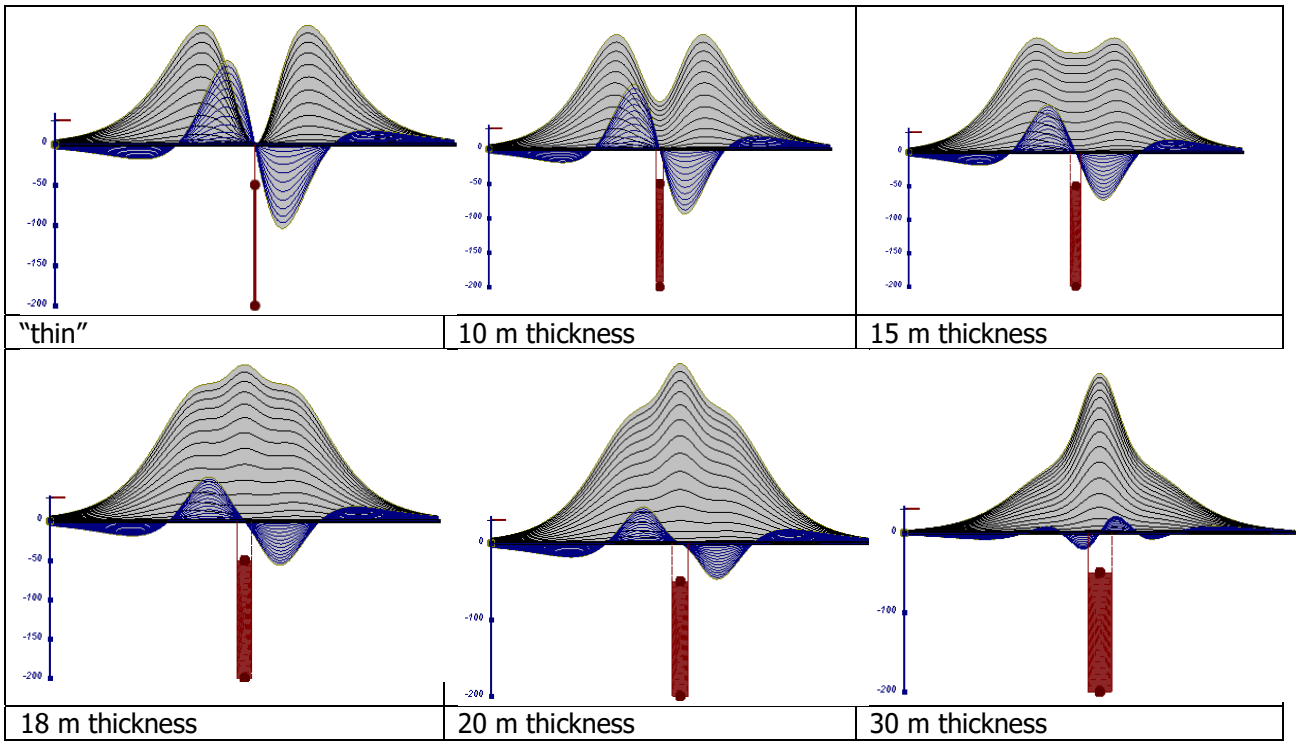


**Figure D-17**: Conductive vertical plate, depth 50 m, strike length 200 m, depth extends 150 m.

Alexander Prikhodko, PhD, P.Geo
**Geotech Ltd.**

September 2010

# APPENDIX E

## EM TIME CONSTANT (TAU) ANALYSIS

Estimation of time constant parameter[1] in transient electromagnetic method is one of the steps toward the extraction of the information about conductances beneath the surface from TEM measurements.

The most reliable method to discriminate or rank conductors from overburden, background or one and other is by calculating the EM field decay time constant (TAU parameter), which directly depends on conductance despite their depth and accordingly amplitude of the response.

## THEORY

As established in electromagnetic theory, the magnitude of the electro-motive force (emf) induced is proportional to the time rate of change of primary magnetic field at the conductor. This emf causes eddy currents to flow in the conductor with a characteristic transient decay, whose Time Constant (Tau) is a function of the conductance of the survey target or conductivity and geometry (including dimensions) of the target. The decaying currents generate a proportional secondary magnetic field, the time rate of change of which is measured by the receiver coil as induced voltage during the Off time.

The receiver coil output voltage ($\mathbf{e_0}$) is proportional to the time rate of change of the secondary magnetic field and has the form,

$$e_0 \, \alpha \, (1 / \tau) \, e^{-(t/\tau)}$$

Where,
$\tau$ = L/R is the characteristic time constant of the target (TAU)
R = resistance
L = inductance

From the expression, conductive targets that have small value of resistance and hence large value of $\tau$ yield signals with small initial amplitude that decays relatively slowly with progress of time. Conversely, signals from poorly conducting targets that have large resistance value and small$\tau$, have high initial amplitude but decay rapidly with time[1] (Fig. E1).

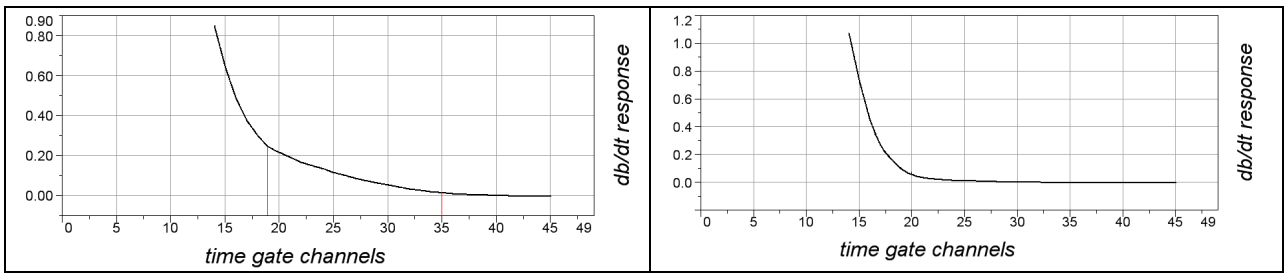


Figure E-1: Left – presence of good conductor, right – poor conductor.

[1] McNeill, JD, 1980, "Applications of Transient Electromagnetic Techniques", Technical Note TN-7 page 5, Geonics Limited, Mississauga, Ontario.

## EM Time Constant (Tau) Calculation

The EM Time-Constant (TAU) is a general measure of the speed of decay of the electromagnetic response and indicates the presence of eddy currents in conductive sources as well as reflecting the "conductance quality" of a source. Although TAU can be calculated using either the measured dB/dt decay or the calculated B-field decay, dB/dt is commonly preferred due to better stability (S/N) relating to signal noise. Generally, TAU calculated on base of early time response reflects both near surface overburden and poor conductors whereas, in the late ranges of time, deep and more conductive sources, respectively. For example early time TAU distribution in an area that indicates conductive overburden is shown in Figure 2.

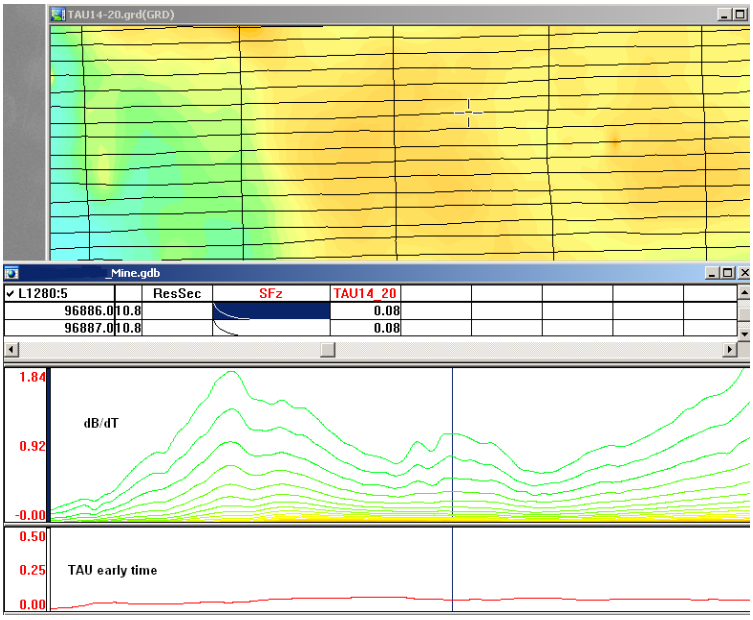


Figure E-2: Map of early time TAU. Area with overburden conductive layer and local sources.

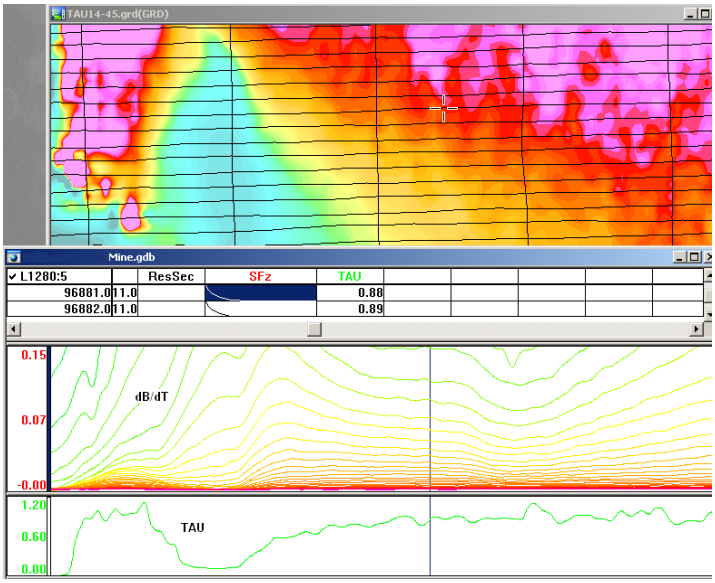

Figure E-3: Map of full time range TAU with EM anomaly due to deep highly conductive target.

There are many advantages of TAU maps:

- TAU depends only on one parameter (conductance) in contrast to response magnitude;
- TAU is integral parameter, which covers time range and all conductive zones and targets are displayed independently of their depth and conductivity on a single map.
- Very good differential resolution in complex conductive places with many sources with different conductivity.
- Signs of the presence of good conductive targets are amplified and emphasized independently of their depth and level of response accordingly.

In the example shown in Figure 4 and 5, three local targets are defined, each of them with a different depth of burial, as indicated on the resistivity depth image (RDI). All are very good conductors but the deeper target (number 2) has a relatively weak dB/dt signal yet also features the strongest total TAU (Figure 4). This example highlights the benefit of TAU analysis in terms of an additional target discrimination tool.

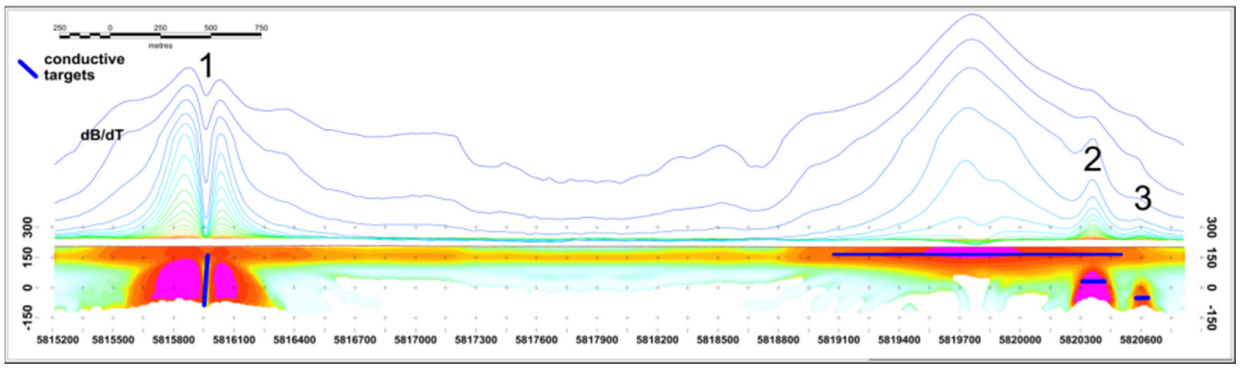


Figure E-4: dB/dt profile and RDI with different depths of targets.

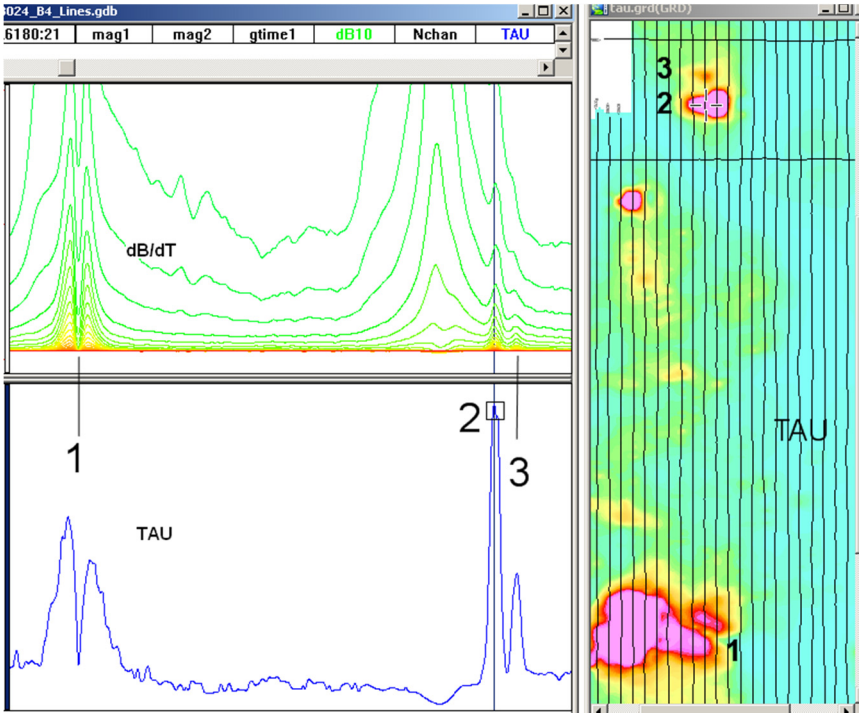

Figure E-5: Map of total TAU and dB/dt profile.

The EM Time Constants for dB/dt and B-field were calculated using the "sliding Tau" in-house program developed at Geotech2. The principle of the calculation is based on using of time window (4 time channels) which is sliding along the curve decay and looking for latest time channels which have a response above the level of noise and decay. The EM decays are obtained from all available decay channels, starting at the latest channel. Time constants are taken from a least square fit of a straight-line (log/linear space) over the last 4 gates above a pre-set signal threshold level (Figure F6). Threshold settings are pointed in the "label" property of TAU database channels. The sliding Tau method determines that, as the amplitudes increase, the time-constant is taken at progressively later times in the EM decay. Conversely, as the amplitudes decrease, Tau is taken at progressively earlier times in the decay. If the maximum signal amplitude falls below the threshold, or becomes negative for any of the 4 time gates, then Tau is not calculated and is assigned a value of "dummy" by default.

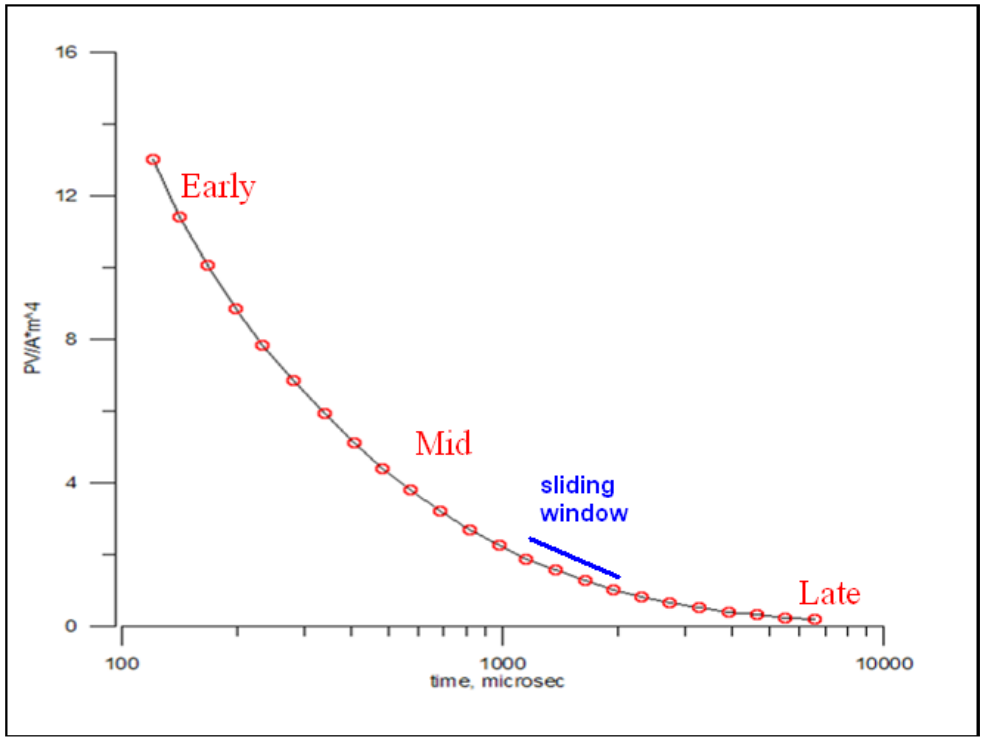


Figure E-6: Typical dB/dt decays of VTEM data

Alexander Prikhodko, PhD, P.Geo
**Geotech Ltd.**

September 2010

[2] by A.Prikhodko

# APPENDIX F

## TEM RESISTIVITY DEPTH IMAGING (RDI)

Resistivity depth imaging (RDI) is technique used to rapidly convert EM profile decay data into an equivalent resistivity versus depth cross-section, by deconvolving the measured TEM data.
The used RDI algorithm of Resistivity-Depth transformation is based on scheme of the apparent resistivity transform of Maxwell A.Meju (1998)[1] and TEM response from conductive half-space. The program is developed by Alexander Prikhodko and depth calibrated based on forward plate modeling for VTEM system configuration (Fig. 1-10).

RDIs provide reasonable indications of conductor relative depth and vertical extent, as well as accurate 1D layered-earth apparent conductivity/resistivity structure across VTEM flight lines. Approximate depth of investigation of a TEM system, image of secondary field distribution in half space, effective resistivity, initial geometry and position of conductive targets is the information obtained on base of the RDIs.

Maxwell forward modeling with RDI sections from the synthetic responses (VTEM system).

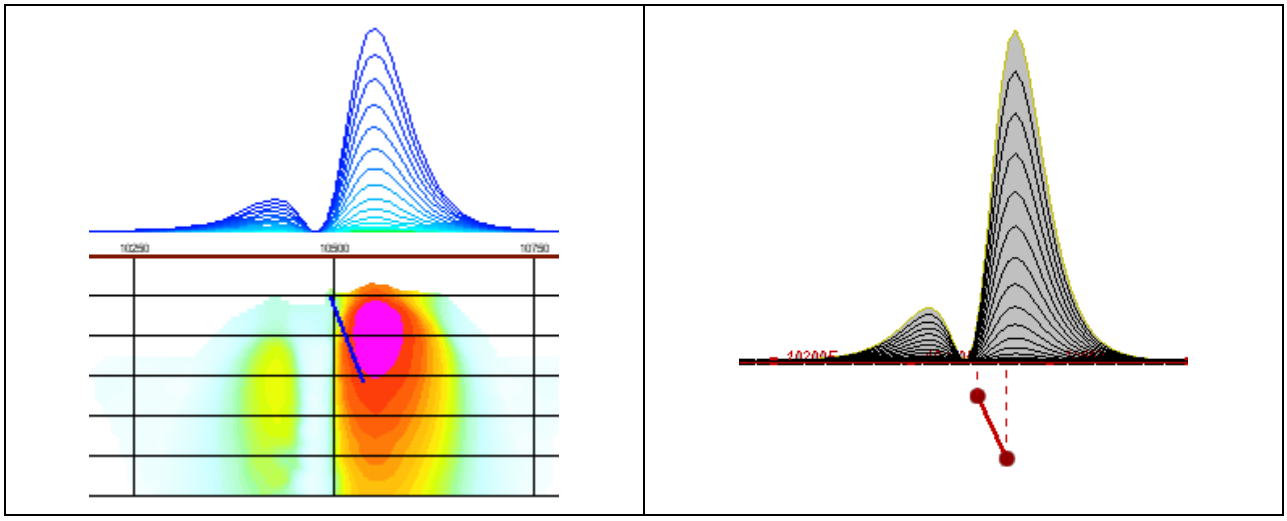

Figure F-1: Maxwell plate model and RDI from the calculated response for conductive "thin" plate (depth 50 m, dip 65 degree, depth extend 100 m).

[1] Maxwell A.Meju, 1998, Short Note: A simple method of transient electromagnetic data analysis, Geophysics, **63**, 405–410.

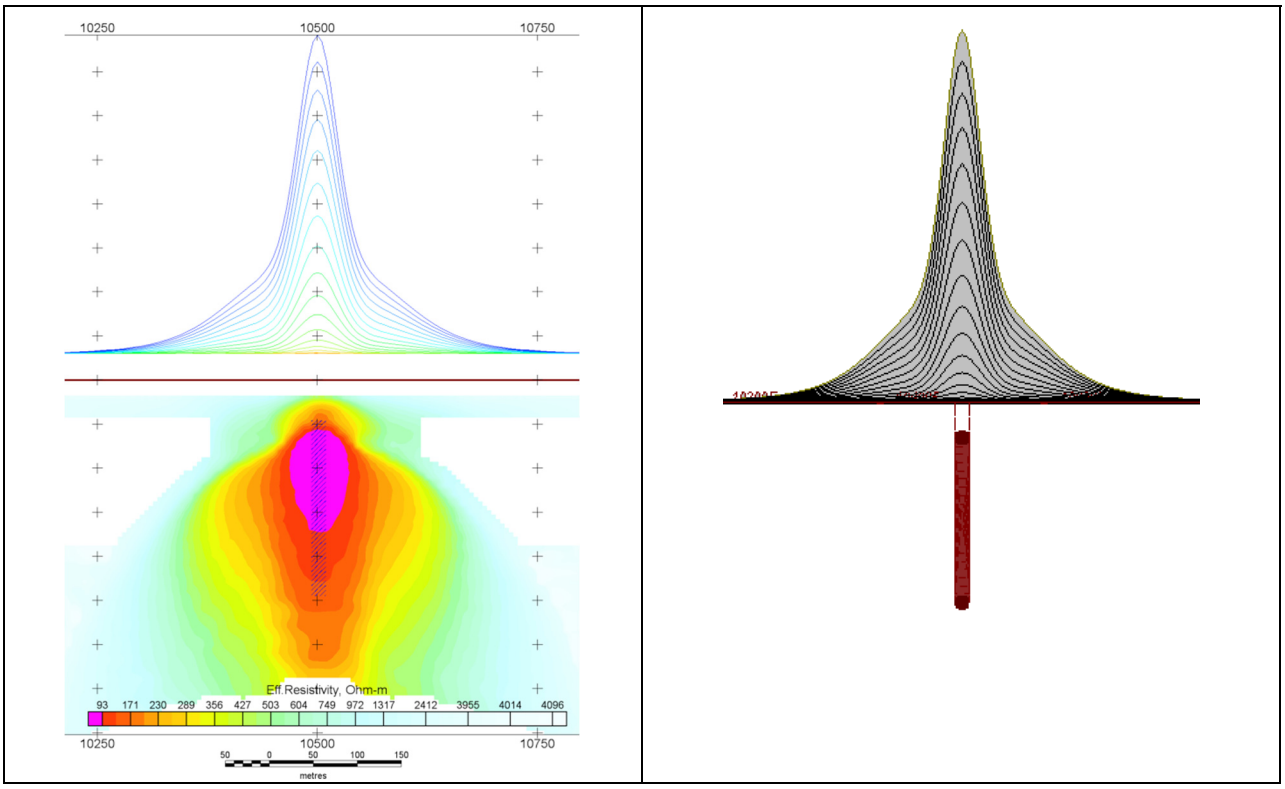


Figure F-2: Maxwell plate model and RDI from the calculated response for "thick" plate 18 m thickness, depth 50 m, depth extend 200 m).

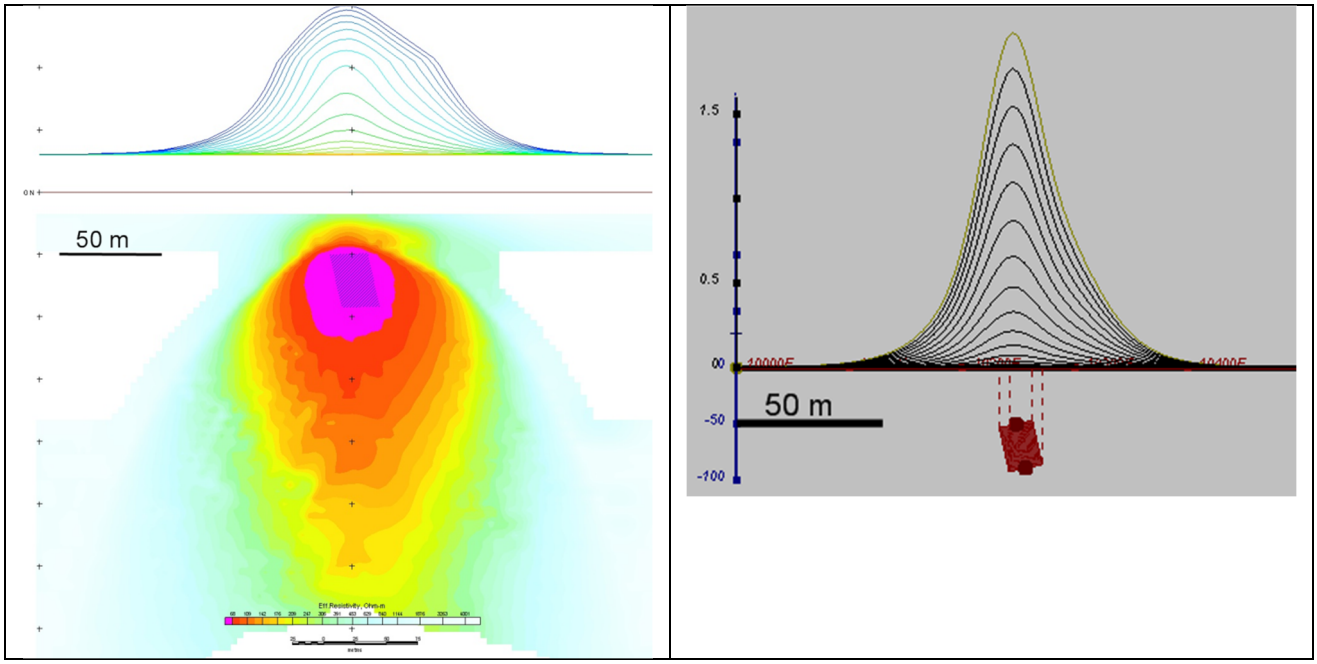


Figure F-3: Maxwell plate model and RDI from the calculated response for bulk ("thick") 100 m length, 40 m depth extend, 30 m thickness

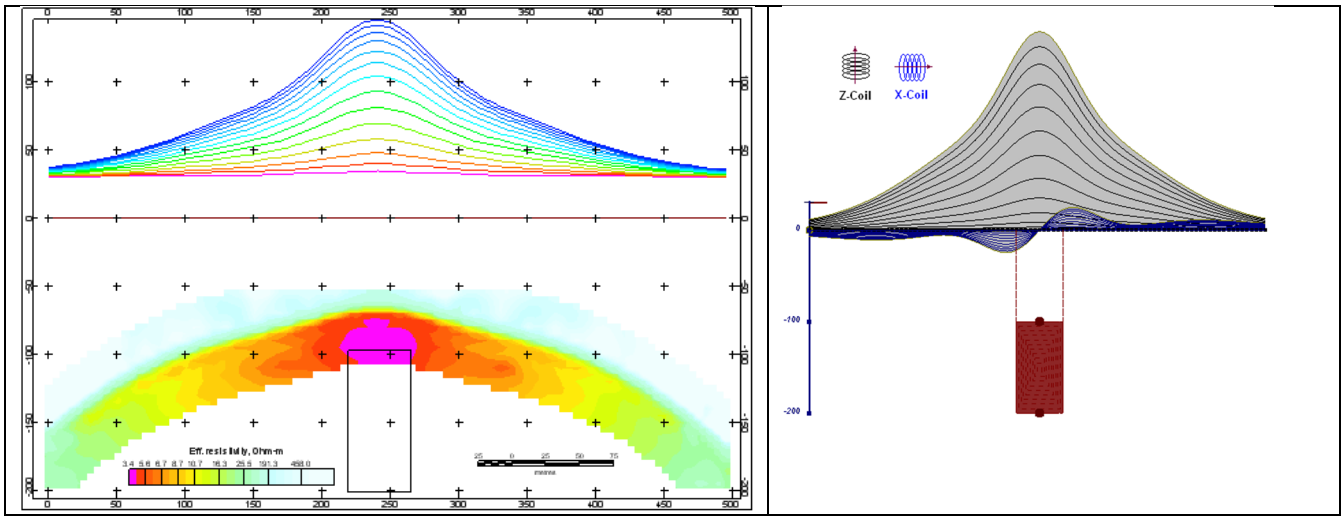


Figure F-4: Maxwell plate model and RDI from the calculated response for "thick" vertical target (depth 100 m, depth extend 100 m). 19-44 chan.

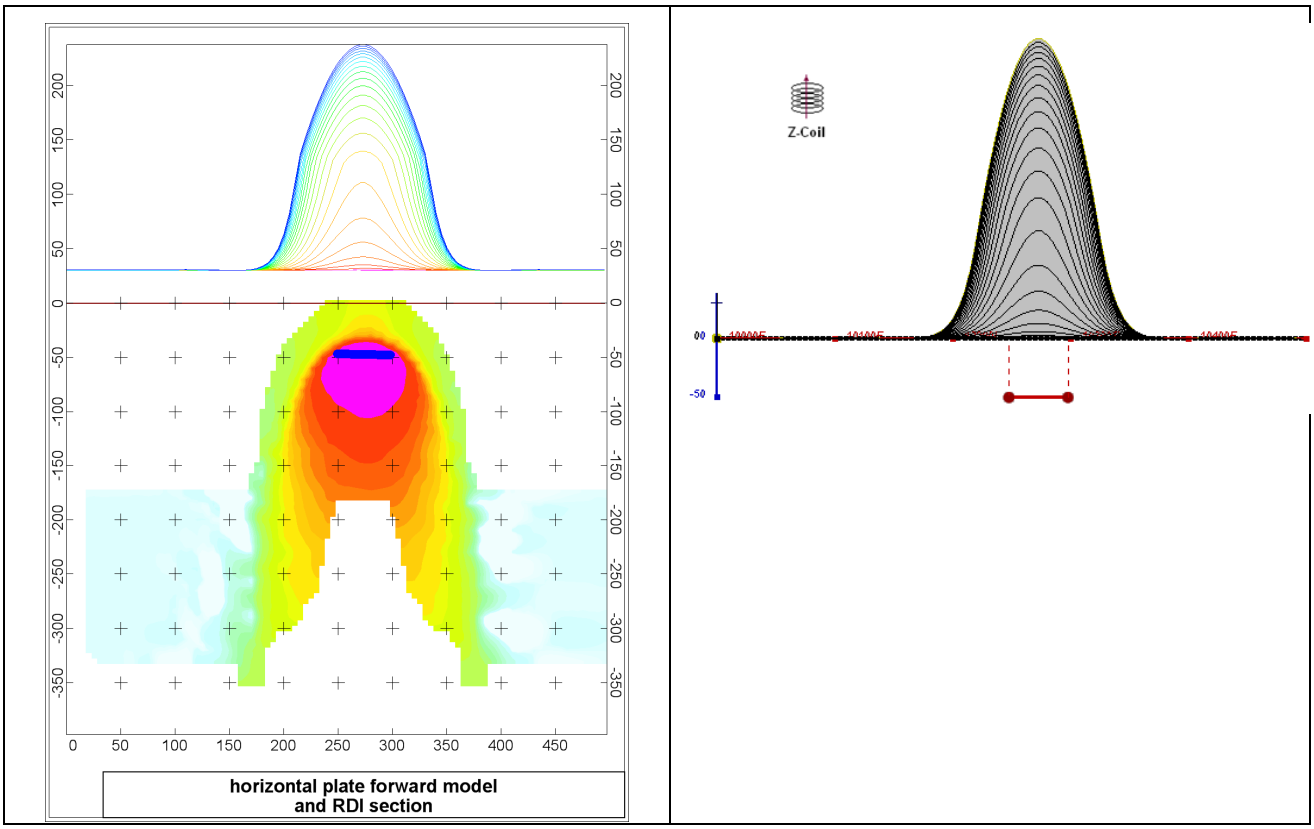


Figure F-5: Maxwell plate model and RDI from the calculated response for horizontal thin plate (depth 50 m, dim 50x100 m). 15-44 chan.

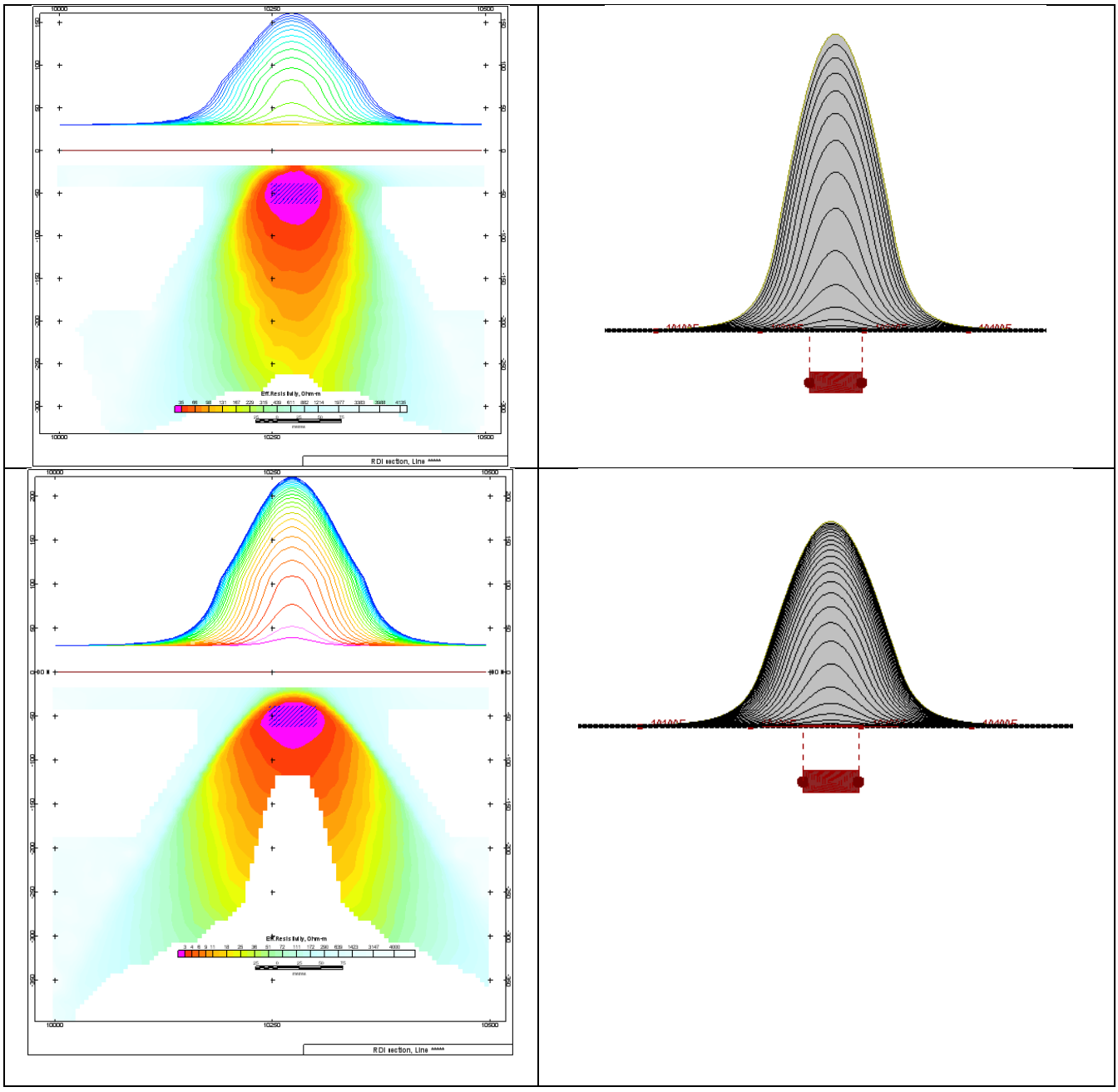


Figure F-6: Maxwell plate model and RDI from the calculated response for horizontal thick (20m) plate – less conductive (on the top), more conductive (below).

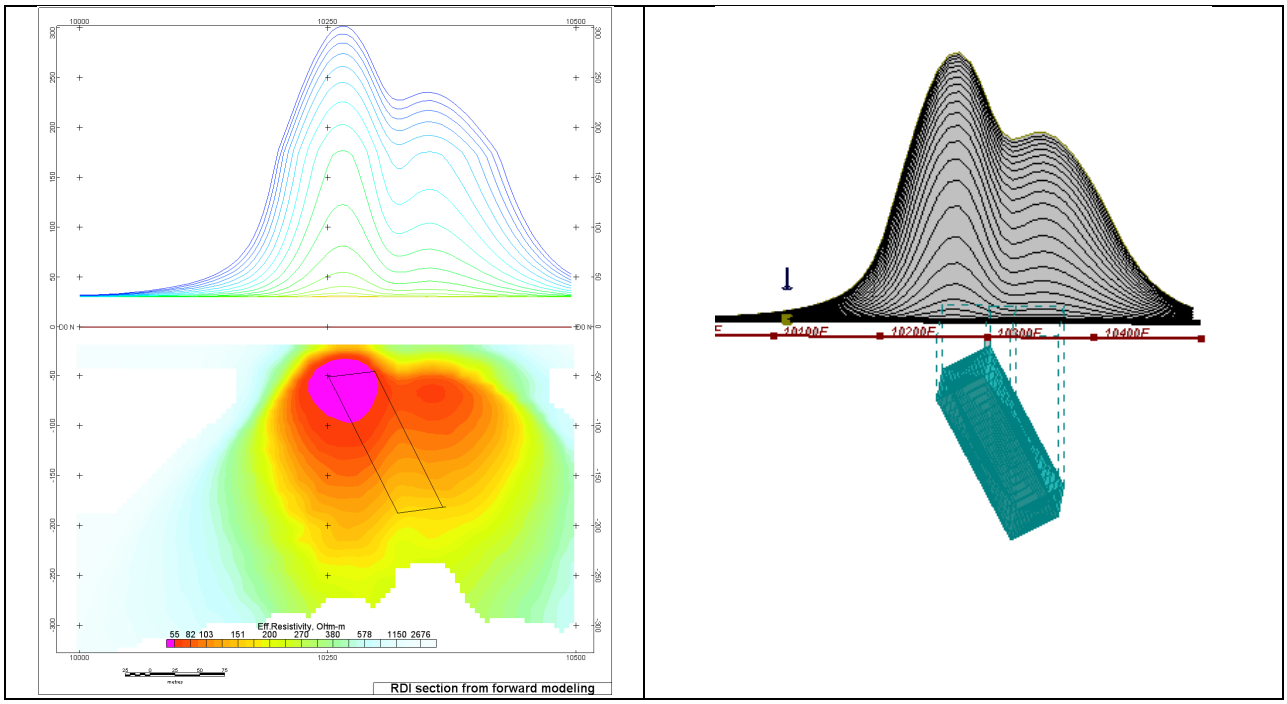


Figure F-7: Maxwell plate model and RDI from the calculated response for inclined thick (50m) plate. Depth extends 150 m, depth to the target 50 m.

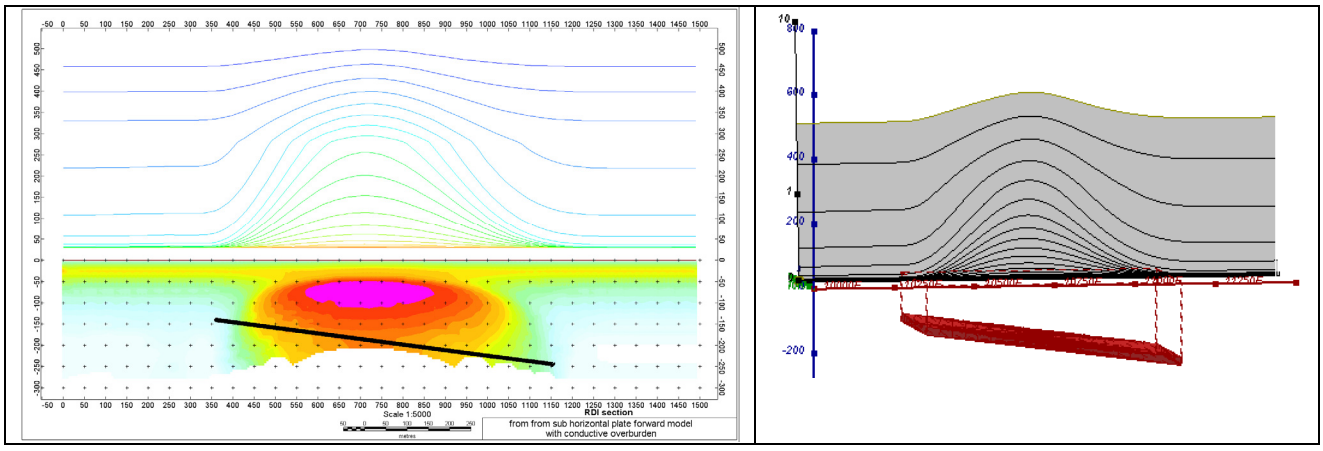


Figure F-8: Maxwell plate model and RDI from the calculated response for the long, wide and deep subhorizontal plate (depth 140 m, dim 25x500x800 m) with conductive overburden.

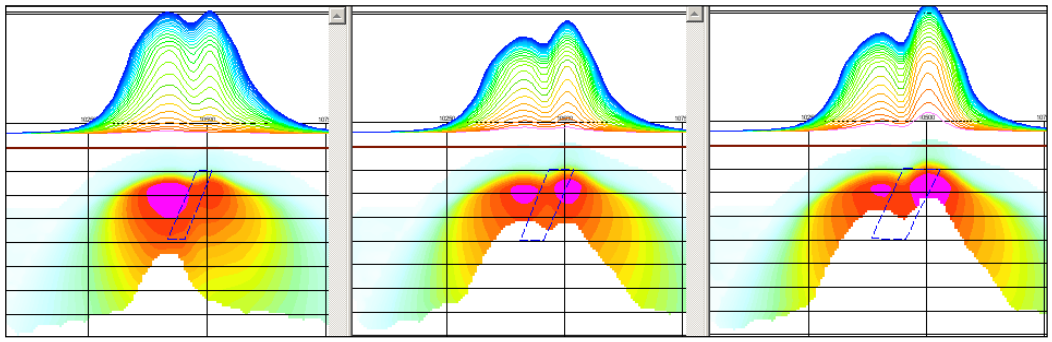

Figure F-9: Maxwell plate models and RDIs from the calculated response for "thick" dipping plates (35, 50, 75 m thickness), depth 50 m, conductivity 2.5 S/m.

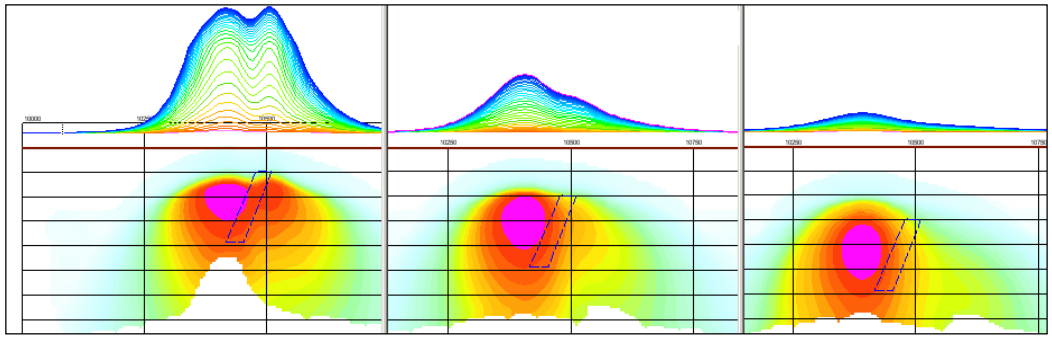

Figure F-10: Maxwell plate models and RDIs from the calculated response for "thick" (35 m thickness) dipping plate on different depth (50, 100, 150 m), conductivity 2.5 S/m.

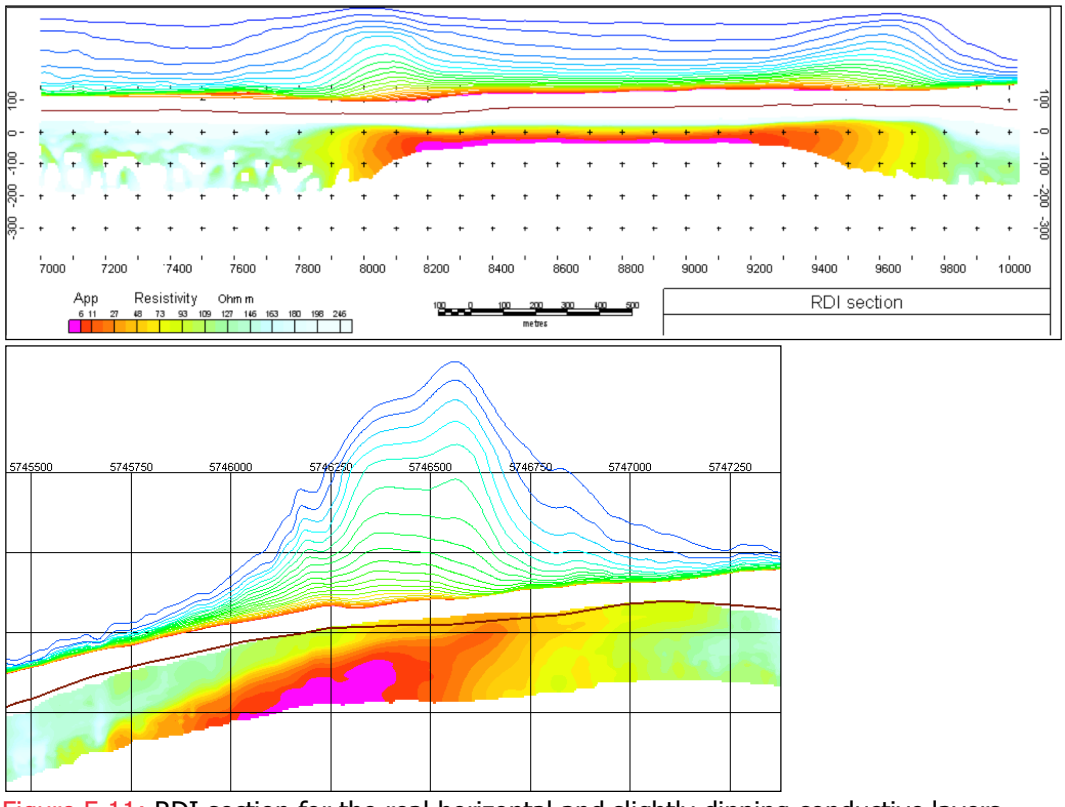


Figure F-11: RDI section for the real horizontal and slightly dipping conductive layers

# FORMS OF RDI PRESENTATION

## PRESENTATION OF SERIES OF LINES

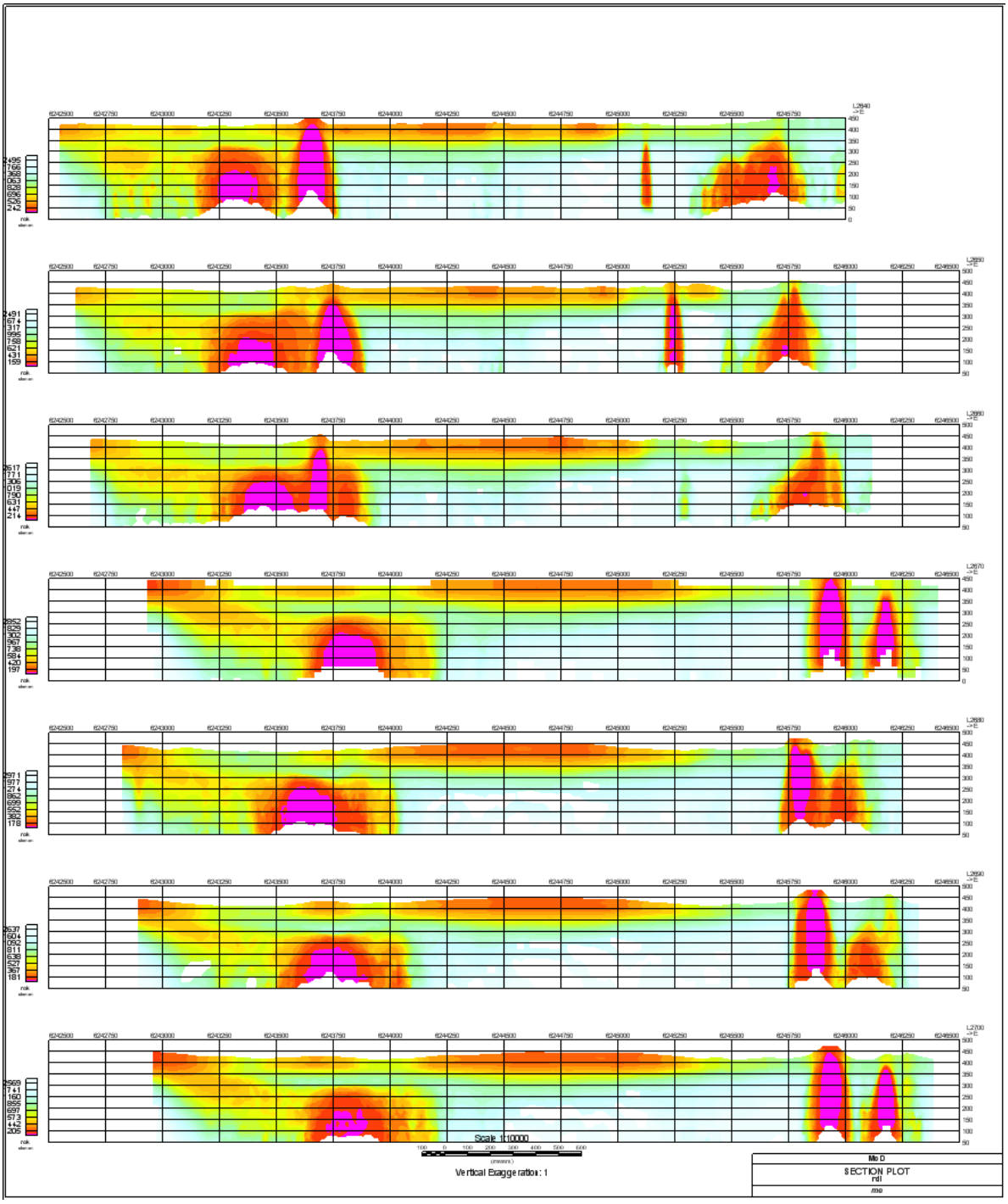

## 3D PRESENTATION OF RDIS

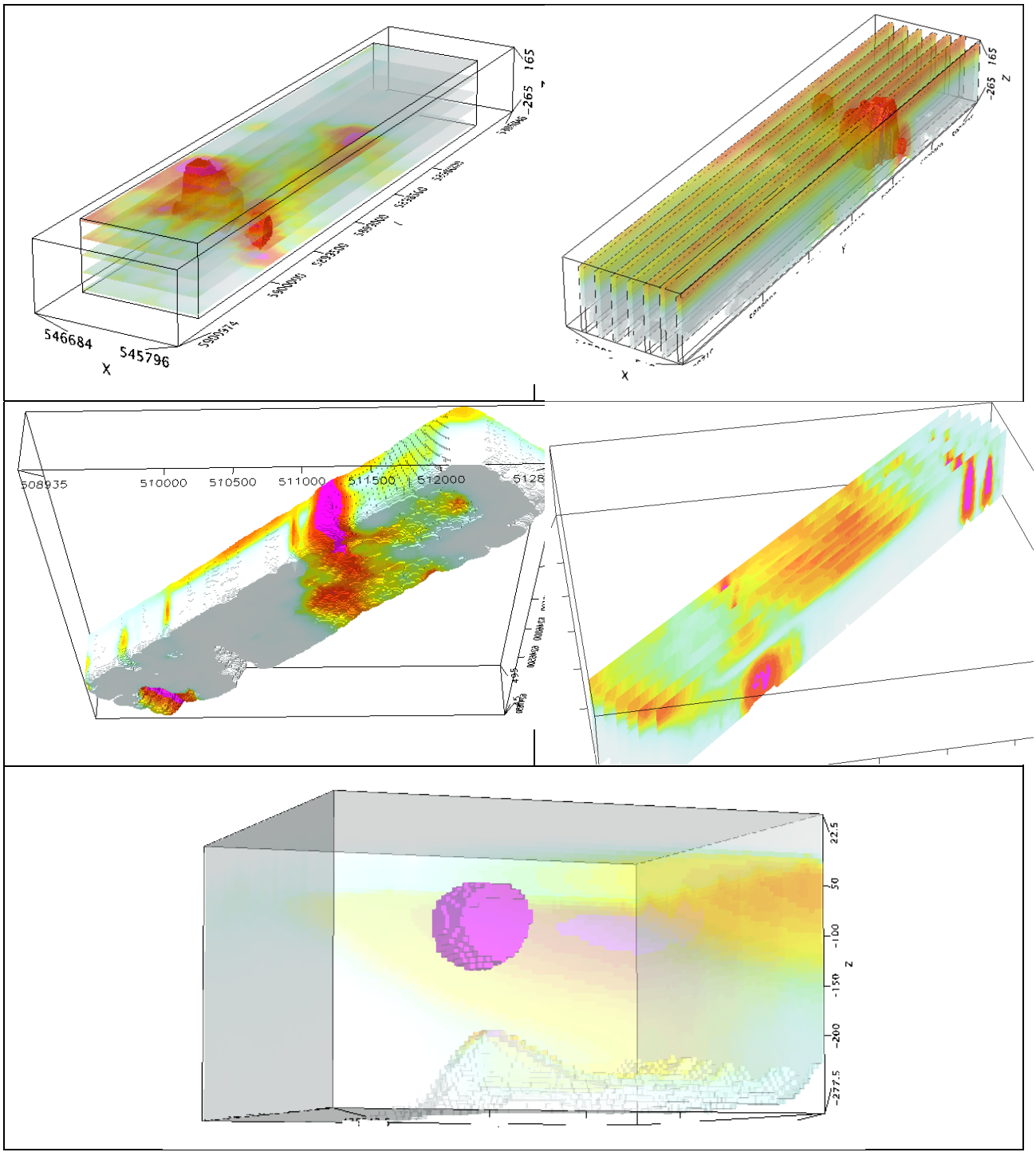

## APPARENT RESISTIVITY DEPTH SLICES PLANS:

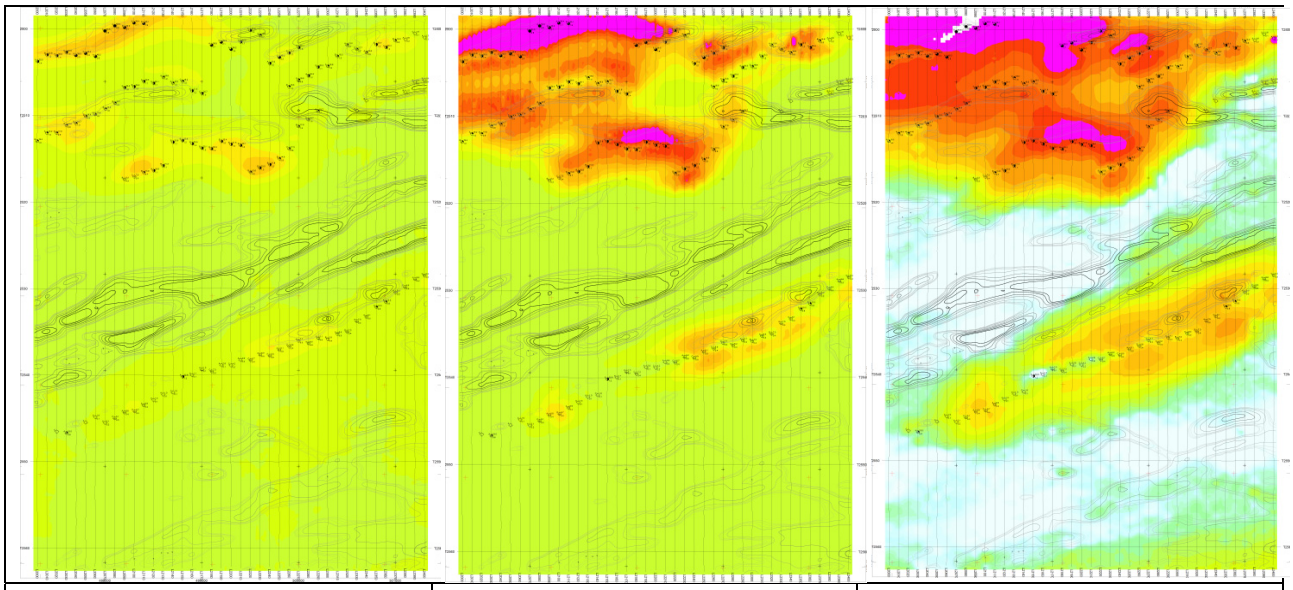

| 0 m (surface) | -100 m | -200 m |
|---|---|---|

## 3D VIEWS OF APPARENT RESISTIVITY DEPTH SLICES:

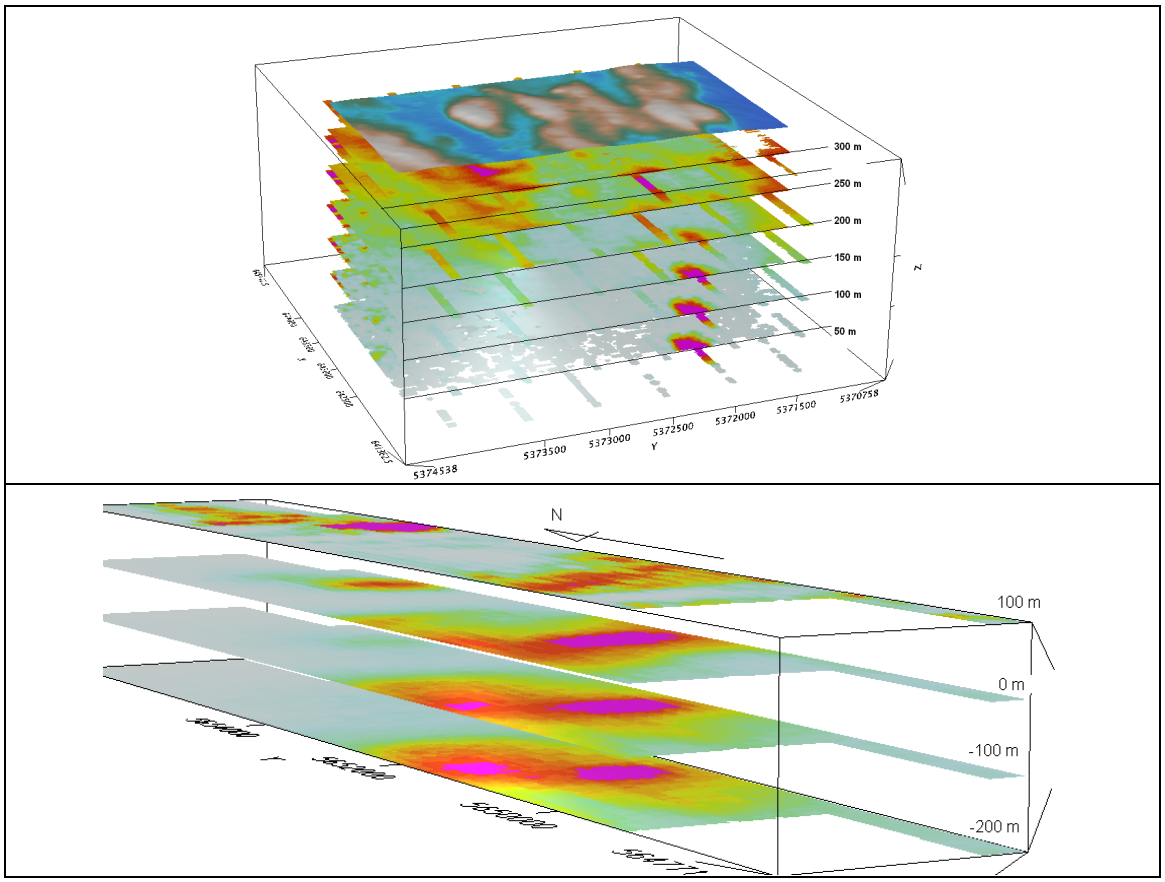

## REAL BASE METAL TARGETS IN COMPARISON WITH RDIS:

RDI section of the line over Caber deposit ("thin" subvertical plate target and conductive overburden.

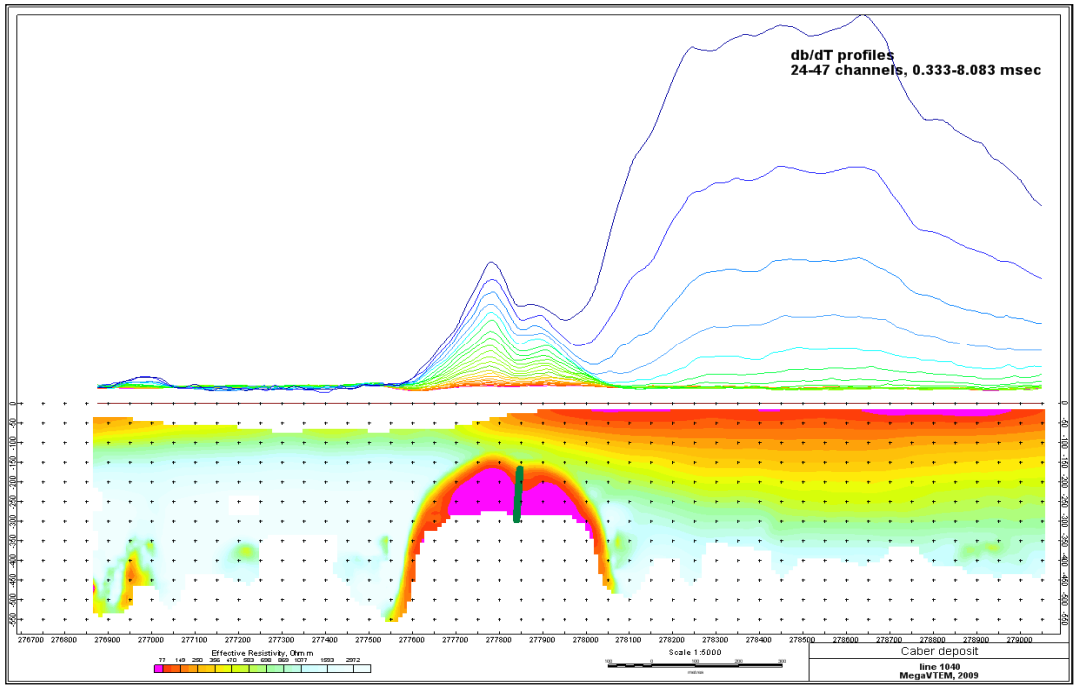


## 3D RDI VOXELS WITH BASE METALS ORE BODIES (MIDDLE EAST):

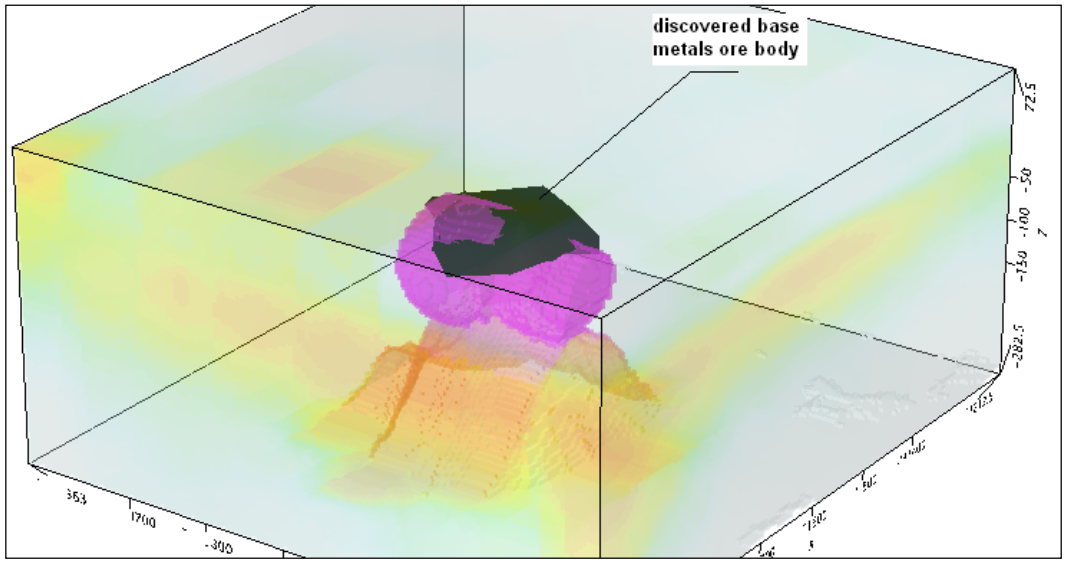

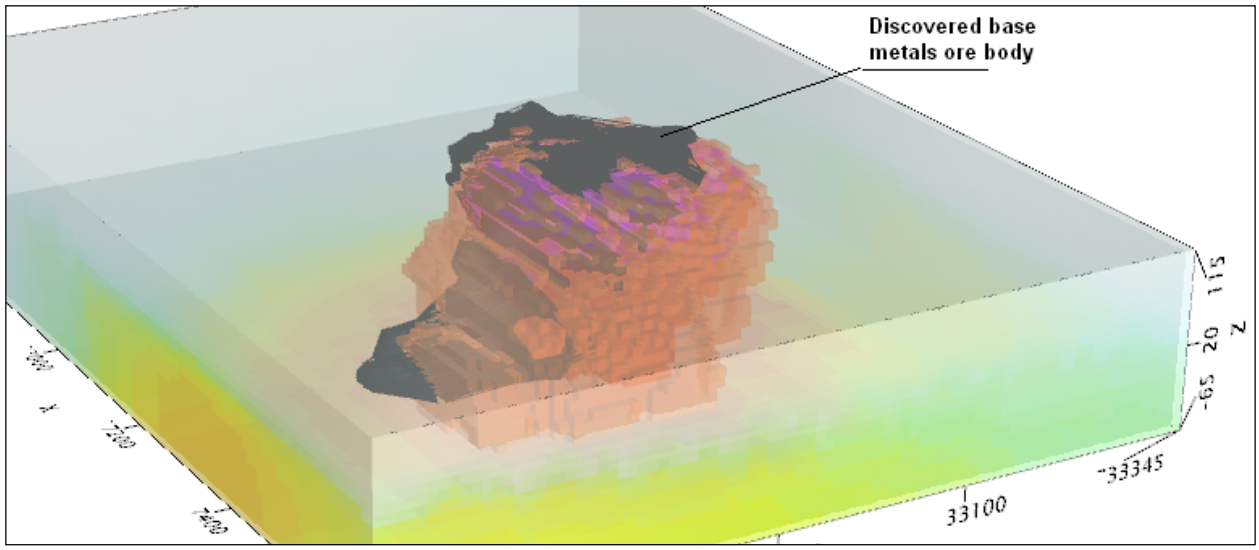


Alexander Prikhodko, PhD, P.Geo
**Geotech Ltd.**
April 2011

# APPENDIX G

## RESISTIVITY DEPTH IMAGES (RDI)

Please see RDI Folder on DVD for the PDF's

# VTEM™ MAX

## EM ANOMALY SUMMARY ON A HELICOPTER-BORNE VERSATILE TIME DOMAIN ELECTROMAGNETIC (VTEM™ MAX) AND AEROMAGNETIC GEOPHYSICAL SURVEY

| | |
|---|---|
| PROJECT: | Sturgeon Lake Property |
| LOCATION: | Sioux Lookout, Ontario |
| FOR: | Odin Metals LTD |
| SURVEY FLOWN: | April-May 2019 |
| PROJECT: | GL190069 |

Geotech Ltd.
245 Industrial Parkway North
Aurora, ON Canada L4G 4C4

Tel: +1 905 841 5004
Web: www.geotech.ca
Email: info@geotech.ca

GEOTECH
AIRBORNE GEOPHYSICAL SURVEYS

# TABLE OF CONTENTS



# LIST OF FIGURES



# LIST OF TABLES

NO TABLE OF FIGURES ENTRIES FOUND.

# APPENDICES

# EXECUTIVE SUMMARY

## EM anomaly summary on VTEM™ MAX survey of Sturgeon Lake property, Sioux Lookout, Ontario

During April 25th to May 15th, 2019 Geotech Ltd. carried out a helicopter-borne geophysical survey over the Sturgeon Lake Property situated near Sioux Lookout, Ontario.

Principal geophysical sensors included a versatile time domain electromagnetic (VTEM™ MAX) system and a caesium magnetometer. Ancillary equipment included a GPS navigation system and a radar altimeter. A total of 414 line-kilometres of geophysical data were acquired during the survey.

Geotech Ltd carried out EM anomaly picking of the VTEM data.

Final deliverable products are:

- EM anomaly picks database and map;
- EM Anomaly summary.

# 1. SURVEY LOCATION

The VTEM MAX survey is located approximately 80 kilometers SE of Sioux Lookout in northwestern Ontario (Figure 1).


Figure 1: The location of the VTEM survey in the James Bay region of Quebec, over Google Earth Image.

The VTEM survey was flown in a north to south (N 0° E Azimut) direction with nominal traverse line spacing of 100 meters.

# 2. EM ANOMALY

### *EM Induction time-constant*

Induction time constant TAU τ is a measure of the rate of decay of electromagnetic (EM) induction in the ground. The EM induction can be created by a man-made EM source from a time-domain electromagnetic (TDEM) system. The measured parameter of an airborne TDEM system, such as VTEM, is the voltage induced in the receiver (RX). It is proportional to the time rate of change of the secondary magnetic field $\frac{dB}{dt}$, according to Faraday's Law. The induced eddy current in a conductor, and the corresponding induced voltage in a receiver (RX), can be analyzed by an equivalent Resistor-Inductor (RL) circuit. The analysis of a RL circuit shows the RX voltage $v(t)$ drops exponentially with a time-constant τ, i.e., $v(t) \propto e^{-\frac{t}{\tau}}$. Time-constant τ can be used to discriminate conductors. Induced eddy-current in good conductors decays slowly, thus having large τ's, while the eddy-current in poor conductors decays rapidly with small τ's (McNeil, 1980). The computation of time constant τ is accomplished using the so-called "Sliding TAU" method developed by Geotech. The method uses a time window (normally consisting of four time channels) moving along the decay curve and above the user-defined noise level. This method tends to favor late-time channels and therefore deep basement conductors.

It was shown by Nabighian 1979 that the EM induction time-constant TAU computed from dB/dt Z channels is proportional to half-space conductivity, i.e., $\tau \propto \sigma\mu a^2$, where σ is the conductivity, μ is the permeability of the half-space and $a$ is the radius of the induced downward and outward moving secondary current filament of diminishing amplitude, the so-called "smoke ring".

The EM induction time-constant TauSF data, computed from the dB/dt Z channels, are shown in Figure 2. There is a conductive trend in the center of the VTEM. Two major conductive trends are observed in the TauSF data in the northeast region of the VTEM block. A minor conductive trend is also seen in the SE corner.

A known Cu occurrence (Claw Lake) is located in the central region of the VTEM survey (sourced from MNDM Mineral Deposit Inventory – MDI).

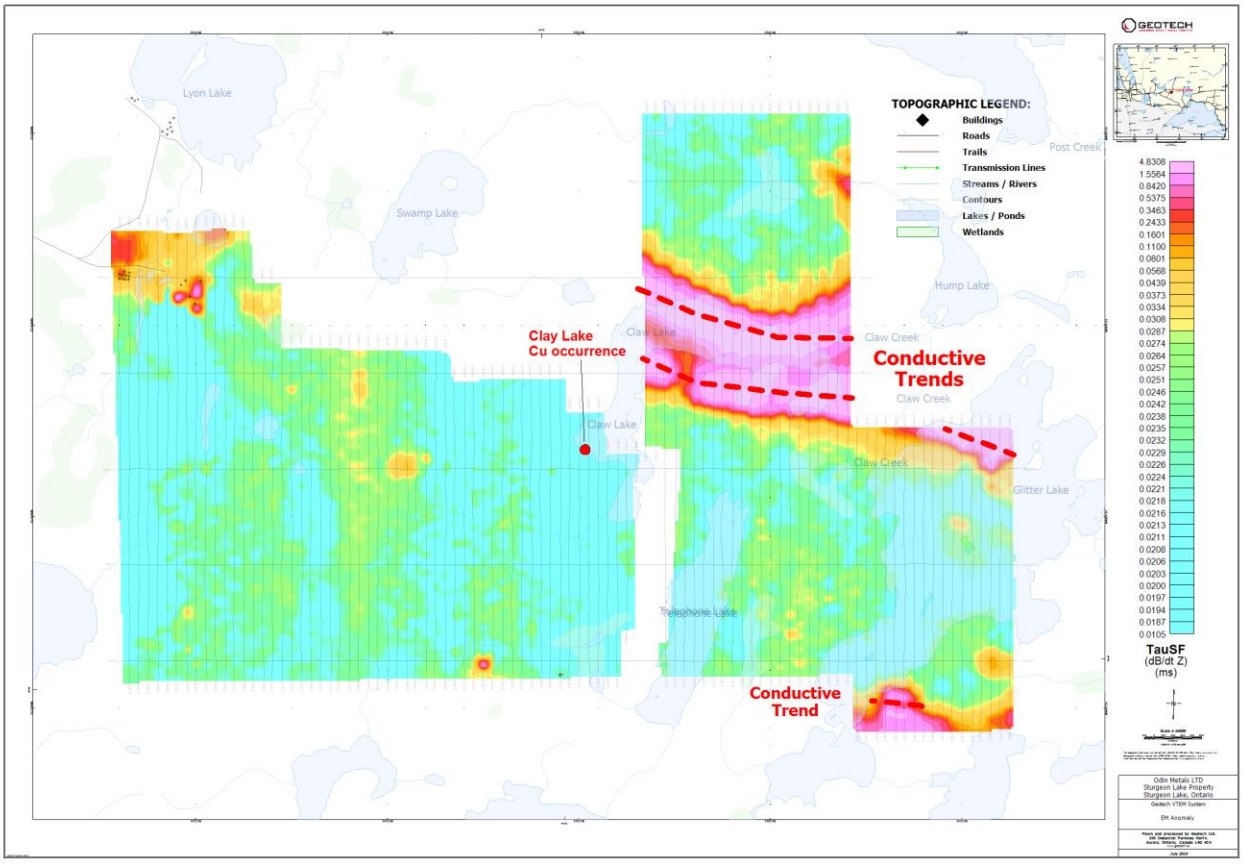


Figure 2: The EM induction time-constant TauSF (from dB/dt Z) data.

## *EM Anomalies*

The objective of picking EM anomalies in the VTEM data from the Pikwa project is to identify local and discrete EM anomalies.

The EM data were examined for anomalous responses using all time domain EM channels for the dB/dt and B-Field profiles. The resulting EM anomaly picks are presented as overlays in a Geosoft map and approximately correspond to the position of the target's center projected onto surface.

Each individual conductor pick is represented by an anomaly symbol classified according to calculated conductance[1].

[1] Note: Conductance values were obtained from the dB/dt and B-Field EM time constants (Tau) whose relationships to Tau were calculated using the oblate spheroid model of McNeill (1980, TN-7, "Applications of Transient EM Techniques").

Identified anomalies were classified into one of six categories, as shown in Figure 3. The anomaly symbol is accompanied by postings denoting the calculated dB/dt conductance, calculated dB/dt and B-field decay constant (Tau). Each symbol is also accompanied by an anomaly identification letter, e.g., A, B, C...etc., uniquely defined for each flight line. Double peak anomalies in the dB/dt data (sub-vertical and thin conductors) are distinguished by an orange dot inside the anomaly symbol. The anomalous responses are picked, reviewed and edited on a line by line basis to discriminate between bedrock, overburden and culture conductors.

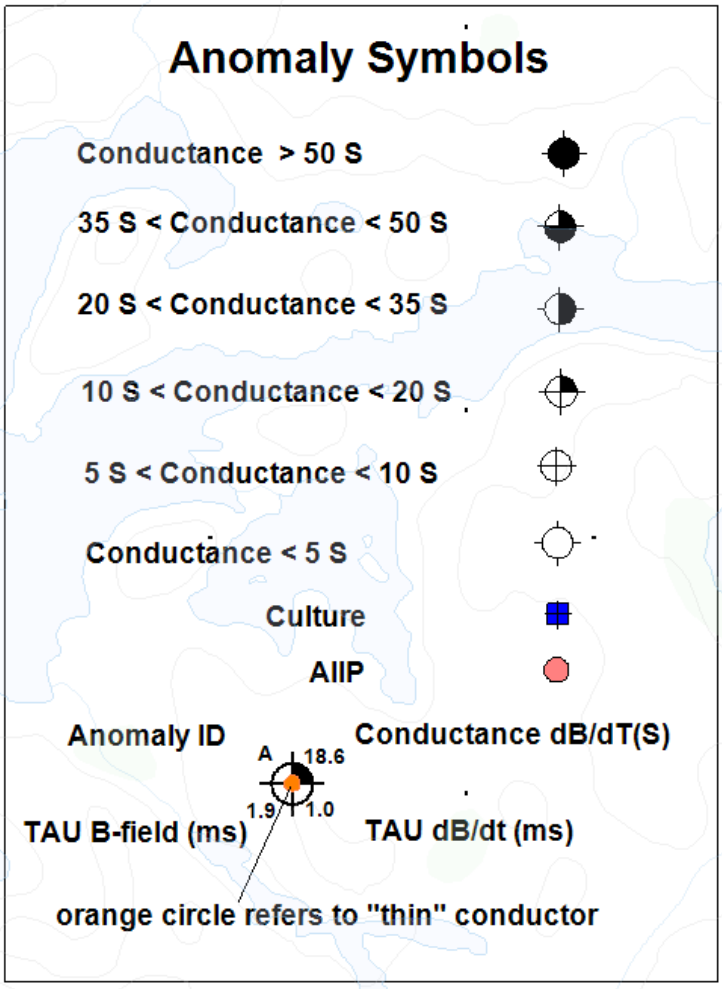


Figure 3: EM anomaly legends.

A total of 123 single and double-peak anomalies were picked in the VTEM block. The EM time-constants and the associated conductances of these anomalies are summarized below.

| Conductance, Siemens dB/dt Z component (min-max) | Conductance, Siemens B-field Z component (min-max) | TAU dB/dt, msec, min-max | TAU B-field, msec, min-max |
|---|---|---|---|
| 0.52- 89.71 | 0.00 - 191.26 | 0.03 - 4.82 | 0.00 - 10.28 |

The picked EM anomalies over the EM induction time-constant TAU data are shown in Figure 4. As shown, most of the strong (high conductance), sub-vertical (thin) conductors are located along the conductive trends. In the NW corner of the block, there is an area with extensive cultural artefacts or buildings. EM anomalies picked in this area should be treated with caution, as they may very well be related to culture.

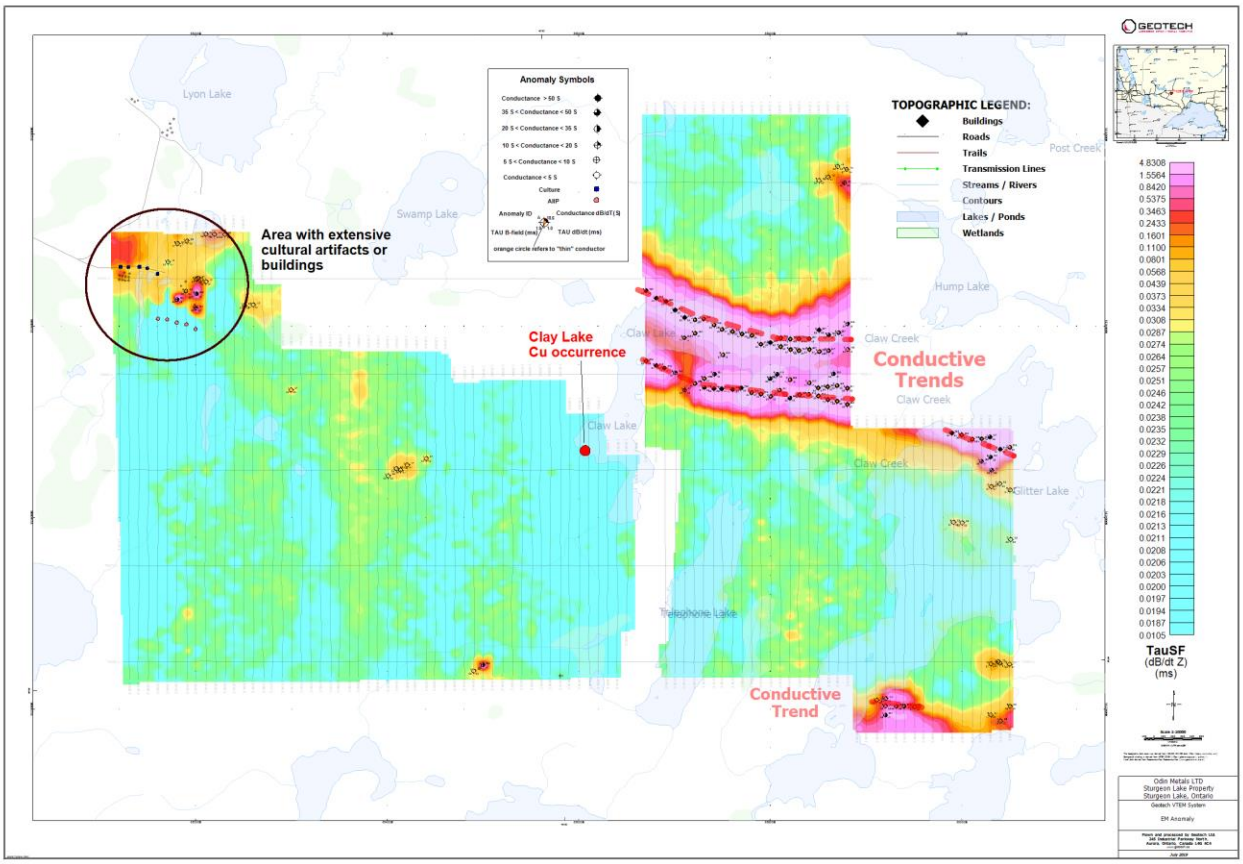


Figure 4: EM anomaly picks over the EM induction time-constant TAU data.

# 3. CONCLUSIONS AND RECOMMENDATIONS

Geotech has carried out the EM anomaly picking of the VTEM data from the Sturgeon Lake property located near Sioux Lookout, Ontario.

The strong (high conductance) conductors in the EM anomalies could be potential exploration targets for polymetallic mineralization, i.e., semi-massive to massive sulphides, including the extremely conductive pyrrhotite (Po).

There is an area in the NW corner of the VTEM block with extensive cultural artefacts or buildings. The EM anomalies picked in the area should be treated with caution, and some may in fact be related to culture.

The EM anomalies are recommended for further follow-up for the exploration of potential polymetallic mineralization in the VTEM survey area over the Sturgeon Lake property.

Respectfully submitted,

_____ _____

Karl Kwan, M.Sc. P.Geo. (Limited[2], Ontario)
Senior Geophysicist/Interpreter

Kanita Khaled, P.Geo. (Ontario)
Project Manager

_____

Jean M. Legault, M.Sc.A, P.Geo. (OGQ #1147)
Chief Geophysicist

**Geotech Ltd.**
July 30, 2019

[2] The designation of P.Geo (Limited) by Association of Professional Geoscientists of Ontario permits the principal interpreter to practice in the field of exploration geophysics only.

# REFERENCES

McNeill, JD, 1980: Applications of Transient Electromagnetic Techniques, Technical Note TN-7, Geonics Limited.

# APPENDIX A: FINAL DELIVERABLES

### *EM Anomaly*

GL190069_ Odin _anoms.gdb; (EM anomaly only Geosoft database)
GL190069_ Odin _anoms.XYZ; (EM anomaly ASCII file)
GL190069_ Odin _anoms2.map; (EM anomaly Geosoft map)

| Channel | Descriptions | Unit |
|---|---|---|
| Line | Line number | |
| x | UTM Easting (WGS84, UTM Z15N) | meter |
| y | UTM Northing (WGS84, UTM Z15N N) | meter |
| z | GPS elevation (WGS84, UTM Z15N) | meter |
| Culture | Culture anomaly (number 7) | |
| AIIP | Airborne Inductively Induced Polarization anomaly (number 5) | |
| Grade | Conductor grad (1 to 6) | |
| Anom_ID | K (thick – single peak) and N( (thin – double peak) | |
| Anom_Labels | Unique letters A, B, C, … anomaly identifier on a line | |
| AnConBF | Conductance (B-field) | Siemens |
| AnConSF | Conductance (dB/dt) | Siemens |
| AnTauBF | EM induction time-constant (B-field) | milliseconds |
| AnTauSF | EM induction time-constant (dB/dt) | milliseconds |